Review of the late Quaternary stratigraphy of the northern Gulf of Cadiz continental margin: New insights into controlling factors and global implications

Thomas MESTDAGH [a,*], Francisco J. LOBO [b], Estefanía LLAVE [c], F. Javier HERNÁNDEZ-MOLINA [d], David VAN ROOIJ [a]

[a] *Renard Centre of Marine Geology, Department of Geology, Ghent University, Krijgslaan 281 (S8), 9000 Gent, Belgium*

[b] *Instituto Andaluz de Ciencias de la Tierra, CSIC-Universidad de Granada, Av. de las Palmeras 4, 18100 Armilla, Spain*

[c] *Instituto Geológico y Minero de España (IGME), Ríos Rosas 23, 28003 Madrid, Spain*

[d] *Department of Earth Sciences, Royal Holloway University of London, Egham, Surrey TW20 0EX, UK*

(*) Corresponding author: Thomas.Mestdagh@UGent.be

Highlights

- A revised late Quaternary seismic and sequence stratigraphic framework for the northern Gulf of Cadiz shelf to middle slope, calibrated to IODP Expedition 339 sites U1386/U1387, is presented.

- The development of the continental margin is governed by an interplay of ~100 kyr eccentricity-driven sea-level cycles, tectonics, oceanography and sediment supply.

- This case has implications for the general understanding of high-resolution sequence stratigraphy, most notably regarding the relationship between glacial lowstands and the formation/preservation of sequence boundaries on the shelf.

Abstract

Over the past decades, the northern Gulf of Cadiz has been the focus of a wide range of late Quaternary seismic and sequence stratigraphic studies, either addressing the slope contourite depositional system (CDS), or the development of the continental shelf. Yet, high-resolution seismic data bridging between these domains and age information have remained sparse. This study, based on new high-resolution reflection seismic profiles calibrated to IODP Expedition 339 sites U1386/U1387, now presents an updated stratigraphic framework, that integrates (for the first time) the late Quaternary records of the northern Gulf of Cadiz middle slope to shelf off the Guadiana River.

Seismic stratigraphic analysis of the stacking, depocenter distribution, stratal architecture and facies of the seismic (sub-)units reveals the influence of ~100 kyr sea-level variations paced by Milankovitch (eccentricity) cycles, tectonics (manifesting as two pulses of uplift and margin progradation), sediment supply and bottom current activity. This work furthermore contributes to the application and understanding of high-resolution, late Quaternary sequence stratigraphy. Firstly, the proposed sequence stratigraphic interpretation shows that adaptations to the basic models are required to integrate the shelf and slope record, and to account for the presence of a significant alongslope (bottom current-controlled) component. Secondly, the results confirm that the sequences are dominantly composed of regressive deposits, whereas the preservation of transgressive to highstand deposits is more irregular. Significantly, the common assumption that successive major glacial lowstands are consistently recorded as well-marked, shelf-wide erosional unconformities, is demonstrated to be occasionally invalid, as tectonics can obliterate this one-to-one relationship.

Keywords: *stratigraphy, sea level, tectonics, oceanography, late Quaternary, Gulf of Cadiz*

1. Introduction

Over the past decades marine geological research has shown that several proxies in deep-sea sediment cores (most notably oxygen isotope records) reflect cyclic variations in the Earth's orbital geometry, or so-called Milankovitch cycles (Emiliani, 1955; Shackleton and Opdyke, 1973; Hays et al., 1976). These variations in precession, obliquity and eccentricity (having a ca. 20, 40 and 100 kyr periodicity respectively) control solar radiation, and as such pace climatic cycles and sea-level variations through changes in global ice-sheet volumes (Milankovitch, 1930; Chappell, 1974; Schwarzacher, 2000). Between 900 and 650 ka, this glacial-interglacial cyclicity shows a marked transition referred to as the Middle Pleistocene Transition (MPT) or Revolution (MPR), from an obliquity-controlled periodicity to a dominant eccentricity-driven periodicity characteristic of the middle to late Pleistocene (Ruddiman et al., 1986; Maslin and Brierley, 2015). Along with the prolongation of the cycles came an intensification in the global ice volume variations and amplification of the sea-level fluctuations up to 100 – 150 m during the past 500 kyr (Chappell and Shackleton, 1986; Bard et al., 1990; Rabineau et al., 2006; Elderfield et al., 2012; Grant et al., 2014; Rohling et al., 2014). 100 kyr sea-level cycles show an asymmetric pattern, with relatively short maximum (glacial) lowstand and (interglacial) highstand phases being separated by rapid sea-level rises on the one hand, and long-lasting sea-level falls on the other (Ruddiman, 2003). Higher frequency 20 kyr sea-level oscillations punctuate 100 kyr cycles, which is especially well-documented for the most recent (full) protracted sea-level fall starting at ca. 125 ka (Gallup et al., 1994; Lambeck and Chappell, 2001; Lambeck et al., 2002; Lea et al., 2002; Waelbroeck et al., 2002; Siddall et al., 2003).

Relative sea-level fluctuations exert a primary control on the sedimentary architecture of continental margins, and it has therefore been proposed that high-resolution, Quaternary seismic/sequence stratigraphy of modern continental margins can also record Milankovitch cycles (Lobo and Ridente, 2014; and references in their review). A basic tenet in these studies is that 100 kyr glacio-eustatic cycles have exerted a primary control on the stratigraphic architecture during the last ca. 800 kyr, by generating well-marked, shelf-wide erosional unconformities that enclose depositional sequences mainly consisting of progradational units. Most of these studies have been based on the premise of a one-to-one correlation between depositional sequences and 100 kyr glacio-eustatic cycles. However, age control is usually restricted to the most recent depositional sequence of last glacial age, whereas indirect age information of older sequences is obtained through correlation between shelf-wide unconformities and relative sea-level falls/lowstands of successive 100 kyr cycles (e.g. Hübscher and Spieß, 2005; Rabineau et al., 2005; Liquete et al., 2008; Riboulot et al., 2012; Ridente et al., 2012; Yoo et al., 2017; Figure 1).

In a number of shelves, recent investigations based on borehole data have provided a more robust age control. These studies show that, although in general terms the glacio-eustatic control on shelf sequences can be confirmed, the one-to-one correlation is too simplistic, and that the sedimentary expression of 100 kyr cycles is much more diverse. For example, the three most recent sequences appear to have developed in consonance with the three most recent 100 kyr cycles in the Adriatic Sea (Ridente et al., 2008; Ridente et al., 2009), and the five most recent sequences formed under the last five 100 kyr cycles on the Gulf of Lions shelf to upper slope (Rabineau et al., 2005; Rabineau et al., 2006; Bassetti et al., 2008; Sierro et al., 2009; Cortina et al., 2015; Cortina et al., 2016a; Cortina et al., 2016b). However, whereas in the Gulf of Lions the bulk of the sequences seem to have developed during the terminal limb of the long-lived sea-level falls, in the Adriatic Sea the preserved regressive deposits rather developed during the initial limb of the sea-level falls, i.e. during higher relative sea-level positions (cfr. Figure 1F vs. Figure 1G). In addition, in other cases (e.g. the Canterbury shelf off New Zealand and the New Jersey margin) only some 100 kyr cycles have been able to generate seismic-scale depositional sequences during the last 800 kyr (Miller et al., 2013; McHugh et al., 2017; Proust et al., 2018).

The higher frequency 20 kyr Milankovitch cycle has proven to be more elusive to recognize in the stratigraphic record at seismic scale, because of the greater spatial and temporal variability in the sedimentary sequence architecture, and because high-resolution age control is mostly lacking (Lobo and Ridente, 2014). An example where it was locally possible to observe major, preserved sequence boundaries that presumable result from 20 kyr cycles, is the Gulf of Mexico (Kolla et al., 2000). In other examples with age control, the higher-frequency cycles are expressed as minor bounding surfaces separating downward stepping parasequences (Bassetti et al., 2008; Ridente et al., 2008; Ridente et al., 2009) or as repetitive patterns of lithofacies successions (McHugh et al., 2017). In these cases, the 20 kyr signal thus appears as a superposition on the dominant 100 kyr cycle, leading to a composite stratigraphic pattern. Only in the Canterbury Shelf the drilling was deep enough to allow reaching the older sedimentary succession dominated by 40 kyr cycles. There, the correlation between sedimentary and glacio-eustatic cycles is even more tenuous than in the case of 100 kyr dominance (McHugh et al., 2017). Finally, sub-Milankovitch (millennial-scale) cyclicity in the stratigraphic organization of late Pleistocene – Holocene successions has as well been identified on a number of modern continental margins using very high-resolution techniques, like the Gulf of Lions (Labaune et al., 2005; Jouet et al., 2006; Berné et al., 2007), Adriatic Sea (Pellegrini et al., 2015; Pellegrini et al., 2018), Black Sea (Aksu et al., 2002) or southern Iberian margin (Hernández-Molina et al., 1994). In these examples, millennial-scale variations in sediment supply and rates of sea-level rise or fall have been demonstrated to be capable of generating resolvable changes in stratal stacking patterns and geometries.

For the northern Gulf of Cadiz shelf, on the southwestern Iberian margin, a composite sequence stratigraphic model was initially suggested based on a seismic stratigraphic approach (Somoza et al., 1997; Hernández-Molina et al., 2000; Hernández-Molina et al., 2002; Lobo et al., 2005a). In such scheme, 100 kyr sequences would be composed of higher frequency sequences, presumably guided by a higher frequency cyclicity. However, this model has remained tentative in the absence of direct age control. On the other hand, a range of seismic stratigraphic studies on the Quaternary stacking patterns of the northern Gulf of Cadiz continental slope (e.g. Nelson et al., 1993; Llave et al., 2001; Hernández-Molina et al., 2006; Llave et al., 2007; Marchès et al., 2010; Llave et al., 2011; Roque et al., 2012) have recently been ground-truthed and synthesized through International Ocean Discovery Program (IODP) Expedition 339 (Stow et al., 2013). This expedition drilled seven sites on the continental slope along the southwestern Iberian margin, targeting the contourite depositional system (CDS) which has developed under the action of the Mediterranean Outflow Water (MOW) during the Pliocene and Quaternary (Hernández-Molina et al., 2006). In addition to the strong imprint of bottom water circulation, the overall Quaternary sedimentary evolution of this system has also been controlled by sediment supply, climate, sea level and, significantly, tectonic activity (Stow et al., 2013; Hernández-Molina et al., 2014a; Hernández-Molina et al., 2016a). Yet, no attempt has been made to extrapolate these findings from the slope to the shelf, and to apply them to a higher-resolution, late Quaternary framework.

Therefore, a dedicated set of new high-resolution reflection seismic profiles that connect the northern Gulf of Cadiz shelf with IODP Expedition 339 sites U1386 and U1387 on the middle slope is presented in this study (Figure 2). This data, in combination with the borehole information, provides the opportunity to create an updated scheme of the stratigraphic patterns of the continental margin during the late Quaternary. Specifically, this study aims to a) revise the previously suggested seismic and sequence stratigraphic models, on a broad scale encompassing the shelf and middle-to-upper slope and integrating recently available age control; b) evaluate the controlling factors leading to this specific stratigraphic architecture; and c) discuss the conceptual implications of the presented case for the understanding and application of high-resolution (Quaternary) sequence stratigraphic schemes in general.

2. Study area

2.1. Geological setting

The large-scale late Cenozoic geological evolution of the Gulf of Cadiz is controlled by the convergence between Eurasia (Iberia sub-plate) and Africa (Nubia sub-plate) since the mid-Oligocene (e.g. Dewey et al., 1989; Srivastava et al., 1990; Rosenbaum et al., 2002). The Azores-Gibraltar fracture zone (AGFZ) constitutes the boundary between these plates in the Atlantic, but in the Gulf of Cadiz the eastern end of this plate boundary becomes somewhat diffuse. Nevertheless, dextral strike-slip faults, referred to as SWIM (South West Iberian Margin) faults, cross-cut the Gulf of Cadiz and are inferred to accommodate the present-day oblique WNW-ESE convergence (Figure 2A; Terrinha et al., 2009; Zitellini et al., 2009), at a rate of ~4 mm/year (Koulali et al., 2011). These faults have been active since at least 1.8 Ma (Rosas et al., 2009; Duarte et al., 2011). In addition, the westward migration of the Gibraltar arc, which marks the propagation of the Mediterranean Alpine collision belt into the Atlantic, resulted in a series of NE-SW-striking thrust faults and the emplacement of an accretionary wedge during the Tortonian (late Miocene) (Maldonado et al., 1999; Gutscher et al., 2002; Medialdea et al., 2004; Duarte et al., 2013). The (in plan view) U-shaped accretionary wedge consists of a pile of westward-thrusted sediments and is generally referred to as the 'allochthonous unit of the Gulf of Cadiz' (AUGC) or the 'olistostrome unit' (Figure 2A; Maldonado et al., 1999; Medialdea et al., 2004; Duarte et al., 2013). The AUGC, together with the Sudiberic paleomargin (part of the Hercynian Iberian Massif) north of the accretionary wedge deformation front, constitutes a relatively unstable base for the so-called Neogene sedimentary basins in the Gulf of Cadiz, which are infilled by late Miocene to Quaternary deposits (Maldonado et al., 1999; Medialdea et al., 2004; Hernández-Molina et al., 2016a). These basins are affected by the continued oblique convergence between the Iberia and Nubia sub-plates since the late Miocene, resulting in episodic uplift of fault blocks, fault reactivation and diapirism (Maldonado et al., 1999; Gràcia et al., 2003; Medialdea et al., 2004; Fernández-Puga et al., 2007; García et al., 2009; Terrinha et al., 2009; Zitellini et al., 2009; Duarte et al., 2011).

2.2. Oceanographic setting

After its opening in the latest Miocene (Duggen et al., 2003; Roveri et al., 2014), the Strait of Gibraltar has acted as an oceanic gateway through which the exchange of Atlantic and Mediterranean water masses has controlled the oceanographic regime in the Gulf of Cadiz (Figure 2A). At present, the eastward movement of the Atlantic Inflow Water (AIW) into the Mediterranean is compensated by the westward outflow of the Mediterranean Outflow Water (MOW) underneath (Price et al., 1993).

The AIW comprises the North Atlantic Superficial Water (NASW) and the Eastern North Atlantic Central Water (ENACW). The overall anticyclonic circulation of the NASW over the outer continental shelf (Johnson and Stevens, 2000; Garcia et al., 2002) confines landward two cyclonic cells that dominate the shallow-water oceanography of the northern Gulf of Cadiz shelf (Figure 2A). These cyclonic cells are subject to significant variability dictated by changes in the direction of the prevailing winds (i.e. easterlies vs. westerlies; García-Lafuente et al., 2006). The western cyclonic cell over the Portuguese shelf constitutes a moderate to high-energy environment with significant activity of storm events (Lobo et al., 2004). In the eastern cyclonic cell, the reworking activity of waves and along-shore currents is significant off the Guadiana River, but decreases towards the east and is moderate to low on the shelf sector off the Guadalquivir River (Lobo et al., 2004). Underneath the NASW, the ENACW flows in a dominant eastward direction between ca. 100 – 250 m water depth, thus affecting the seabed on the outer shelf and upper slope in the northern Gulf of Cadiz (Figure 2A). At present, it is characterized by an average temperature of ca. 14.5 °C and relatively low salinity of < 36.2 ‰ (Bellanco and Sánchez-Leal, 2016). These hydrographic conditions (temperature, salinity and flow depth) are subject to intra-annual variability caused by seasonal changes in the stratification of the water column (Bellanco and Sánchez-Leal, 2016).

The MOW and modified Antarctic Intermediate Water (AAIW) occupy intermediate water depths below the ENACW (Figure 2A). The AAIW circulates cyclonically between 600 and 1500 m water depth and has an average temperature and salinity of ~10 °C and ~35.62 ‰ respectively (Louarn and Morin, 2011). The MOW results from the mixing and advection of Mediterranean waters (i.e. the Levantine Intermediate Water and part of the West Mediterranean Deep Water), and has in the northern Gulf of Cadiz a temperature range of 10.5 – 14 °C and relatively high salinity between 36 and 38 ‰ (Ambar and Howe, 1979; Gascard and Richez, 1985; Bryden et al., 1994; Bellanco and Sánchez-Leal, 2016; Hernández-Molina et al., 2016a; Sánchez-Leal et al., 2017). Upon its exit through the Strait of Gibraltar, the MOW reaches very high current velocities of up to 300 cm/s (Ambar and Howe, 1979; Mulder et al., 2003), and then gradually decelerates as it flows to the northwest along the Iberian margin as a contour current within the mid-slope region (400 - 1400 m water depth; Baringer and Price, 1999). The MOW splits in different branches due to the interaction with the complex seafloor morphology (a.o. created by diapiric ridges) and potentially also because of vertical layering within the MOW west of the Strait of Gibraltar (Ambar and Howe, 1979; Borenäs et al., 2002; Millot, 2009; Copard et al., 2011; Sánchez-Leal et al., 2017). Two main branches can be distinguished, the Mediterranean Upper branch (MU) and the Mediterranean Lower branch (ML), flowing at depths of 400 – 800 m and 800 – 1400 m respectively (Figure 2A). The MU has an average velocity of 40 – 50 cm/s, whereas the current velocity of the ML is 20 – 30 cm/s on average (Ambar et al., 1999; Borenäs et al., 2002; Llave et al., 2007; Marchès et al., 2007; García et al., 2009). After the onset of the MOW in the Gulf of Cadiz around 5.3 Ma, it underwent a step-wise increase in intensity during the Pliocene, leading to the present-day vigorous MOW circulation that was established during the Quaternary (Hernández-Molina et al., 2014a; Hernández-Molina et al., 2016a). Superimposed on this long-term evolution, several studies have reported variations in MOW circulation on shorter timescales, which are presumably governed by climatic and sea-level changes. The present-day consensus, primarily based on analysis of the last glacial-interglacial cycle, is that the MU is enhanced during warm (highstand) intervals and reduced or absent during cool (lowstand) intervals, whereas the ML is enhanced during cold intervals (Nelson et al., 1993; Nelson et al., 1999; Cacho et al., 2000; Llave et al., 2006; Voelker et al., 2006; Llave et al., 2007; Rogerson et al., 2010; Bahr et al., 2014; Hernández-Molina et al., 2014b; Kaboth et al., 2016). However, changes in the water mass sourcing of the MOW could reduce MU influence on the slope also during interglacials, which was suggested to be the case between ~475 ka and ~130 ka (Kaboth et al., 2017).

Finally, at depths greater than 1500 m, the MOW is underlain by the cold and less saline (3 – 8 °C; < 35.2 ‰) North Atlantic Deep Water (NADW; see Figure 2A; Zenk, 1975; Caralp, 1988; Ochoa and Bray, 1991; Baringer and Price, 1999).

2.3. Margin physiography, morphology and stratigraphy

The northern Gulf of Cadiz continental margin comprises three well-defined physiographic domains: continental shelf, continental slope (further subdivided into upper, middle and lower slope) and abyssal plain (Hernández-Molina et al., 2006). This study focuses on the continental shelf and upper-to-middle continental slope (Figure 2).

The continental shelf is widest in the central part of the Spanish zone off the Guadalquivir River (~ 30 km) and narrows towards the Strait of Gibraltar to the E and Portuguese margin to the W. It is relatively flat (< 0.3° on average offshore Spain), with the shelf break occurring between 120 and 140 m water depth (Hernández-Molina et al., 2006). The two main fluvial input sources are the Guadiana and Guadalquivir, which drain most of the southern half of the Iberian Peninsula (Lobo et al., 2018). Offshore the Guadiana River, an inner shelf domain dominated by prodeltaic facies with scattered rocky outcrops, a middle shelf domain covered by shore-parallel muddy deposits cross-cut by an across-shelf sandy zone, and a predominantly fine-grained outer shelf domain with occasional coarser-grained veneers can be distinguished (Figure 2B; Gonzalez et al., 2004; Lobo et al., 2018). Stratigraphically, two asymmetric depositional sequences have been described that primarily consist of regressive-to-lowstand facies (Figure 3B). In the absence of direct age control, these sequences have tentatively been interpreted to be related to the two last glacial cycles (Somoza et al., 1997; Hernández-Molina et al., 2000; Lobo et al., 2005a). They are bounded by well-marked shelf-wide unconformities, the most recent one being attributed to subaerial erosion during the Last Glacial Maximum (LGM) lowstand and transgressive ravinement during the subsequent sea-level rise (Figure

3B; Lobo et al., 2018). Both sequences are internally composed of higher-frequency units, leading to a composite stratigraphic pattern, which has been attributed to 100 and 20 kyr Milankovitch-driven sea-level fluctuations (Somoza et al., 1997; Hernández-Molina et al., 2000; Hernández-Molina et al., 2002; Lobo et al., 2005a). During the deposition of these sequences the margin shows a strong progradation and limited aggradation (Figure 3B; Lobo and Ridente, 2014). The post-glacial and Holocene transgressive and highstand deposits overlying these depositional sequences on the shelf can be imaged and studied with greater detail, and record short-term (millennial-scale) changes in the rate of sea-level rise, sediment supply, hydrodynamic regime and shelf circulation patterns (Lobo et al., 2001; Lobo et al., 2004; Lobo et al., 2005b).

The upper slope (130 – 400 m water depth) has an average width of ~ 10 km, and gradients between 1 and 3° (Hernández-Molina et al., 2006). Morphologically, depositional features, erosive surfaces, neotectonic elements (related to diapiric movements and faults), gravitational elements (e.g. slides, slumps and creeps) and fluid flow features (e.g. pockmarks) have been distinguished (e.g. Baraza et al., 1999; Rodero et al., 1999; Hernández-Molina et al., 2006). Submarine canyons are absent, except in the western part of the Gulf of Cadiz off Portugal (Hernández-Molina et al., 2003; Mulder et al., 2006). The middle slope (400 – 1200 m water depth) is more gently dipping (gradients around 1°) and very wide (up to 100 km), and as such can be considered as a slope "terrace" (Hernández-Molina et al., 2003; García et al., 2009). A vast CDS has formed on this middle slope terrace during the Pliocene and Quaternary under the action of the MOW (e.g. Nelson et al., 1999; Llave et al., 2001; Habgood et al., 2003; Hernández-Molina et al., 2003; Hernández-Molina et al., 2006; Hanquiez et al., 2007; Llave et al., 2007; Llave et al., 2011; Hernández-Molina et al., 2014b). Five morphosedimentary sectors have been defined (Hernández-Molina et al., 2003), of which the focus area of this study is located within the "contourite deposition" sector. The main depositional elements in this sector are the elongated, mounded and separated Faro-Albufeira Drift, which laterally transitions into the Faro-Cadiz and Bartolome Dias sheeted drifts, whereas the Alvarez Cabral contourite moat represents an important erosional element (Figures 2B and 3A; Stow et al., 1986; Llave et al., 2001; Stow et al., 2002). The drifts consist of mixed biogenic and terrigenous muddy and silty to sandy sediments (Gonthier et al., 1984). The Late Quaternary stratigraphy of the middle slope CDS (Figure 3A) comprises one major depositional sequence (QIII), which is bound at the base by the mid-Pleistocene Discontinuity (MPD) occurring around 0.7-0.9 Ma (Lofi et al., 2016; Hernández-Molina et al., 2016a). Within this main unit, two sub-units (Q5 and Q6) are separated by the Late Quaternary Discontinuity (LQD), the second important late Quaternary hiatus between 0.3-0.6 Ma (Figure 3A; Hernández-Molina et al., 2016a). These marked late Quaternary discontinuities (MPD and LQD) relate to tectonic activity and uplift-induced erosion (Llave et al., 2007; Hernández-Molina et al., 2016a). Sub-units Q5 and Q6 are in turn build up by higher-frequency sedimentary cycles, which are presumably controlled by changes in bottom current circulation and climatic (orbital) and eustatic variations (Llave et al., 2001; Llave et al., 2006; Llave et al., 2007; Toucanne et al., 2007; García et al., 2009; Bahr et al., 2014; Hernández-Molina et al., 2014b; Kaboth et al., 2016). These short-term depositional cycles (i.e. cycles < 0.4 Ma) typically show a distinct, repetitive facies motif in seismic profiles wherein a weak or transparent acoustic facies at the base grades into a more reflective facies at the top that is truncated by an erosional surface. This is inferred to correspond to mud dominated deposits at the base and upward increase in grain size and detrital content (Llave et al., 2001; Stow et al., 2002; Llave et al., 2006).

3. Material and methods

3.1. IODP Expedition 339 sites U1386 and U1387

In total, IODP Expedition 339 drilled seven sites along the southwestern Iberian margin (Stow et al., 2013), of which the two adjacent sites U1386 and U1387 on the middle-to-upper slope contourite terrace (targeting the Faro-Albufeira Drift) are integrated with the seismic dataset (Figure 2). Drilling at site U1386 yielded 850 m of core material from three parallel holes, reaching a maximal borehole depth of 526 m below sea floor (mbsf). 1085 m of core was retrieved at site U1387 from three parallel holes, with a maximum penetration of 870 mbsf. Physical properties (gamma ray attenuation density, magnetic susceptibility, P-wave velocity and natural gamma radiation) were determined onboard on whole-round core sections using a multi-sensor core logger (MSCL). In addition, a limited number of discrete P-wave velocity measurements were performed on split cores (generally 1 measurement per core section), using the measurement gantry (Stow et al., 2013). Downhole logging was performed at both sites, using the triple combo, Formation MicroScanner (FMS)-sonic, and Versatile Sonic Imager (VSI) tool strings (Stow et al., 2013). After filtering out erroneous values (i.e. values < 1400 m/s, due to poor sediment-liner coupling, small cracks in the sediments etc; Stow et al., 2013), the discrete P-wave velocity measurements on the split cores (available in the upper tens of meters of the borehole) and downhole logging velocities (available below 100 m borehole depth) were integrated to convert borehole depth to two-way travel time (twtt) in the reflection seismic data. With this approach, a borehole-seismic tie was obtained for both sites that is consistent with a few additional travel time – borehole depth control points from vertical seismic profiling (VSP) deeper in the boreholes (Figure S1). High-resolution age control at sites U1386 and U1387 is provided by the age models of Kaboth et al. (2016) (36 control points) and Bahr et al. (2014) (32 control points), which cover the upper ~40 m of the boreholes, corresponding to a time span of ~150 kyr (Table S1). These age models are based on tuning normalized bromine counts, derived from XRF scanning of sediment cores from U1386/U1387, to the $\delta^{18}O$ record of the Iberian Margin core MD01-2444 (Hodell et al., 2013). For borehole depths > 40 m, the chronostratigraphic framework proposed by Lofi et al. (2016) for the last 500 kyr was adopted (consisting of 11 control points; Table S1), which was established through the regional correlation of downhole and core Gamma Ray data from five IODP Expedition 339 drilling sites in the Gulf of Cadiz.

3.2. Acquisition, processing and interpretation of reflection seismic data

The main dataset used for the seismic interpretation and correlation is a set of high-resolution single-channel reflection seismic profiles acquired over IODP sites U1386/U1387 and the northern Gulf of Cadiz shelf during the RV Belgica COMIC 2013 and RV Ramón Margalef LASEA 2013 cruises, using a SIG sparker source (with an energy of 300 J, shot interval of 2 s and sampling frequency of 10 kHz). The approximate vertical resolution of the system is 1 – 1.5 m. Basic post-processing included bandpass filtering, amplitude corrections (spherical divergence), 2D spike removal (burst noise removal), swell static corrections and top muting. To refine the dataset for mapping and gridding the seismic surfaces, the aforementioned data was complemented with LASEA 2013 TOPAS (parametric echo-sounder) profiles, which have a higher resolution but lower penetration than the sparker data, and with data from previous surveys in the study area (i.e. GOLCA 93 and FADO 96, which used a Uniboom source, and NOMADS 2007, which deployed a sparker source and a six-channel streamer). The complete seismic grid is shown in Figure 2B.

Seismic horizons and discontinuities were interpreted following the principles of seismic stratigraphy (Mitchum et al., 1977) using the commercially available software IHS Kingdom®. First, margin-wide surfaces (mws) of discontinuity that can be traced from the middle slope to the shelf were identified based on the analysis of reflection terminations. These mws delineate the major seismic units. Within the major seismic units, less pronounced minor internal surfaces (is) of discontinuity, which generally do not have a margin-wide extent, are picked and used to define sub-units. The seismic facies analysis of these sub-units consisted of a description of the internal reflection characteristics (e.g. reflection continuity and amplitude). Based on these seismic stratigraphic analyses, a sequence stratigraphic interpretation is proposed (the adopted approach is clarified in chapter 5). A qualitative analysis of shoreline/shelf-edge trajectories is herein also taken into account, following the concepts and nomenclature of Helland-Hansen and Hampson (2009), on the dip-oriented seismic sections over the shelf.

The margin-wide surfaces were gridded using a minimum curvature gridding algorithm, from which thickness maps and basic volume estimations (combined sediment + porous volumes, uncorrected for compaction) for the major seismic units were generated using Golden Software Surfer®. In the volume calculations, a (vertically and laterally) uniform P-wave velocity of 1600 m/s was assumed to convert thicknesses in seconds twtt to meters. This velocity is in accordance with the fine-grained nature of surficial and (shallow) subsurface sediments on the upper slope and shelf (Maldonado et al., 1999; Nelson et al., 1999; Lobo et al., 2018), and approximates the average of values measured in the upper ~100 m of the boreholes on the middle slope (see above; Figure S1). Likewise, this velocity was adopted in the quantification of the subsidence, which followed the method proposed by Rabineau et al. (2014).

4. Results

4.1. Seismic stratigraphy

A seismic stratigraphic analysis for the northern Gulf of Cadiz continental margin is presented in this section. Two key correlation profiles which cross IODP site U1386 on the middle slope and connect to the available regional seismic grid on the upper slope and shelf to the NE are shown (Figures 4 and 5; detailed sections of these profiles in Figures 6 – 13). These profiles, further named '(correlation) profile 1' and '(correlation) profile 2', are similar on the middle slope, but connect to different shelf sectors. This allows to illustrate the lateral variability in the seismic stratigraphic architecture both downslope (shelf vs. upper slope vs. middle slope) and along-strike. A summary of the seismic stratigraphic analysis, together with a reference to previous stratigraphic work in the study area, is provided in Table 1.

4.1.1. Major seismic surfaces

Five major seismic surfaces were identified on a margin-wide scale (mws5 – mws1, from oldest to youngest). The oldest surfaces (mws5 – mws3) are partly located below the multiple reflection on the upper slope. This impedes a full seismic stratigraphic characterization on the upper slope in correlation profiles 1 and 2 (Figures 4 and 5), yet the available seismic grid allows to infer a tentative slope-to-shelf correlation.

mws5. The lateral extent of the oldest major seismic surface, mws5, is limited to the slope and outer to middle shelf, where mws5 is truncated by mws4 (Figures 10 and 13). It is a high-amplitude, laterally continuous and concordant seismic surface on the middle slope, except where a depression in mws4 (described below) incises mws5 directly east of site U1386 (Figure 6). Towards the eastern part of the middle slope, occasional erosional truncation and onlap occurs, while the amplitude of mws5 becomes moderate to weak (Figures 8 – 9 and 11). The lateral continuity of mws5 (and of the shallower major seismic surfaces mws4 – mws2) is locally disturbed on the upper slope in profile 2 by a diapiric structure (characterized by low-amplitude, chaotic seismic reflections; Figures 5 and 11). On the outer shelf, mws5 displays moderate amplitudes, with toplap terminations and erosional truncation below and downlap above.

mws4. Mws4 laterally extends from the middle slope to the middle shelf, and merges in profile 1 with mws1 (description below) towards the inner shelf (Figure 4). On the middle slope, mws4 is characterized by high amplitudes and mostly conformable contacts, except for the smooth, channel-like incision immediately east of site U1386. This incision is 45 ms twtt deep, has an asymmetrical U-shape (the western flank is steeper than the eastern flank), and truncates underlying reflections (Figure 6). This incision causes a depression in the overall planar morphology of mws3 – mws1 above (with the depth of the depression decreasing from mws3 to mws1), and still leaves a faint depression on the present-day seabed. Towards the upper slope, amplitudes decrease and occasional low-angle erosional truncation below can be observed (Figure 8). On the shelf, mws4 varies from a regular, moderate- to high-amplitude surface on the outer shelf to a more irregular, high-amplitude surface towards the middle shelf. The reflection termination pattern shows toplap (on the outer shelf) and erosional truncation (on the middle shelf) below mws4, and downlap above (Figures 10 and 13).

mws3. Mws3 extends from the middle slope to the middle shelf. It is marked as a smooth surface on the middle slope (where the amplitude is high) and upper slope (where the amplitude is low). The contact with reflections below is conformable to faintly erosive, whereas contacts above show a conformable pattern and sporadic onlap at the foot of the upper slope (Figures 8 – 9). Mws3 itself onlaps the aforementioned diapir on the upper slope in profile 2 (Figure 11). The amplitude of mws3 increases on the shelf, and its character changes from smooth on the outer shelf to slightly irregular towards the middle shelf. Toplap below and onlap above mws3 on the outer shelf grade landwards into erosional truncation and downlap (Figures 10 and 12 – 13).

mws2. The extent of mws2 spans the middle slope to the outer shelf, where it is truncated by mws1 (see below). Mws2 varies laterally from a planar, moderate- to high-amplitude surface on the middle slope, to an irregular, wavy surface of low to moderate amplitude on the upper slope, and eventually to a rugged, high-amplitude surface on the outer shelf. On the continental slope, it is a concordant to slightly erosive surface, with sporadic onlap or downlap of reflections above. On the outer shelf, mws2 shows a general concordant to slight erosional truncation pattern in profile 1 (Figure 10). In profile 2, more clear toplaps and erosional truncation can be observed below mws2, in addition to onlap (on the upper slope to outer shelf) and downlap (towards the middle shelf) of reflections above (Figures 12 – 13).

mws1. The most recent major seismic surface, mws1, can be traced over the entire extent of the correlation profiles, i.e. from the middle slope to the middle shelf. Only locally, in the upper slope to outer shelf transition in correlation profile 1, mws1 is truncated by the seabed. It appears as a planar surface of moderate- high amplitude on the middle slope, that becomes slightly wavy on the upper slope (Figures 6 – 9). On the slope, mws1 is generally concordant with sporadic slight erosion of reflections below and local onlap above. On the shelf, mws1 is characterized by a high amplitude and an irregular appearance, with occasional incision (up to 15 ms twtt) of larger-scale channels. The reflection termination pattern against mws1 on the shelf displays erosional truncation below and a concordant pattern or onlap (in the deeper incisions) above (Figures 10 and 12 – 13).

4.1.2. Major seismic units

The major seismic surfaces, together with the present-day seabed, delineate five major seismic units (U5 – U1, from oldest to youngest). Their shape, stacking patterns, distribution and internal architecture are presented below and summarized in Table 1.

U5. U5 stacks seawards of the older packages on the shelf and upper slope in profile 1 (Figure 10), whereas towards the eastern part of the shelf (e.g. in profile 2), it builds outwards and upwards (Figure 12). On the middle slope, U5 shows an aggradational stacking pattern. It has a sheeted external geometry on the middle slope, becoming wedge-shaped towards the upper slope and outer shelf in profile 1, and towards the middle shelf in profile 2. The thickness distribution map (Figure 14A) shows that U5 reaches its maximal thickness (> 120 ms twtt) on the outer shelf and upper slope in the western part of the mapped area, where the landward termination of the unit is located most distally. Towards the east, as the landward termination of U5 moves closer to the present coastline, U5 becomes thinner, and eventually thickens again towards the southeastern edge of the mapped area. On the middle slope, U5 is relatively thin (app. 10 – 50 ms twtt) and shows a rather uniform distribution without major depocenters.

Internally, U5 can be subdivided into two sub-units, which are separated by minor seismic surface is5. This surface is characterized by moderate to high amplitudes and is generally conformable to slightly erosive on the middle and upper slope (Figures 6 – 9 and 11). On the eastern part of the shelf, is5 shows moderate amplitudes and an irregular character, with downlap terminations above and conformable contacts below. Is5 itself onlaps mws5 on the middle shelf (Figures 12 – 13). In contrast, is5 could not be correlated to the western part of the shelf (profile1; Figure 10), as it cannot be traced below the multiple on the upper slope. The lower sub-unit, U5.2, shows smooth, parallel and continuous low-amplitude reflections on the middle slope, that laterally become subparallel to slightly wavy and very weak in amplitude towards the upper slope (Figures 6 – 9). On the shelf in profile 2, the seismic facies of U5.2 displays subparallel to slightly chaotic reflections of low to moderate amplitude (Figures 12 – 13). The upper sub-unit (U5.1) is also characterized by smooth, parallel and continuous reflections on the middle slope, but with higher amplitudes than U5.2. The amplitudes and lateral continuity decrease slightly towards the upper slope, the latter becoming wavy to hummocky (Figures 6 – 9). On the outer shelf, U5.1 shows low-amplitude seismic reflections with a contorted to parallel-oblique progradational reflection configuration (Figures 10 and 12 – 13).

U4. U4 shows a progradational-aggradational motif. It has a sheeted external geometry on the middle and upper slope, passing into a wedge (in profile 1; Figure 4) or a lobate to bank-shaped geometry (in profile 2; Figure 5) on the shelf. Overall, U4 is a relatively thin unit on the shelf (< 20 ms twtt), that thickens downdip into a vaguely alongslope elongated depocenter on the upper slope, which is most clearly expressed in the western part of the study area (Figure 14B). Further downslope, U4 becomes thinner towards the middle to upper slope transition, and eventually slightly thickens on the middle slope (to thicknesses between app. 20 to 40 ms twtt).

The internal architecture of U4 comprises 2 sub-units, separated by minor seismic surface is4. This is a smooth, high-amplitude surface that onlaps mws4 at the base of the upper slope (Figure 8). Except for the incision directly east of U1386, is4 is a concordant surface. The seismic facies of lower unit U4.2 is characterized by parallel, continuous reflections on the middle slope, with laterally varying amplitudes (generally weak to moderate, but sporadically high). U4.2 pinches out at the foot of the upper slope (Figures 6 – 8). Upper sub-unit U4.1 is typified by a parallel reflection pattern on the middle slope, that becomes subparallel towards the upper slope. Amplitudes decrease updip from moderate on the middle slope to low on the upper slope (Figures 6 – 9). On the shelf, U4.1 shows parallel-oblique progradation that is locally contorted to chaotic, while the amplitude increases landwards from moderate on the outer shelf to high on the middle shelf (Figures 10 and 12 – 13).

U3. On the shelf and upper slope, U3 stacks on top and seawards of U4, while it builds mainly upwards on the middle slope (Figures 4 – 5). U3 has a sheeted external geometry on the (middle and upper) slope, and becomes wedge-shaped on the shelf. It is a relatively thick unit with a major linear, alongslope elongated depocenter on the upper slope (> 160 ms twtt; Figure 14C).

Three minor internal seismic surfaces divide U3 into four sub-units (U3.4 – U3.1, from oldest to youngest). Internal surfaces is3.3 and is3.1 are smooth, concordant, high-amplitude surfaces on the middle slope, that evolve into slightly wavy surfaces of moderate amplitude towards the transition to the upper slope (Figures 6 – 9). On the upper slope and shelf, their amplitude increases again, and reflection terminations display toplap below, and onlap (on the upper slope for is3.3) and downlap (on the outer and middle shelf) above (Figures 10 – 13). Is3.2 is characterized by moderate-high amplitudes, is conformable to slightly erosive, and merges with is3.3 at the base of the upper slope (Figures 6 – 9). Sub-unit U3.4 is characterized by parallel, continuous, low- to moderate-amplitude reflections on the middle slope, that decrease in amplitude and become subparallel to wavy on the upper slope (Figures 6 – 9 and 11). At the top of the upper slope and on the shelf, U3.4 shows a low-angle parallel-oblique progradational reflection configuration (Figures 10 and 12 – 13). The internal architecture of the sub-unit above, U3.3, is also characterized by a laminar, aggradational pattern of moderate- to high-amplitude reflections on the middle slope, before it pinches out at the foot of the upper slope (Figures 6 – 9). Continuous and parallel seismic reflections constitute the seismic facies of sub-unit U3.2 on the middle slope, with amplitudes upwardly increasing from low at the base to high at the top of the sub-unit (Figures 6 – 7). In the transition to the upper slope, U3.2 shows a wavy to slightly chaotic reflection pattern of moderate amplitude, while on the upper slope the amplitude decreases again and reflections become subparallel to wavy (Figures 8 – 9 and 11). On the shelf, U3.2 is located landward of sub-unit U3.4. It has a lens-shaped external geometry with internal low-angle parallel-oblique progradation composed of low- to moderate-amplitude reflections (Figures 10 and 13). Finally, the reflection configuration within the uppermost sub-unit (U3.1) varies laterally from parallel continuous on the middle slope, to discontinuous or disrupted at the base of the upper slope, to wavy/hummocky or contorted on the upper slope and shelf edge (Figures 6 – 11). There is a marked increase in amplitude from the base to the top of this sub-unit on the middle slope (Figure 6), while amplitudes become relatively high throughout U3.1 at the base of the upper slope, and low throughout U3.1 updip on the upper slope. On the shelf, U3.1 is characterized by parallel to tangential oblique progradation and moderate to high amplitudes. In profile 1, the inclination of the foresets increases seawards (Figure 10), while profile 2 rather shows uniform, low angle progradation (Figure 12).

U2. U2 stacks dominantly seawards of the underlying units on the shelf and upper slope (Figures 4 – 5). It has a sheeted external geometry on the middle slope that becomes wedge-shaped on the upper slope and shelf. The thickness distribution map (Figure 14D) illustrates that U2 is restricted to the outer shelf and slope, with its landward termination showing a slightly undulating pattern and located in a more distal position (closer to the shelf edge) towards the W. A major linear, alongslope elongated depocenter (> 120 ms twtt) is identified on the upper slope, while the thickness is rather uniform (~10 – 40 ms twtt) on the middle slope.

Internally, a minor seismic surface (is2) separates U2 into two sub-units. Is2 appears as a smooth, conformable, high-amplitude surface that onlaps mws2 on the more eastern part of the middle slope (Figure 7). The lower sub-unit (U2.2) shows parallel, low-amplitude seismic reflections on the middle slope around site U1386. It thins and increases in amplitude towards the E, where it eventually pinches out (Figures 6 – 7). The upper sub-unit (U2.1) is characterized by (sub)parallel continuous reflections on the middle slope, with an overall upward increase in amplitude (Figures 6 – 7). On the upper slope, the reflection configuration becomes complex, as chaotic to transparent bodies alternate both laterally and vertically with more continuous, wavy facies of moderate amplitude (Figures 8 – 9 and 11). Also, a localized incision can be observed within this sub-unit on the upper slope in correlation profile 1 (Figure 9). On the outer shelf, the reflection configuration is dominantly progradational (Figures 10 and 12), where reflections show moderate amplitudes and lateral variations in character ranging from subparallel – wavy to contorted – chaotic.

U1. The most recent unit (U1) aggradationally stacks on top of the underlying units over the entire margin (i.e. from middle slope to inner shelf). It has a sheeted geometry, except towards the inner shelf in profile 1 where a more bank-shaped geometry can be observed (Figure 4). Locally, U1 also infills depressions in mws1 on the shelf (Figure 10). The thickness distribution is therefore somewhat patchy on the shelf. Two depocenters (up to ~ 80 ms twtt thick) that are slightly elongated alongslope, can be observed on the upper slope (Figure 14E). The thickness of U1 on the middle slope is limited (< 20 ms twtt) and uniform. Internally, U1 shows continuous and parallel reflections on the middle slope, which gradually increase from low amplitudes at the base to high amplitudes at the top (Figures 6 – 8). Towards the upper slope, amplitudes become overall high and the reflection configuration subparallel to wavy (Figures 9 and 11). On the shelf, U1 generally shows an aggradational reflection configuration with subparallel reflections of moderate amplitude. Where U1 infills the topographic depressions in mws1, the internal configuration is chaotic and variable in amplitude. Also, towards the inner shelf, a parallel-oblique progradational reflection configuration can be observed (Figures 10 and 12 – 13).

4.2. Borehole-seismic tie and chronology

Through the borehole-seismic tie and available age models at IODP sites U1386 and U1387, a chronology and correlation to sea-level/ $\delta^{18}O$ curves and Marine Isotope Stages (MIS) can be obtained for the above described seismic stratigraphy (Figure 15 and Table 2). As such, it appears that major seismic surfaces mws5 – mws1 consistently formed towards the end of the five most recent major glacial lowstands (i.e. MIS12, MIS10, MIS8, MIS6 and MIS2 respectively); hence major seismic units U5 – U2 correspond to glacial-interglacial cycles of app. 100 kyr in duration, while U1 represents an incomplete cycle comprising the most recent deglaciation and present-day highstand. Within the major units, the basal sub-units (i.e. U5.2, U4.2, U3.4, U2.2 and U1) correspond to glacial terminations and (early) highstands, whereas the upper sub-units (i.e. U5.1, U4.1, U3.1 and U2.1) are formed during gradual sea-level falls and lowstands. In U3 two additional sub-units were defined between the basal and upper sub-unit (U3.3 and U3.2), which respectively coincide with a sea-level fall and subsequent sea-level rise/highstand superimposed on the 100 kyr sea-level cycle.

5. Sequence stratigraphic interpretation

5.1. Sequence stratigraphy: background

Modern sequence stratigraphy started to develop after it was originally conceived in the 1970's as 'seismic stratigraphy' (AAPG memoir 26, Payton, 1977). This early work introduced the analysis of reflection terminations and configurations in seismic data as a tool to subdivide seismic sections into packages of concordant reflections, interpreted as genetically related strata ('depositional sequences') bounded by unconformities or their correlative conformities ('sequence boundaries') (Mitchum et al., 1977). This original 'depositional sequence' model by Mitchum et al. (1977) was refined by the Exxon group (e.g. Posamentier et al., 1988; Posamentier and Vail, 1988) to include a threefold systems tract division (lowstand, transgressive and highstand systems tract; LST – TST – HST), each of them being attributed to a specific stage of the relative sea-level curve (Table 3). The LST was herein proposed to be split into an (early) LST fan and (late) LST wedge, to differentiate between forced regression and lowstand normal regression, with the marine portion of the sequence boundary (i.e. the correlative conformity) positioned at the base of the LST fan (Table 3; Posamentier et al., 1992; Kolla et al., 1995). Another group of sequence stratigraphy practitioners further advocated the fourfold depositional sequence concept by defining a fourth systems tract, the forced regressive or falling-stage systems tract (FSST), but argued to place the correlative conformity above the forced regressive deposits (Table 3; Hunt and Tucker, 1992; Helland-Hansen and Gjelberg, 1994; Hunt and Tucker, 1995). In this work, the latter definition of the correlative conformity (i.e. in the sense of Hunt and Tucker, 1992; Hunt and Tucker, 1995) is adopted, while the former correlative conformity (sensu Posamentier et al., 1992; Kolla et al., 1995) will hereinafter be referred to as 'basal surface of forced regression' (following Hunt and Tucker, 1992). Alternatives to the depositional sequence models are the 'genetic stratigraphic sequence' model (Galloway, 1989), which uses the maximum flooding surface as sequence boundary, and the 'transgressive-regressive (T-R) sequence' model (Johnson and Murphy, 1984; Johnson et al., 1985), which designates the maximum regressive surface as sequence boundary (Table 3). A modification to the original definition of the T-R sequence was proposed to incorporate the subaerial unconformity as the continental portion of the sequence boundary (Embry and Johannessen, 1993).

The existence of competing approaches and inherent confusion (in terms of terminology and the classification of sequences) eventually prompted efforts towards a standard, model-independent approach to sequence stratigraphy (Catuneanu et al., 2011; Catuneanu, 2019). This evolution was accompanied by a growing focus on observation and the elimination of assumptions on (and interpretations of) underlying controlling factors (e.g. eustasy, subsidence/uplift, sediment supply) from the sequence stratigraphic workflow (Miall, 1991, 1992; Catuneanu et al., 2011). Alternative methods proposed to maintain a clear distinction between the observation of stratal geometries and the interpretation of the driving mechanisms behind them, are 'trajectory analysis' (Helland-Hansen and Hampson, 2009; Henriksen et al., 2009) and the 'accommodation succession' method (Neal and Abreu, 2009; Neal et al., 2016).

The sequence stratigraphic interpretation in this study is based on the observed stacking trends, stratal terminations and bounding discontinuities as described in the previous section (summarized in Table 1). The model-independent approach (Catuneanu, 2019) is here adopted, separating the identification of the model-independent sequence stratigraphic components (i.e. sequence stratigraphic surfaces and systems tracts) from the model-dependent choice of the sequence boundary and nomenclature, which is partly driven by the setting and data available in this specific study as well. Trajectory analysis (of the shoreline and shelf edge) is also incorporated in the interpretation. The resulting sequence stratigraphic elements are delineated in Figures 6C – 13C, and a synthetic scheme of the interpretation is provided in Figure 17. A supplementary dip-oriented seismic section over the shelf is provided in Figure S2 to support the trajectory analysis.

5.2. Model-independent interpretation for the northern Gulf of Cadiz (sequence stratigraphic surfaces, systems tracts and trajectory analysis)

On the shelf, major seismic surfaces mws5 to mws1 are interpreted as subaerial unconformities, based on their erosional character, truncation and toplap contacts below, and onlap (in shelf incisions) above (Catuneanu, 2006; Zecchin and Catuneanu, 2013). The basinward portions of mws5 to mws1 are conformable to slightly erosive on the middle slope but show sporadic marine onlap above on the upper slope to outer shelf, which is the main criterion to interpret them as maximum regressive surfaces (Figure 17; Catuneanu, 2006). Likewise, minor surface is3.2 is inferred to represent a maximum regressive surface. The other minor surfaces preserved on the shelf to upper slope (i.e. is5, is3.3 and is3.1) are downlap surfaces that separate the retrogradational to aggradational-progradational depositional trend in the lower sub-units from the more outspoken progradational trend in the upper sub-units. Accordingly, they are interpreted as basal surfaces of forced regression, bounding transgressive to highstand normal regressive deposition (TST to HST) below, and regressive deposition comprising forced regression (FSST) and lowstand normal regression (LST) above (Catuneanu, 2006; Zecchin and Catuneanu, 2013; Catuneanu, 2019). Minor surfaces is4 and is2, whose extent is limited to the middle to upper slope, are equally considered as basal surfaces of forced regression because their seismic expression on the slope is very similar to the minor surfaces that can be correlated to the shelf (i.e. is5, is3.3 and is3.1). The trajectories of the shoreline and shelf edge within the units (indicated in Figures 10, 17 and S2) support above sequence stratigraphic interpretations: the descending regressive trajectory within the upper sub-units (U2.1, U3.1, U4.1 and U5.1) confirms their interpretation as forced regressive deposits (the shoreline can be assumed to coincide with the shelf edge during these intervals), whereas the transgressive to ascending regressive trajectory within U3.2 and U3.4 supports their interpretation as transgressive to (highstand) normal regressive deposits (Figure 17; Helland-Hansen and Hampson, 2009; Catuneanu, 2019).

5.3. Setting- and data-driven choices for the northern Gulf of Cadiz (sequence boundary and systems tracts nomenclature)

The above identified systems tracts and sequence stratigraphic surfaces are shown in Table 3 (last column), next to the sequence classification adopted in the standard models discussed above. Maximum regressive surfaces appear to be consistently recorded in the northern Gulf of Cadiz stratigraphic record. These surfaces furthermore connect to the subaerial unconformities on the upper slope to outer shelf, as such forming well-marked margin-wide surfaces (mws5 – mws1; Figure 17). Hence, mws5 – mws1 are in this study selected as the sequence-bounding surfaces, with the continental portion of the sequence boundary thus corresponding to the subaerial unconformity, and the marine portion to the maximum regressive surface. They delineate five margin-wide sequences that correspond to major seismic units U5 – U1 and which follow a ~100 kyr (4th order) cyclicity as indicated by the chronology (Figures 15 – 17; Table 2). Compared to the standard sequence stratigraphic models outlined in Table 3, an alternative systems tract classification and nomenclature is applied in this study. Due to the absence of identifiable maximum flooding surfaces, a combined TST + HST is considered. Similarly, the absence of easily identifiable correlative conformities prompts the use of a combined FSST + LST, hereinafter referred to as RST (Table 3). These deviations from standard sequence stratigraphic frameworks result partly from the resolution and type of the available data, but mostly from the interplay of underlying controls (both allogenic and autogenic) in the study area, which are discussed in the next chapter. Finally, it should also be noted that the most recent sequence (corresponding to U1) is incomplete, as it only comprises the TST + HST between mws1 and the present-day seabed.

6. Discussion

6.1. Controls on the late Quaternary stratigraphy of the northern Gulf of Cadiz continental margin

6.1.1. Seismic stacking pattern of main units and controlling factors

Clues on the factors controlling the late Quaternary architecture of the northern Gulf of Cadiz margin can be inferred from the stacking pattern of the major seismic units. On the middle continental slope, U5 – U1 show an aggradational stacking pattern, which goes along with the accretion of a sheeted drift to slightly mounded drift towards the NW under the action of the MOW (Hernández-Molina et al., 2006). In contrast, on the continental shelf the stacking pattern is progradational-aggradational, with (for the considered time frame) two episodes of pure shelf-edge progradation composed by respectively U5 and U2, that punctuate aggradation-progradation during U4, U3 and U1 (as schematically summarized in Figure 17). Accordingly, the shelf-edge positions on the major seismic surfaces (indicated by the red dots in Figures 10, 17 and S2) indicate an ascending trajectory over U4 and U3, and a descending trajectory over U5 and U2. The resulting progradational-aggradational pattern is most clearly expressed in correlation profile 1 (Figures 4 and 10), as correlation profile 2 (Figures 5 and 12 – 13) generally shows lower inclinations of prograding reflections on the outer shelf to upper slope. The laterally variable progradation has previously been attributed to the different proximity to the Guadiana River, which is the dominant source of sediment in the studied shelf sector (Lobo et al., 2005a), although there may also be an observational bias since the shelf cross-sections in profiles 1 and 2 have been acquired under different angles relative to the dominant progradation direction.

The question now arises what mechanisms control the overall stacking pattern. The integration of the seismic data with the chronostratigraphic framework at IODP site U1386 provides clear evidence that U5 – U1 formed in concert with 100 kyr glacio-eustatic cycles, with the bounding surfaces consistently forming towards the end of major glacial lowstand periods (Figures 15 – 17). This confirms previous stratigraphic studies and hypotheses focusing on the middle slope contourite terrace in the northern

Gulf of Cadiz (Llave et al., 2001; Llave et al., 2007). However, continental shelves where the dominant control of 100 kyr sea-level cycles has been demonstrated through drilling, like the Gulf of Lions (Rabineau et al., 2005; Bassetti et al., 2008; Sierro et al., 2009) or the Adriatic margin (Ridente et al., 2008; Ridente et al., 2009), show a uniform stacking pattern of self-similar sequences bounded by clearly erosional shelf-wide unconformities (Figure 1). With successive 100 kyr glacio-eustatic sea-level variations during the late Quaternary having a fairly similar amplitude (e.g. Zazo, 1999; Waelbroeck et al., 2002), such a uniform stacking pattern on the shelf can be achieved under conditions of a relatively steady subsidence and sediment supply (e.g. as demonstrated in the Gulf of Lions; Rabineau et al., 2006; Rabineau et al., 2014). Oppositely, the purely progradational intervals on the northern Gulf of Cadiz shelf suggest two pulses of tectonic uplift (during the deposition of U5 and U2), interrupted by a period of subsidence that allows for the combined aggradation-progradation of U4 and U3 (Figures 15 and 17). As a result of this tectonic control, the one-to-one correlation between major glacial sea-level lowstands and the formation/preservation of major seismic surfaces mws5 – mws1 (like on the middle slope) is lost on the shelf. There, mws4 and mws1 respectively overprint mws5 (during the first tectonic pulse) and mws2 (during the second tectonic pulse). As such, on the middle to inner shelf mws4 and mws1 form composite surfaces that encompass multiple glacial lowstand intervals (i.e. MIS10, MIS12 and potentially older in the case of mws4, and MIS2 and MIS6 in the case of mws1). On the other hand, mws3 formed during a period of subsidence, was hence prevented from reworking during the subsequent glacial lowstand (during which mws2 developed), and is therefore entirely preserved on the shelf (Figure 17). Following the method proposed by Rabineau et al. (2014), the total subsidence during U4 and U3 can be quantified by assuming that mws4, mws3 and mws2 correspond to a similar palaeodepth (Figure S3). The calculated 2D subsidence values near the shelf break in correlation profile 2 are 18 and 49 m during U4 and U3 respectively (at point A in Figure S3). The corresponding angle of tilt between mws4 and mws2 is 0.077 °, with a rotation point that is located 4 km offshore the present-day coastline (Figure S3). Using the available chronology for mws4, mws3 and mws2, a subsidence rate of 247 m/Myr for U4 and 386 m/Myr for U3 is obtained (Figures 17 and S3). These values compare to subsidence rates calculated for other dated margins like the central Adriatic (300 m/Myr between MIS10 and MIS2; Maselli et al., 2010) and Gulf of Lions (240 m/Myr ±15 m/Myr for the Pliocene-Quaternary at the shelf break; Rabineau et al., 2014), but are higher than previous (basic) estimates for the northern Gulf of Cadiz shelf (50-100 m/Myr for the Pliocene-Quaternary; Maldonado et al., 1999). Subsidence ceases after the deposition of U3, and passes into uplift during U2 as evidenced by the strong erosional character of mws1 (Figures 10 and 12 – 13). Such relatively rapid changes in the tectonic context have previously been reported to impact on the late Quaternary development of the shelf sector proximal to the Strait of Gibraltar, based on the analysis of seismic stacking patterns (Rodero et al., 1999) and coastal uplift rates from marine terraces (Zazo et al., 1999). The present study now demonstrates that this tectonic control should be expanded to the shelf sector off the Guadiana River to the west, thus influencing the entire northern Gulf of Cadiz continental shelf.

As mentioned above, further offshore on the continental slope the tectonic control is not reflected in the stacking pattern of the major units. Yet, some elements in the slope seismic record might be indicative of tectonic activity. Firstly (yet speculatively in the absence of a denser seismic grid), the channel-like incision affecting U5 and U4 on the middle slope east of site U1386 (Figure 15) could be caused by an intensification or local deviation of bottom currents forced by changes in the seabed topography, or by the enhanced activity of downslope gravitational processes. Both hypotheses could be related to the first tectonic phase, since active incision of the channel into U5 coincides with the onset of tectonic uplift, while the incision starts to be infilled when uplift ceases (Figure 15).. Notably, mws4 correlates to the LQD, a regional discontinuity described in earlier stratigraphic studies on the Gulf of Cadiz middle slope which has been associated with tectonic activity (between 0.3 – 0.6 Ma) as well (Figure 3A; Llave et al., 2007; Llave et al., 2011; Lofi et al., 2016; Hernández-Molina et al., 2016a). Secondly, some diapirs in the study area (e.g. the Guadalquivir and Cadiz diapiric ridges) locally suggest recent deformation (García et al., 2009; Hernández-Molina et al., 2016a). Indeed, the diapir on the upper slope in correlation profile 2 (Figure 11) affects sedimentary packages up to (and including) U2, which attests of salt or mud flowage that could be responding to regional pressure changes induced by the second uplift phase. Furthermore, the occurrence of chaotic, transparent bodies at the foot of the upper slope within U2 (Figure 8), which are interpreted as mass transport deposits (MTD's) based on the similarity with ground-truthed seismic facies in basin floor fans in the Gulf of Mexico (Beaubouef and Friedmann, 2000), could be indicative of margin instability related to this tectonic movement. These two tectonic pulses confirm the previously suggested importance of tectonics on the (late) Quaternary development of the northern Gulf of Cadiz slope, on relatively short timescales with pulses of ~0.8 – 0.9 and ~0.4 – 0.5 Myr (Stow et al., 2013; Hernández-Molina et al., 2014a; Hernández-Molina et al., 2016a), but have until now never been described to also affect the continental shelf off the Guadiana River.

6.1.2. Depocenter distribution of main units and controlling factors

Based on the position of the major depocenters on the outer shelf to upper slope, their clear alongslope elongation (especially evident in U3 and U2; Figure 14), and their wedge-shaped external geometry in cross-section (Table 1), U5 – U2 can be interpreted as laterally continuous shelf-margin wedges. U1, since it does not encompass a full 100 kyr sea-level cycle, shows a deviant distribution pattern that is more sheeted to patchy. In line with previous research (Lobo et al., 2005a), shelf-margin wedges U5 – U2 are inferred to be deltaic in nature, forming as a result of fluvial encroachment on the shelf during major sea-level falls and lowstands. This is supported by the occurrence of incised valleys on the middle to inner shelf, as observed in this study (e.g. in mws1; Figures 12 – 13) and in previous work in the study area (Somoza et al., 1997; Hernández-Molina et al., 2000; Lobo et al., 2018), through which terrigenous sediment can be conveyed to the shelf edge. Most terrigenous sediments derive from the Guadiana River, as the study area is located directly off this major river that drains a significant part of the southern Iberian Peninsula (Lobo et al., 2018). U3 stands out in terms of thickness of the upper slope depocenters (Figure 14C) and total (preserved) volume over the studied margin sector (numbers indicated in Figure 14). This likely results from an increased sediment supply during the deposition of U3, in combination with a relatively high subsidence rate (see section 6.1.1) which leads to enhanced preservation of sediments on the shelf. In contrast, U2 also has relatively thick upper slope depocenters but a moderate preserved volume over the considered area (Figure 14D), because tectonic uplift during the deposition of U2 hinders the preservation of deposits on the shelf. The calculated volumes allow to compare accumulation rates (i.e. the volume of the units over the duration of the accumulation interval; Figure 14) with the sedimentation rates at IODP site U1386 on the middle slope (Figure S4). For comparison, average sedimentation rates at U1386 for the respective units were derived from the (higher-resolution) sedimentation rates from Kaboth et al. (2017). Although there is relatively little variation in these averaged sedimentation rates, the maximal sedimentation rate at U1386 corresponds to the high overall accumulation rate during U3 (Figure S4). It is further noteworthy that the high accumulation rate of U1 is not reflected in the sedimentation rate at U1386 (Figure S4). This implies that a relatively large portion of the accumulated volume during U1 is stored on the shelf, which can be linked to the fact that U1 encompasses an incomplete sea-level cycle comprising the post-LGM sea-level rise and present-day highstand.

Regardless of the involved thicknesses or volumes, the alongslope elongation of the depocenters in both the older and younger units (U5 – U2) implies uniform margin progradation over the studied shelf sector, and suggests an overall linear sediment supply. Enhanced longshore current activity and high wave energy herein play a significant role by redistributing sediments (e.g. Chiocci, 2000; Lu and Fulthorpe, 2004; Rabineau et al., 2005; Ridente et al., 2009; Lobo and Ridente, 2014; Pellegrini et al., 2015). In the northern Gulf of Cadiz, the continental shelf has indeed been characterized by dominantly eastward shore-parallel shelf currents and littoral drift throughout the late Quaternary (Lobo et al., 2005a), whereas the outer shelf and upper slope domain have been under the influence of the dominant eastward flow of the ENACW (Figure 2A; Bellanco and Sánchez-Leal, 2016). Further downslope, the upper MOW flows in the opposite direction as the surficial waters (i.e. westwards) and is well-known to be capable of eroding, transporting and redepositing sediments on the middle slope terrace, as such shaping the northern part of the Cadiz CDS (Figure 2A; Hernández-Molina et al., 2006). Besides the direct influence of these water masses on depocenter distribution, associated oceanographic processes at the interface between the MOW and ENACW, like internal tides or waves, have also been shown to play a role on the sedimentation and physiography of the Iberian continental margin (Hernández-Molina et al., 2016b).

6.1.3. Internal architecture, seismic facies and controlling factors

Shelf. The seismic and sequence stratigraphic interpretation (summarized in Figure 17) illustrates that the internal architecture of U5 – U2 is dominated by regressive deposits, showing as seaward dipping clinoform foresets in the seismic data. Locally, towards the top of regressive sub-unit U2.1 (Figure 12), occasional landward dipping and prograding reflections can be observed, which supposedly result from the interaction of the cyclonic circulation on the outer shelf (Figure 2A) with the underlying inclined topography. The preservation of transgressive deposits is limited and variable, which is a common observation on modern shelves recording 100 kyr cyclicity (Lobo and Ridente, 2014). Preservation of sediments deposited during transgressions to early highstands on the shelf is supposedly favored under conditions of considerable sediment supply, effective dispersal (e.g. through waves or tides), tectonic stability and subsidence, which would prevent their complete erosion during subsequent sea-level falls (Carey et al., 1998; Sheridan et al., 2000; Browne and Naish, 2003; Rabineau et al., 2006; Lobo and Ridente, 2014; Rabineau et al., 2014). Indeed, the tectonic history inferred from the sedimentary stacking patterns (see section 6.1.1.) indicates that U3.4 and U3.2 were deposited under a period of subsidence (Figures 15 and 17). Lobo et al. (2002), who previously interpreted U3.4 – U3.2 as a transgressive to highstand complex as well (although in the absence of age control tentatively attributed to the MIS4 to MIS3 sea-level rise and relative highstand), additionally suggested that the duration, rate and magnitude of the sea-level rise and highstand might have an effect on the preservation potential of the transgressive-highstand complex. This has been postulated for the preservation of post-LGM transgressive deposits on Mediterranean continental shelves as well (e.g. Berné et al., 2007; Pellegrini et al., 2015). The present study indeed confirms that U3.4 and U3.2 were deposited during a relatively protracted and stepped sea-level rise and highstand (Figures 15 – 17).

The long duration of the sea-level rise preluding MIS11 could similarly be one of the reasons for the preservation of U5.2 in correlation profile 2. It is further noted that the expression of higher-frequency precessional cycles remains elusive on the continental shelf. Distinct seismic surfaces or changes in stacking trends within the major seismic units that point at a higher-frequency ~20 kyr cyclicity superimposed on the dominant 100 kyr cycle, as for example observed on the Adriatic margin (Ridente et al., 2008; Ridente et al., 2009), could not consistently be identified. The only detectable manifestation of 20 kyr (5^{th} order) cyclicity in the shelf record is the above discussed stacking of U3.4 and U3.2, separated by minor surface is3.3, attributed to the stepped sea-level rise into marine isotope substages 7e and 7c that is interrupted by a ~60 m relative sea-level fall during substage 7d (Table 2 and Figures 15 – 17). Relative sea-level falls punctuating other highstand intervals over the considered timeframe do not reach such high amplitudes and hence are apparently too small to generate observable changes in seismic stacking trends and facies in the studied data.

Upper slope. On the upper slope, the variable seismic facies (characterized by chaotic, wavy or continuous reflections, with varying amplitudes), reflect an interplay of (hemi)pelagic sedimentation, downslope gravitational processes (leading to mass transport deposits and/or turbiditic deposition), and oceanographic processes related to the upper MOW, ENACW or associated oceanographic processes at their interface. The gravitational control is enhanced during the above inferred pulses of tectonic uplift and instability, as the internal architecture of U2 (deposited during tectonic pulse 2; Figure 15) is the most disturbed (i.e. showing the highest degree of chaotic facies and lateral discontinuity, margin instability, MTD's). This hypothesis cannot be assessed for tectonic pulse 1, as the upper slope domain of U5 is largely located below the multiple. The infill of the upper slope incision within U2 in correlation profile 1 (Figures 4 and 9) is also inferred to be controlled by downslope (deltaic) deposition towards the end of the sea-level fall to MIS2 lowstand, as it is likely spatially connected to (and thus fed through) incised valleys on the shelf. Yet, the seismic facies and internal architecture of the upper part of this infill, i.e. U1, can be interpreted to represent a plastered drift, according to the criteria of Faugères and Stow (2008). This points at a significant alongslope (bottom current) control on the upper slope, at least during the development of U1 (i.e. during the sea-level rise and highstand following MIS2). This interpretation is in line with Llave et al. (2007), who identified this plastered drift on the upper slope in older seismic data as well, and attributed its formation to the upper MOW. The salinity data (Figure 18) confirms that this feature is indeed located below the present-day flow path of this water mass on the upper slope, although the shallower ENACW or processes at the interface between the MOW and ENACW cannot be ruled out to play a role too. Also, the wavy seismic facies observed at the foot of the upper slope in U1 (and older sub-units; Figures 8 and 9) can be interpreted as (migrating) sedimentary waves, which further documents the importance of oceanographic processes in this part of the margin (even though additional oceanographic data and morphometric information of these sedimentary waves is needed to infer the exact formation mechanism).

Middle slope. To understand the internal architecture of the units and seismic facies of the sub-units on the middle slope, sediment supply to the middle slope (as traditionally conceived; Figure 19A) should be assessed in combination with the intensity and alongslope redistribution capacity of the upper MOW (Figure 19B). The IODP sites on the middle slope allow to tentatively compare the deposits resulting from the combined effect of sediment input and bottom current activity (using the shipboard visual core descriptions) with their expression in the seismic data (Figure 19C). The relatively thin basal sub-units (U5.2, U4.2, U3.4, U3.2, U2.2, U1) show a low-amplitude to transparent seismic facies linked to rather uniform sedimentation. This is interpreted as fine-grained contouritic deposition and/or reworking of (low-density) turbidites, resulting from the effect of increasingly vigorous bottom current activity on fine-grained sediments (brought into the system as (hemi)pelagic deposits or low-density turbidites) during rising and high sea-level positions (Figure 19). Amplitudes become high towards the top of the basal sub-units, as the upper MOW reaches its peak intensity leading to deposition of coarser-grained sediments or winnowing of the finer fraction. On the other hand, the observed increase in amplitude from the base to the top within the upper sub-units (U5.1, U4.1, U3.3, U3.1, U2.1) corresponds to an increase in the frequency of (relatively) coarse-grained, sharp-based beds

(Figure 19). This is interpreted as deposition becoming increasingly turbiditic, as the shoreline moves closer to the shelf edge and upper MOW activity decreases (and eventually disappears) during gradual sea-level falls (Figure 19). It is further noteworthy that sub-unit U2.1 shows a higher frequency of thin coarser-grained beds than sub-unit U3.1, which could reflect the uplift and shelf tilting during tectonic pulse 2 and a subsequent increased turbiditic input. Future detailed sedimentological analysis is however required to verify the exact nature of the coarser-grained beds at the IODP sites (contouritic vs. turbiditic) and test above established links between sedimentation and the seismic facies characterizing the sub-units. As on the shelf, the expression of higher-frequency (20 kyr) Milankovitch cyclicity can be distinguished in the internal structure of U3 (i.e. regressive sub-unit U3.3, related to the marine isotope substage 7d relative sea-level fall, punctuating transgressive deposition of U3.4 and U3.2), while in the other units the precessional signal is less readily discernable in the seismic data. This indicates that also for the middle slope seismic record, relative sea-level falls punctuating interglacial highstand intervals must exceed a certain threshold (~60 m in the case of U3.3) to generate clear changes in seismic facies through modification of the sediment input (Figures 15 – 17).

6.1.4. Controlling factors: final considerations and summary

From the above discussion, a synthetic figure was compiled on the controlling factors on margin development in the northern Gulf of Cadiz (Figure 20). The controls that can most readily be derived from the seismic stratigraphic analysis are tectonics, glacio-eustatic sea-level variations driven by orbital cycles and oceanographic processes. The relative importance of these controls changes with the considered timescales and seismic stratigraphic elements: tectonics mainly control the seismic stacking patterns on timescales of several hundreds of kyr, sea level plays a role in all seismic stratigraphic elements on timescales ≤ ~100 kyr, while on similar timescales oceanography mostly impacts on the depocenter distribution, internal architecture and seismic facies.

The dominant sea-level signal is the one driven by ~100 kyr eccentricity cycles; higher-frequency ~20 kyr precessional cycles are only sporadically resolved in the studied seismic stratigraphic record.

However, sediment cores, core physical properties and downhole logs of IODP Expedition 339 reveal an omnipresent precessional control on Quaternary sedimentation at all drilled sites on the northern Gulf of Cadiz slope (Stow et al., 2013; Lofi et al., 2016; Hernández-Molina et al., 2016a). The fact that precession is rather reflected in sedimentological data (i.e. at core-scale) than in larger-scale features recorded in seismic data likely illustrates that the dominant effect of precessional cycles, which are climatic variations resulting in fluctuations in sediment supply and biogenic production (Lofi et al., 2016), might not generate sufficient contrasts in the acoustic properties or stacking patterns of sediments. Alternatively, precession could be expressed in cyclic sediment beds that are below the scale of observation in this study or that are too thin or too closely spaced to be resolved by the used reflection seismic method. Future efforts in integrating core material and seismic data at very high resolution are needed to further elucidate this question.

Sediment supply should be considered as a central element, since tectonics, sea-level fluctuations and oceanography all impact on the temporal and spatial variations in the amount and type of sediments supplied to the different continental margin domains, sediment pathways, and the dominance of alongslope vs. downslope vs. (hemi)pelagic processes. Also, the input of terrigenous sediment, dominantly sourced from the Guadiana River, is of considerable importance in controlling the position, shape and thickness of the late Quaternary stratigraphic units on the studied margin sector.

A final consideration is that the above discussed controlling factors (Figure 20) do not act independently, but in fact are strongly interrelated. Furthermore, variations in sea level, oceanographic processes and sediment supply are underlain by climatic (orbital) mechanisms, which in turn can be influenced by plate tectonic rearrangements (e.g. Hernández-Molina et al., 2014a). Interpreting the development of a specific margin architecture therefore requires caution and a case-by-case approach, which takes into account the local variability of the different driving factors. Also, the ability to date and correlate the stratigraphic record to a sea-level curve proves to be essential to thoroughly comprehend the different controlling factors and the timescales at which they operate.

6.2. Sequence stratigraphic considerations and implications

Through the sequence stratigraphic interpretation presented in chapter 5 and analysis of controlling factors on margin development in section 6.1, this study also contributes to some key aspects in the research field of high-resolution late Quaternary sequence stratigraphy. This current section discusses sequence boundary formation, internal sequence architecture (systems tracts) and composite cyclicity (hierarchy) on the northern Gulf of Cadiz middle slope to shelf, focusing on the practical constraints and model-dependent choices to the applied sequence stratigraphic approach, the comparison with previous interpretations for the northern Gulf of Cadiz and other late Quaternary margins, and the general implications arising from the presented case regarding the understanding and application of high-resolution (late Quaternary) sequence stratigraphy on continental margins worldwide.

6.2.1. Sequence boundary formation in the northern Gulf of Cadiz

Whereas many high-resolution sequence stratigraphic studies exclusively focus on the inner to outer shelf domain, this study integrates the (middle to upper) slope and shelf record. Sequence stratigraphic surfaces to promote to sequence boundaries on this margin-wide scale should therefore not only be easily identifiable, but also traceable from the shelf to the middle slope. On the shelf, in line with the basic tenets (as outlined by Lobo and Ridente, 2014), the subaerial unconformities forming during gradual sea-level falls of successive 100 kyr glacio-eustatic cycles are the best marked seismic surfaces. The erosional behavior on the outer shelf is noteworthy (e.g. for mws1 at 0.2 s twtt or ~150 m below present-day sea level; Figures 9 and 12), while sea level was docked at shallower depths at the time of formation of these surfaces (e.g. ~100 to 120 m below the present-day sea level during the formation of mws1 according to the sea-level curves in Figure 17). This offset has in the case of mws1 previously been explained by subsidence (i.e. mws1 is at a deeper level at present than during the time of its formation; see also section 6.1.1) and subaqueous erosion by wave activity (Lobo et al., 2018), which is likely to have similarly affected the deeper mws as well. Further offshore, the maximum regressive surfaces are most easily recognizable (chapter 5), and are hence selected as the marine portion of the sequence boundary. Maximum regressive surfaces are clearly expressed in the Gulf of Cadiz stratigraphic record, because they mark a sharp transition from a regime controlled by downslope processes and sediment supply below, to a bottom-current controlled regime with dominant alongslope sediment supply above (see discussion in section 6.1.3; Figure 19). The timing of formation of the maximum regressive surfaces generally, yet not always exactly, coincides with the minimum sea-level positions of successive glacial-interglacial cycles (Figures 15 – 17). Where the timing of the maximum regressive surface shortly precedes (e.g. in the case of mws1) or follows after (e.g. in the case of mws4, mws3 or mws2) the timing of minimum sea level, it is inferred that the supply of coarser-grained sediments to the middle slope respectively ceases shortly before or continues after sea level has reached its lowest position.

The adopted sequence boundary definition (i.e. with the subaerial unconformity as continental portion and maximum regressive surface as marine portion) follows Embry and Johannessen (1993), and requires that the maximum regressive surfaces physically connect to the subaerial unconformities on the shelf (Catuneanu et al., 2009; Catuneanu, 2019). This is indeed the case in this study, since lowstand normal regressive deposits are generally absent on the shelf (see discussion in the next section).

In view of the current state-of-the-art in high-resolution sequence stratigraphy, the presented case complies with the tenet that sequence boundaries (subaerial unconformities) form on the continental shelf during major 100 kyr sea-level falls (Lobo and Ridente, 2014; Ridente, 2016). However, in contrast to other examples where sequences are generally inferred to be self-similar with consistent well-marked and shelf-wide sequence boundaries, the 100 kyr sea-level pattern is obliterated by tectonics on the northern Gulf of Cadiz shelf (cfr. examples in Figure 1 vs. Figure 16). As a result of the tectonic control, some sequence boundaries comprise multiple major glacial lowstand intervals on the middle to inner shelf, which implies a loss of the one-to-one correlation between 100 kyr glacio-eustatic cycles and sequence (boundary) formation/preservation (Figure 17; section 6.1.1). Such a situation has been demonstrated on the Canterbury margin as well by integrating lower-resolution (multi-channel) seismic data and borehole information (McHugh et al., 2017). A one-to-one correlation between the formation (and preservation) of shelf-wide unconformities and 100 kyr glacio-eustatic cycles should thus not straightforwardly be assumed, although this is a commonly applied approach when direct age control is not available (e.g. the examples shown in Figure 1A-E). Tectonic activity, although traditionally considered to be expressed on longer timescales of > 1 Myr (e.g. Johnson, 1971; Cloetingh, 1988), is here demonstrated to be able to obscure this pattern, even on the relatively short timescales considered in late Quaternary studies. Other examples in which a tectonic influence has been demonstrated are the Southern Tuscany margin and Gulf of Lions margin, where the sedimentary stacking patterns and depocenter distribution are governed by continued regional subsidence (Ridente et al., 2012; Rabineau et al., 2014), and the Eel River Basin, where episodic uplift was demonstrated to have impacted on the distribution and thickness of the late Quaternary sequences (Burger et al., 2002).

6.2.2. Systems tracts in the northern Gulf of Cadiz

The sequence stratigraphic interpretation shows an asymmetric depositional architecture, i.e. a dominance of progradational units of the RST vs. scarce and variable occurrence/preservation of the TST to HST (Figure 17; section 6.1.3), which is in line with the current state-of-the-art in high-resolution sequence stratigraphy (Lobo and Ridente, 2014; Ridente, 2016). However, with respect to the internal division of the sequences into component systems tracts, none of the standard sequence stratigraphic approaches (Table 3; section 5.1) appears applicable in the northern Gulf of Cadiz. Firstly, in the here presented case and in previous stratigraphic studies in the northern Gulf of Cadiz (Hernández-Molina et al., 2000; Hernández-Molina et al., 2002), the correlative conformity has seemingly no clear expression in the seismic record on the upper and middle slope, presumably because it falls within a progressive increase in downslope sediment transport under gradually falling sea level and a decreasing alongslope (oceanographic) component (cfr. Figure 19). As a result, the FSST cannot confidently be distinguished from the LST, and a combined RST is considered instead (Figure 17; Table 3). Anyway, since the maximum regressive surfaces generally form shortly after sea level starts to rise

(Figures 15 – 17), lowstand normal regressive deposition is inferred to be limited on the middle slope, and even absent on the upper slope and shelf, as indicated by the descending regressive shoreline trajectories (Figures 10, 17 and S2; Helland-Hansen and Hampson, 2009; Catuneanu, 2019). This is a common trait in late Quaternary stratigraphic records, because transgression follows the onset of sea-level rise very shortly within 100 kyr (and higher frequency) glacio-eustatic cycles (Catuneanu et al., 2009; Ridente, 2016). Only locally and in minor amounts normal regressive deposits may be preserved on the upper slope (e.g. the infill of the upper slope incision within U2 up to mws1, discussed in 6.1.3, could be interpreted as a lowstand delta; Figure 9). Secondly, there seem to be no criteria to distinguish the TST from the HST on the middle slope in the seismic data (i.e. no formation of seismically identifiable maximum flooding surfaces), and therefore a combined TST + (early) HST is used (Table 3). This indistinct gradation between the TST and HST has been discussed in previous studies (Hernández-Molina et al., 2002; Brackenridge et al., 2011), and is due to the gradual increase to peak bottom current activity as sea-level rises and reaches (early) highstand positions, which dominates the sediment dispersal and supply mechanisms rather than a pure sea-level control. In relation to this, since the studied middle slope sector in the northern Gulf of Cadiz is part of an extensive and well-studied contourite depositional system, this work also contributes to previous efforts in integrating contourites in sequence stratigraphic models. Brackenridge et al. (2011) conceptualized two end-members, depending on whether bottom currents are intensified during sea-level highstand or lowstand; the here presented example can be verified against the former model. Our case complies with the model of Brackenridge et al. (2011) in that it indeed suggests that downslope deposition (e.g. turbidites, debrites) masks alongslope processes in the FSST and LST, whereas the seismic facies of the TST and HST reflect dominant contouritic deposition, with an indistinct gradation from TST to HST and supposedly coarser grained facies towards the top (Figure 19). Yet, the model of Brackenridge et al. (2011) foresees mounded and relatively thick TST+HST's, whereas the TST+HST's on the middle slope in this study are thin and sheeted. This difference could result from the fact that Brackenridge et al. (2011) based their model on the analysis of larger-scale examples of 2nd - 3rd order depositional sequences (using low-resolution 2D reflection seismic profiles) and the assumption of a relatively symmetric sea-level curve. In contrast, the 100 kyr (4^{th} order) sequences in this study formed under the asymmetric sea-level curve that is typical of the late Quaternary, in which rising sea level and early highstand only encompass a short interval of time. More (dated) examples of 100 kyr (or higher-frequency) sequences on margins with a pronounced alongslope (contouritic) component are required to capture all possible variations and to test if the original concepts of Brackenridge et al. (2011) can be applied to higher-resolution (late Quaternary) sequence stratigraphy as well.

6.2.3. Hierarchy in the northern Gulf of Cadiz sequence stratigraphic framework and comparison with previous models

Previous high-resolution, late Quaternary sequence stratigraphic work in the study area (see section 2.3) mostly focused either on the continental shelf (e.g. Somoza et al., 1997; Hernández-Molina et al., 2000; Lobo et al., 2005a), or on the middle slope contourite terrace (e.g. Llave et al., 2001; Llave et al., 2006; Llave et al., 2007; Hernández-Molina et al., 2016a). The present research, based on more recently available high-resolution seismic data and the updated chronostratigraphy at IODP Expedition 339 sites U1386 and U1387, now further updates, refines and ties together these late Quaternary sequence stratigraphic interpretations over the northern Gulf of Cadiz continental margin. It thus appears that the basic conclusions outlined in previous (middle) slope studies are largely confirmed, whereas the shelf is shown to predominantly record a 100 kyr (eccentricity) cyclicity that is modulated by a longer-term tectonic control (Figure 17), rather than a composite 100 kyr and 20 kyr Milankovitch cyclicity.

The concept of composite cyclicity or hierarchy in sequence stratigraphy addresses the possibility to build stratigraphic frameworks at different scales of observation (hierarchical levels), with the smaller-scale frameworks or sequences composing the larger-scale sequences (Catuneanu et al., 2009). On late Quaternary timescales, this concept has mainly been applied to the superposition of 20 kyr (5^{th} order) on 100 kyr (4^{th} order) Milankovitch/sea-level cyclicity (Lobo and Ridente, 2014). However, at the high-resolution seismic scale of observation in this study, the 20 kyr pattern remains tenuous (see section 6.1.3), as is the case in numerous other modern shelf settings (Lobo and Ridente, 2014). Instead, the studied seismic stratigraphic record reveals that a superposition of ~100 kyr glacio-eustatic cycles and tectonic pulses can also generate composite patterns (Figure 17 and section 6.1.1). This variability in the tectonic context, as it is conceived here to manifest on potentially relatively short timescales (i.e. in the studied case, tectonic pulses separated by ~0.3 – 0.4 Ma), is a hitherto often overlooked factor in evaluating composite stacking patterns in high-resolution seismic/sequence stratigraphic studies. In this respect, age control proves to be a valuable tool to correctly identify the various orders of cyclicity and their drivers in a certain dataset.

7. Conclusions

This work presents an updated late Quaternary stratigraphic framework for the northern Gulf of Cadiz continental margin off the Guadiana River. Through the slope-to-shelf correlation of high-resolution seismic profiles and the connection with IODP Expedition 339 sites U1386 and U1387, earlier slope and shelf stratigraphic models are integrated, refined and dated. As such, this study provides a useful revised framework for future fundamental and applied research in the study area. It further constitutes a first step in enhancing the understanding of the sediment routing on the margin from source (shelf) to sink (middle slope CDS). In this respect, the upper slope appears to be a significant, but relatively underemphasized depositional area, that requires increased attention in future research.

Moreover, the seismic stratigraphic interpretation linked to the chronostratigraphic data allows to review the factors controlling the late Quaternary margin architecture in the study area. As suggested in earlier work, the northern Gulf of Cadiz margin bears the imprint of Milankovitch-driven sea-level cycles. The ~100 kyr eccentricity cycle appears pervasive in the margin record, as it guides the formation of major seismic surfaces and units. The ~20 kyr precessional cycle, although pervasive in the slope sedimentary record retrieved by IODP Expedition 339, could only sporadically be identified at seismic scale. The apparent absence of the precessional signal in the seismic stratigraphic record, especially on the shelf, requires a more detailed integration of core and seismic data to verify if precession truly fails to leave a mark on the margin architecture, or if this is rather an observational bias linked to the resolution and/or scale of observation of this study. Besides sea level, several seismic stratigraphic elements indicate that additional controls should be considered. Firstly, the stacking pattern of major units on the shelf suggests an additional tectonic control. Two pulses of late Quaternary tectonic uplift with about ~0.3 – 0.4 Ma between them were identified, leading to two episodes of pure margin progradation, punctuating periods of subsidence and mixed progradational-aggradational stacking. Secondly, on shorter timescales (< 100 kyr) oceanographic processes have also been shown to impact on the depocenter distribution, internal architecture and seismic facies of the seismic (sub-)units. In addition, above controlling factors are interrelated and furthermore linked to variations in sediment supply and climate. Therefore, from a general perspective, the northern Gulf of Cadiz constitutes an interesting case to decipher the effects of the different controlling mechanisms on sedimentation, which contributes to the comprehension of how late Quaternary continental margins develop worldwide.

Finally, a sequence stratigraphic interpretation is presented as well, although it requires some adaptations to the basic model due to the set-up of this study (i.e. the integration of both the shelf and slope record) and setting-specific conditions in the study area (i.e. the imprint of tectonics and oceanography next to sea-level fluctuations). This interpretation, together with the aforementioned new insights into the governing processes, has implications for the general understanding and application of high-resolution (late Quaternary) sequence stratigraphy. Most significantly, it is shown that tectonic activity is able to obscure the one-to-one relationship between the formation of shelf-wide unconformities and 100 kyr glacio-eustatic cycles. This prevalent premise in sequence stratigraphic interpretations when age control is absent should therefore be used with caution. In this respect, chronostratigraphic information (obtained through e.g. ocean drilling) appears essential in establishing firm seismic and sequence stratigraphic frameworks, and more dated examples are required to further evaluate and develop the basic tenets in high-resolution (late Quaternary) sequence stratigraphic research. Yet, the presented case further underlines the argument posited in early sequence stratigraphic works that the local variability of controlling factors within a specific basin demands a case-by-case approach, rather than a straightforward implementation of generalized sequence stratigraphic schemes.

Acknowledgements

T. Mestdagh is supported by a doctoral scholarship of the Ghent University Special Research Fund (BOF). This research was conducted in connection with 'The Drifters Research Group' of the Royal Holloway University of London (UK), and is related to projects CTM 2012-39599-C03, CGL2016-80445-R 'SCORE' (AEI/FEDER, UE), CTM2016-75129-C3-1-R, CGL2011-30302-C02-02 and CTM2017-88237-P. We wish to thank the captains, crews and scientific parties of research cruises COMIC 2013 on board of RV Belgica and LASEA 2013 on board of RV Ramón Margalef. Ship time on RV Belgica was provided by BELSPO and RBINS-OD Nature. Editor A. Negri, C. Pellegrini and one anonymous reviewer are kindly acknowledged for providing constructive reviews and feedback.

Declarations of interest: none.

Table captions

Table 1. Overview of the seismic stratigraphic analysis, summarizing the observed external geometrical shape, internal reflection configuration and seismic facies, and reflection terminations of the seismic (sub-)units per margin domain. Abbreviations and symbols: e.t. = erosional truncation, conf. = conformable contact, progr. = progradational, (sub)par. = (sub)parallel, A = amplitude, mod. = moderate, incr. = increase, * = feature only manifesting in landward direction, ( ) = feature rather faint or only manifesting sporadically, X = sub-unit absent on the considered margin domain. Previous stratigraphic nomenclature (at the left side of the table) from Llave et al. (2001, 2007, 2011) and Hernández-Molina et a. (2002, 2016a).

Table 2. Overview of the seismic stratigraphic (sub-)units with their corresponding ages and marine isotope stages (MIS).

Table 3. Choice of the sequence boundary (SB), nomenclature of systems tracts and sequence stratigraphic surfaces, and their timing with respect to the events and stages of the relative sea-level curve (after Catuneanu et al., 2011; Catuneanu, 2019), for (i) the 'depositional sequence' model of Posamentier et al. (1992) (indicated by *), (ii) the 'depositional sequence' model of Hunt and Tucker (1992), Helland-Hansen and Gjelberg (1994) (indicated by **), (iii) the 'genetic sequence' model (Galloway, 1989), (iv) the 'transgressive – regressive (T – R) sequence' model (Johnson and Murphy, 1984; Embry and Johannessen, 1993), and (v) the approach adopted in this study. In the present study, the maximum regressive surfaces (mrs) are well-marked and connect on the upper slope to outer shelf to the subaerial unconformities, and are hence selected as sequence boundary. Basal surfaces of forced regression (bsfr) can be identified as well, whereas the correlative conformities (cc; in the sense of Hunt and Tucker, 1992)) and maximum flooding surfaces (mfs) remain cryptic (see text for discussion). Other abbreviations: (w) = wedge; (f) = fan; T = transgression; HNR, FR, LNR = highstand normal, forced, lowstand normal regression; HST = highstand systems tract; FSST = falling-stage

systems tract; LST = lowstand systems tract; TST = transgressive systems tract; RST = regressive systems tract.

Supplementary table S1. Overview of age-depth control points used in this study. For the upper ~45 mbsf at site U1386 and upper ~30 mbsf at site U1387 the high-resolution age models of respectively Kaboth et al. (2016) and Bahr et al. (2014) were adopted. At greater depths, age control is provided by the lower-resolution age model proposed by Lofi et al. (2016). The depths in the age models of Kaboth et al. (2016) and Bahr et al. (2014) are originally provided in meters composite depth (mcd), since they are based on spliced records. This mcd-scale is here converted to meters below sea floor (mbsf) by applying the constant expansion factors determined by the stratigraphic correlators during IODP Expedition 339 (Stow et al., 2013).

Figure captions

Figure 1. (A-E) Summary of shelf stratigraphic architectures driven by 100 kyr cyclicity, as interpreted in different settings with variable shelf dimensions (shelf dimensions decreasing from a to e). In all these cases, age control is limited to the most recent subaerial unconformity, and older unconformities/sequences are correlated with previous 100 kyr glacio-eustatic cycles assuming a one-to-one correlation. Major phases of shelf growth guided by regressive (and occasionally lowstand) deposition are represented by different colors, which are each related to a specific glacial-interglacial cycle, whereas transgressive deposition is left blank. Sequence boundaries are indicated in red. Examples from: (a) the Bengal Shelf (modified after Hübscher and Spieß, 2005); (b) the Korea Strait (modified after Yoo et al., 2017); (c) the Tuscany margin, Tyrrhenian Sea (modified after Ridente et al., 2012); (d) the Niger Delta (modified after Riboulot et al., 2012); (e) the Catalan margin off the Llobregat River (modified after Liquete et al., 2008). **(F-G)** Stratigraphic development of shelf sequences where age control is available for the middle to late Quaternary: (f) interpretation for the Gulf of Lions shelf (modified after Bassetti et al., 2008); (g) interpretation for the Adriatic shelf (modified after Ridente et al., 2008). Note that the timing of formation of the different sequences within a specific 100 kyr sea-level cycle differs between (f) and (g). **(H)** Correlation between the major progradational phases and 100 kyr cycles during the last 500 kyr. Sea-level curve from Grant et al. (2014).

Figure 2. (A) Gulf of Cadiz map, showing the main tectonic features (AWDF = Accretionary Wedge Deformation Front; CF = Cadiz Fault; PF = Portimao Fault: PH= Portimao High; SVF = San Vicente Fault) and pathways of the Mediterranean Outflow Water (MOW; MU = upper branch, ML = lower branch), Antarctic Intermediate Water (AAIW), Eastern North Atlantic Central Water (ENACW) and North Atlantic Deep Water (NADW). **(B)** Detail of the study area of this work, showing the locations of IODP sites U1386 and U1387, reflection seismic profiles (solid line = 2D single-channel profile; dotted line = TOPAS profile). Three physiographic domains are shown (shelf; U. Sl. = Upper slope; middle slope), with indication of the shelf geomorphological elements and depositional – erosional elements of the contourite depositional system (CDS) on the middle slope. Tectonic features from Duarte et al. (2013);

CDS elements and oceanography from Hernández-Molina et al. (2016a) and García-Lafuente et al. (2006); distribution of shelf geomorphological elements from Vanney and Mougenot (1981), Lobo (1995), Roque (1998) and Lobo et al. (2004).

Figure 3. (A) Late Quaternary stratigraphic architecture of the contourite depositional system (CDS) on the northern Gulf of Cadiz middle slope. The late Quaternary depositional sequence (QIII) comprises two sub-units (Q5 and Q6) bounded by two regional discontinuities, the MPD and LQD (older sequences are QI-II = early to middle Quaternary, P = Pliocene). The location of the profile is shown in Figure 2B. Modified after Hernández-Molina et al. (2014a), Hernández-Molina et al. (2016a). **(B)** Late Quaternary stratigraphic architecture of the northern Gulf of Cadiz continental shelf off the Guadiana River. Two depositional sequences, dominantly composed of regressive-to-lowstand deposits, have tentatively been attributed to the two most recent glacial cycles. Internally, they are inferred to consist of higher-frequency sub-units guided by precessional cycles. The location of the profile is shown in Figure 2B. Modified after Hernández-Molina et al. (2000), Lobo and Ridente (2014).

Figure 4. Correlation profile 1. **(A)** Location of the profile, connecting IODP Expedition 339 site U1386 on the middle slope with the shelf. The letters indicate the segments of the profile as shown in (B). **(B)** Uninterpreted reflection seismic profile. **(C)** Seismic stratigraphic interpretation. Details of this figure are provided in Figures 6 - 10, as indicated in (B).

Figure 5. Correlation profile 2. **(A)** Location of the profile, connecting IODP Expedition 339 site U1386 on the middle slope with the shelf. The letters indicate the segments of the profile as shown in (B). **(B)** Uninterpreted reflection seismic profile. **(C)** Seismic stratigraphic interpretation. Details of this figure are provided in Figures 11 – 13, as indicated in (B).

Figure 6. (A) Detail of correlation profile 1 (as indicated in Figure 4B). **(B)** Seismic stratigraphic interpretation. **(C)** Sequence stratigraphic interpretation. Abbreviations: su = subaerial unconformity; mrs = maximum regressive surface; bsfr = basal surface of forced regression.

Figure 7. (A) Detail of correlation profile 1 (as indicated in Figure 4B). **(B)** Seismic stratigraphic interpretation. **(C)** Sequence stratigraphic interpretation. Abbreviations: su = subaerial unconformity; mrs = maximum regressive surface; bsfr = basal surface of forced regression.

Figure 8. (A) Detail of correlation profile 1 (as indicated in Figure 4B). **(B)** Seismic stratigraphic interpretation. **(C)** Sequence stratigraphic interpretation. Abbreviations: su = subaerial unconformity; mrs = maximum regressive surface; bsfr = basal surface of forced regression.

Figure 9. (A) Detail of correlation profile 1 (as indicated in Figure 4B). **(B)** Seismic stratigraphic interpretation. **(C)** Sequence stratigraphic interpretation. Abbreviations: su = subaerial unconformity; mrs = maximum regressive surface; bsfr = basal surface of forced regression.

Figure 10. (A) Detail of correlation profile 1 (as indicated in Figure 4B). **(B)** Seismic stratigraphic interpretation. **(C)** Sequence stratigraphic interpretation and trajectory analysis, performed at two scales: at the larger scale, shoreline positions are indicated at the sequence-bounding surfaces (red dots); at the smaller scale, shoreline positions are indicated at clinoforms within the seismic units (blue and green dots). In the case of the descending regressive trends (i.e. blue and red dots), the shoreline can be assumed to be coincident with the shelf edge (see text for discussion). Abbreviations: su = subaerial unconformity; mrs = maximum regressive surface; bsfr = basal surface of forced regression.

Figure 11. (A) Detail of correlation profile 2 (as indicated in Figure 5B). **(B)** Seismic stratigraphic interpretation. **(C)** Sequence stratigraphic interpretation. Abbreviations: su = subaerial unconformity; mrs = maximum regressive surface; bsfr = basal surface of forced regression.

Figure 12. (A) Detail of correlation profile 2 (as indicated in Figure 5B). **(B)** Seismic stratigraphic interpretation. **(C)** Sequence stratigraphic interpretation. Abbreviations: su = subaerial unconformity; mrs = maximum regressive surface; bsfr = basal surface of forced regression.

Figure 13. **(A)** Detail of correlation profile 2 (as indicated in Figure 5B). **(B)** Seismic stratigraphic interpretation. **(C)** Sequence stratigraphic interpretation. Abbreviations: su = subaerial unconformity; mrs = maximum regressive surface; bsfr = basal surface of forced regression.

Figure 14. Thickness (in ms two-way travel time) and distribution of major seismic units U5 – U1. The volumes and accumulation rates of U5 – U1 (calculated for the white dashed polygon) are indicated below the thickness maps.

Figure 15. Seismic and sequence stratigraphic interpretation tied to IODP Expedition 339 site U1386 (the shown seismic section is indicated in Figure 5B). Five major late Quaternary seismic units are defined (denominated as U1 to U5 at the right side of the figure, with their internal subdivision and comparison to seismic stratigraphic interpretations in previous work). In sequence stratigraphic terms, two systems tracts are recognized: a combined transgressive and highstand systems tract (T), and a regressive systems tract (R), comprising forced and lowstand normal regression (see Table 3 and text for discussion). Relative sea-level (RSL) and $\delta^{18}O$ curves, marine isotopic stages (MIS), inferred pulses of tectonic uplift and upper MOW variability at the borehole location are plotted on a time scale. Sea-level curve from Grant et al. (2014); $\delta^{18}O$ LR04 stack curve and MIS definition from Lisiecki and Raymo (2005).

Figure 16. Late Quaternary sequences and sequence stratigraphic surfaces on the northern Gulf of Cadiz continental margin, from the middle slope to shelf, in **(A)** correlation profile 1, and **(B)** correlation profile 2 (locations shown in Figures 4A and 5A respectively). Similar to the examples shown in Figure 1, major phases of margin growth are guided by forced and (occasionally) lowstand normal regressive deposition of the RST (sub-units U2.1, U3.1, U3.3, U4.1 and U5.1), and colored according to the corresponding gradual sea-level fall. Transgressive to (early) highstand deposition of the TST+HST (U1, U2.2, U3.2, U3.4, U4.2 and U5.2) is left blank.

Figure 17. Synthetic seismic and sequence stratigraphic interpretation for the northern Gulf of Cadiz. **(A)** Schematic representation of the margin architecture, with indication of the sequence stratigraphic elements (surfaces, systems tracts and stratal terminations) and shoreline/shelf-edge trajectories. The stacking pattern of the major seismic units is rather uniform on the slope, whereas on the shelf the tectonic imprint leads to a non-uniform stacking pattern and dissimilarities in the bounding surfaces (see text for discussion). Trajectory analysis is performed at two scales: at the larger scale, shoreline positions are indicated at the sequence-bounding surfaces (red dots); at the smaller scale, shoreline positions are indicated at clinoforms within the seismic units (blue and green dots). In the case of the descending regressive trends (i.e. blue and red dots), the shoreline can be assumed to be coincident with the shelf edge (see text for discussion). **(B)** Timing of the formation of the seismic (sub-)units and surfaces, with reference to a number of sea-level curves (purple, light blue, dark blue and green respectively from Siddall et al., 2003; de Boer et al., 2014; Grant et al., 2014; Rohling et al., 2014), reconstructed tectonic curve (subsidence vs. uplift; see also Figure S3) and curve of the accumulation rates (see also Figure S4). The dashed part of the tectonic curve is not quantified and should only be regarded as a qualitative indication of the tectonic regime (subsidence vs. uplift). Abbreviations: su = subaerial unconformity; mrs = maximum regressive surface; bsfr = basal surface of forced regression.

Figure 18. Present-day salinity of the water column above correlation profile 1 (shown in Figures 4 and 16A). The high-salinity water mass that drapes the middle slope and foot of the upper slope corresponds to the upper branch of the Mediterranean Outflow Water (MU). ENACW = Eastern North Atlantic Central Water. Salinity data retrieved from Ocean Data View (Schlitzer, 2017).

Figure 19. Overview of the seismic/sequence stratigraphic architecture, involved controls and depositional processes on the middle slope of the northern Gulf of Cadiz. **(A)** Sequence stratigraphic elements and sediment supply to slope (with basinward extent indicated by the blue arrows): (hemi)pelagic input dominates during sea-level highstands, whereas the downslope (gravitational) supply of sediments to the middle slope increases as the shoreline moves closer to the shelf edge

during regressions (Posamentier and Allen, 1993; Catuneanu, 2006; Carvajal et al., 2009; Helland-Hansen and Hampson, 2009). Sequence stratigraphic surfaces indicated with * are cryptic in this case study, and therefore an alternative sequence stratigraphic approach was adopted (see Table 3 and text for discussion). **(B)** Variability of the upper MOW (and according alongslope sediment supply and redistribution capacity) in the study area over one sea-level cycle (following Llave et al., 2006; Rogerson et al., 2010; Hernández-Molina et al., 2014b; Kaboth et al., 2016; Lofi et al., 2016). **(C)** Inferred interpretation and comparison of the deposits at IODP Expedition site U1386 and seismic facies, which result from the combined action of (A) and (B). Visual core descriptions adapted from Stow et al. (2013). Abbreviations: ST = systems tracts; SB = sequence boundary; mfs = maximum flooding surface; mrs = maximum regressive surface; cc = correlative conformity; bsfr = basal surface of forced regression.

Figure 20. Summary of the controls on margin development and architecture in the northern Gulf of Cadiz. The relative importance of the different controlling factors (SL = sea level, TECT = tectonics, OC = oceanography, and sediment supply) changes with the considered timescales and seismic stratigraphic elements: (i) = stacking patterns of the major seismic units, (ii) = depocenter distribution of the major seismic units, (iii) = internal architecture and seismic facies of the (sub-)units. At the scale of 100 kyr glacial-interglacial cycles (central triangle), the relative importance of sea level increases during glacials, while the relative importance of oceanography increases during interglacials (as indicated by the black bars at the bottom).

Supplementary figure S1. P-wave velocities (Vp) from the split core measurement gantry (SCMG) in automatic and manual mode, whole-round multisensor core logger (WRMSL) and interval velocities derived from vertical seismic profiling (VSP) for IODP Expedition 339 sites U1386 **(A)** and U1387 **(B)** (data from Stow et al., 2013). The time-depth charts are based on the integration of the split core measurement gantry velocities (in automatic mode) and downhole logging velocities. The VSP checkshot surveys confirm this approach.

Supplementary figure S2. (A) Dip-oriented seismic section over the northern Gulf of Cadiz continental shelf (location indicated in Figure 2B). **(B)** Seismic stratigraphic interpretation. **(C)** Sequence stratigraphic interpretation and trajectory analysis, performed at two scales: at the larger scale, shoreline positions are indicated at the sequence-bounding surfaces (red dots); at the smaller scale, shoreline positions are indicated at clinoforms within the seismic units (blue and green dots). In the case of the descending regressive trends (i.e. blue and red dots), the shoreline can be assumed to be coincident with the shelf edge (see text for discussion). Abbreviations: su = subaerial unconformity; mrs = maximum regressive surface; bsfr = basal surface of forced regression.

Supplementary figure S3. (A) Quantification of the total 2D subsidence along correlation profile 2 during U3 and U4, following the two methods proposed by Rabineau et al. (2014). Method 1 evaluates the accommodation evolution at point A on the outer shelf (location shown in B). Eustatic variations are not taken into account since the sea-level positions during the formation of mws4, mws3 and mws2 were fairly similar (see Figure 15). Method 2 assesses the change in tilt of mws4 and mws2. The rotation point R is located 4 km off the present-day coastline (indicated in B). **(B)** Map showing the location of correlation profile 2 (yellow line), rotation point R, and point A for which the evolution in accommodation is calculated.

Supplementary figure S4. Comparison of sedimentation rates at IODP site U1386 (location in Figure 2) with the accumulation rates of U1 – U5. **(A)** Late Quaternary sedimentation rates at site U1386 from Kaboth et al. (2017) (in black), on which the calculated average sedimentation rates (in blue) for the respective seismic units are based. **(B)** Accumulation rates of U1 – U5 (i.e. total preserved volume of U1 – U5 over the area indicated in Figure 14, divided by the duration of the interval over which the unit accumulated as indicated in Table 2).

References

Aksu, A.E., Hiscott, R.N., Yaşar, D., Işler, F.I. and Marsh, S., 2002. Seismic stratigraphy of Late Quaternary deposits from the southwestern Black Sea shelf: evidence for non-catastrophic variations in sea-level during the last ∼10 000 yr. Marine Geology, 190(1): 61-94.

Ambar, I., Armi, L., Bower, A. and Ferreira, T., 1999. Some aspects of time variability of the Mediterranean Water off south Portugal. Deep Sea Research Part I: Oceanographic Research Papers, 46: 1109-1136.

Ambar, I. and Howe, M.R., 1979. Observations of the Mediterranean Outflow-II. Deep Circulation in the Vicinity of the Gulf of Cadiz. Deep-Sea Research Part a: Oceanographic Research Papers, 26(5): 555-568.

Bahr, A., Jiménez-Espejo, F.J., Kolasinac, N., Grunert, P., Hernández-Molina, F.J., Röhl, U., Voelker, A.H.L., Escutia, C., Stow, D.A.V., Hodell, D. and Alvarez-Zarikian, C.A., 2014. Deciphering bottom current velocity and paleoclimate signals from contourite deposits in the Gulf of Cádiz during the last 140 kyr: An inorganic geochemical approach. Geochemistry, Geophysics, Geosystems, 15(8): 3145-3160.

Baraza, J., Ercilla, G. and Nelson, C.H., 1999. Potential geologic hazards on the eastern Gulf of Cadiz slope (SW Spain). Marine Geology, 155: 191-215.

Bard, E., Hamelin, B. and Fairbanks, R.G., 1990. U-Th ages obtained by mass-spectrometry in corals from Barbados - Sea-level during the past 130,000 years. Nature, 346: 456-458.

Baringer, M.O. and Price, J.F., 1999. A review of the physical oceanography of the Mediterranean outflow. Marine Geology, 155(1-2): 63-82.

Bassetti, M.A., Berné, S., Jouet, G., Taviani, M., Dennielou, B., Flores, J.A., Gaillot, A., Gelfort, R., Lafuerza, S. and Sultan, N., 2008. The 100 ka and rapid sea level changes recorded by prograding shelf sand bodies in the Gulf of Lions (western Mediterranean Sea). Geochemistry, Geophysics, Geosystems, 9(11).

Beaubouef, R.T. and Friedmann, S.J., 2000. High Resolution Seismic/Sequence Stratigraphic Framework for the Evolution of Pleistocene Intra Slope Basins, Western Gulf of Mexico: Depositional Models and Reservoir Analogs. In: P. Weimer (Editor), Deep-Water Reservoirs of the World. SEPM Society for Sedimentary Geology, pp. 40-60.

Bellanco, M.J. and Sánchez-Leal, R.F., 2016. Spatial distribution and intra-annual variability of water masses on the Eastern Gulf of Cadiz seabed. Continental Shelf Research, 128: 26-35.

Berné, S., Jouet, G., Bassetti, M.A., Dennielou, B. and Taviani, M., 2007. Late Glacial to Preboreal sea-level rise recorded by the Rhône deltaic system (NW Mediterranean). Marine Geology, 245(1): 65-88.

Borenäs, K.M., Wåhlin, A., Ambar, I. and Serra, N., 2002. The Mediterranean outflouw splitting - a comparison between theoretical models and CANIGO data. Deep Sea Research II, 49: 4195-4205.

Brackenridge, R., Stow, D.A.V. and Hernández-Molina, F.J., 2011. Contourites within a deep-water sequence stratigraphic framework. Geo-Marine Letters, 31(5-6): 343-360.

Browne, G.H. and Naish, T.R., 2003. Facies development and sequence architecture of a late Quaternary fluvial-marine transition, Canterbury Plains and shelf, New Zealand: implications for forced regressive deposits. Sedimentary Geology, 158(1): 57-86.

Bryden, H.L., Candela, J. and Kinder, T.H., 1994. Exchange through the Strait of Gibraltar. Progress In Oceanography, 33: 201-248.

Burger, R.L., Fulthorpe, C.S., Austin, J.A. and Gulick, S.P.S., 2002. Lower Pleistocene to present structural deformation and sequence stratigraphy of the continental shelf, offshore Eel River Basin, northern California. Marine Geology, 185(3): 249-281.

Cacho, I., Grimalt, J.O., Sierro, F.J., Shackleton, N. and Canals, M., 2000. Evidence for enhanced Mediterranean thermohaline circulation during rapid climatic coolings. Earth and Planetary Science Letters, 183(3-4): 417-429.

Caralp, M.H., 1988. Late Glacial to Recent Deep-sea Benthic Foraminifera from the Northeastern Atlantic (Cadiz Gulf) and Western Mediterranean (Alboran Sea): Paleoceanographic Results. Marine Micropaleontology, 13: 265-289.

Carey, J.S., Sheridan, R.E. and Ashley, G.M., 1998. Late Quaternary sequence stratigraphy of a slowly subsiding passive margin, New Jersey continental shelf. AAPG Bulletin, 82(5A): 773-791.

Carvajal, C., Steel, R. and Petter, A., 2009. Sediment supply: The main driver of shelf-margin growth. Earth-Science Reviews, 96(4): 221-248.

Catuneanu, O., 2006. Principles of Sequence Stratigraphy. Elsevier, Amsterdam.

Catuneanu, O., 2019. Model-independent sequence stratigraphy. Earth-Science Reviews, 188: 312-388.

Catuneanu, O., Abreu, V., Bhattacharya, J.P., Blum, M.D., Dalrymple, R.W., Eriksson, P.G., Fielding, C.R., Fisher, W.L., Galloway, W.E., Gibling, M.R., Giles, K.A., Holbrook, J.M., Jordan, R., Kendall, C.G.S.C., Macurda, B., Martinsen, O.J., Miall, A.D., Neal, J.E., Nummedal, D., Pomar, L., Posamentier, H.W., Pratt, B.R., Sarg, J.F., Shanley, K.W., Steel, R.J., Strasser, A., Tucker, M.E. and Winker, C., 2009. Towards the standardization of sequence stratigraphy. Earth-Science Reviews, 92(1-2): 1-33.

Catuneanu, O., Galloway, W.E., Kendall, C.G.S.C., Miall, A.D., Posamentier, H.W., Strasser, A. and Tucker, M.E., 2011. Sequence Stratigraphy: Methodology and Nomenclature. Newsletters on Stratigraphy, 44(3): 173-245.

Chappell, J., 1974. Relationships between sealevels, ^{18}O variations and orbital perturbations, during the past 250,000 years. Nature, 252: 199-202.

Chappell, J. and Shackleton, N.J., 1986. Oxygen isotopes and sea level. Nature, 324: 137-140.

Chiocci, F.L., 2000. Depositional response to Quaternary fourth-order sea-level fluctuations on the Latium margin (Tyrrhenian Sea, Italy). In: D. Hunt and R.L. Gawthorpe (Editors), Sedimentary Responses to Forced Regressions. Geological Society, London, Special Publications, 172, pp. 271-289.

Cloetingh, S., 1988. Intraplate Stresses: A Tectonic Cause for Third-Order Cycles in Apparent Sea Level? In: C.K. Wilgus, B.S. Hastings, H. Posamentier, J.V. Wagoner, C.A. Ross and C.G.S.C. Kendall (Editors), Sea-Level Changes: An Integrated Approach. SEPM Society for Sedimentary Geology.

Copard, K., Colin, C., Frank, N., Jeandel, C., Montero-Serrano, J.C., Reverdin, G. and Ferron, B., 2011. Nd isotopic composition of water masses and dilution of the Mediterranean outflow along the southwest European margin. Geochemistry Geophysics Geosystems, 12(6): Q06020.

Cortina, A., Grimalt, J.O., Martrat, B., Rigual-Hernández, A., Sierro, F.J. and Flores, J.A., 2016b. Anomalous SST warming during MIS 13 in the Gulf of Lions (northwestern Mediterranean Sea). Organic Geochemistry, 92: 16-23.

Cortina, A., Grimalt, J.O., Rigual-Hernández, A., Ballegeer, A.-M., Martrat, B., Sierro, F.J. and Flores, J.A., 2016a. The impact of ice-sheet dynamics in western Mediterranean environmental conditions during Terminations. An approach based on terrestrial long chain n-alkanes deposited in the upper slope of the Gulf of Lions. Chemical Geology, 430: 21-33.

Cortina, A., Sierro, F.J., Flores, J.A., Martrat, B. and Grimalt, J.O., 2015. The response of SST to insolation and ice sheet variability from MIS 3 to MIS 11 in the northwestern Mediterranean Sea (Gulf of Lions). Geophysical Research Letters, 42(23): 10,366-10,374.

de Boer, B., Lourens, L.J. and van de Wal, R.S.W., 2014. Persistent 400,000-year variability of Antarctic ice volume and the carbon cycle is revealed throughout the Plio-Pleistocene. Nature Communications, 5: 2999.

Dewey, J.F., Helman, M.L., Turco, E., Hutton, D.H.W. and Knott, S.D., 1989. Kinematics of the Western Mediterranean. In: M.P. Coward, D. Dietrich and R.G. Park (Editors), Alpine Tectonics. Geological Society, London, Special Publications, 45, London, pp. 265-283.

Duarte, J.C., Rosas, F.M., Terrinha, P., Gutscher, M.-A., Malavieille, J., Silva, S. and Matias, L., 2011. Thrust–wrench interference tectonics in the Gulf of Cadiz (Africa–Iberia plate boundary in the North-East Atlantic): Insights from analog models. Marine Geology, 289(1-4): 135-149.

Duarte, J.C., Rosas, F.M., Terrinha, P., Schellart, W.P., Boutelier, D., Gutscher, M.-A. and Ribeiro, A., 2013. Are subduction zones invading the Atlantic? Evidence from the southwest Iberia margin. Geology, 41(8): 839-842.

Duggen, S., Hoernle, K., van den Bogaard, P., Rupke, L. and Morgan, J.P., 2003. Deep roots of the Messinian salinity crisis. Nature, 422: 602-606.

Elderfield, H., Ferretti, P., Greaves, M., Crowhurst, S., McCave, I.N., Hodell, D.A. and Piotrowski, A.M., 2012. Evolution of Ocean Temperature and Ice Volume Through the Mid-Pleistocene Climate Transition. Science, 337: 704-709.

Embry, A.F. and Johannessen, E.P., 1993. T–R sequence stratigraphy, facies analysis and reservoir distribution in the uppermost Triassic–Lower Jurassic succession, western Sverdrup Basin, Arctic Canada. In: T.O. Vorren, E. Bergsager, Ø.A. Dahl-Stamnes, E. Holter, B. Johansen, E. Lie and T.B. Lund (Editors), Norwegian Petroleum Society Special Publications. Elsevier, pp. 121-146.

Emiliani, C., 1955. Pleistocene temperatures. Journal of Geology, 63(6): 538-578.

Faugères, J.C. and Stow, D.A.V., 2008. Contourite Drifts: nature, evolution and controls. In: M. Rebesco and A. Camerlenghi (Editors), Contourites, Developments in Sedimentology, 60. Elsevier, Amsterdam, pp. 257-288.

Fernández-Puga, M.C., Vázquez, J.T., Somoza, L., Díaz del Rio, V., Medialdea, T., Mata, M.P. and León, R., 2007. Gas-related morphologies and diapirism in the Gulf of Cádiz. Geo-Marine Letters, 27(2-4): 213-221.

Galloway, W.E., 1989. Genetic Stratigraphic Sequences in Basin Analysis I: Architecture and Genesis of Flooding-Surface Bounded Depositional Units. The American Association of Petroleum Geologists Bulletin, 73(2): 125-142.

Gallup, C.D., Edwards, R.L. and Johnson, R.G., 1994. The Timing of High Sea Levels Over the Past 200,000 Years. Science, 263: 796-800.

García-Lafuente, J., Delgado, J., Criado-Aldeanueva, F., Bruno, M., del Río, J. and Miguel Vargas, J., 2006. Water mass circulation on the continental shelf of the Gulf of Cádiz. Deep Sea Research Part II: Topical Studies in Oceanography, 53(11-13): 1182-1197.

Garcia, C.M., Prieto, L., Vargas, M., Echevarría, F., García-Lafuente, J., Ruiz, J. and Rubin, J.P., 2002. Hydrodynamics and the spatial distribution of plankton and TEP in the Gulf of Cádiz (SW Iberian Peninsula). Journal of Plankton Research, 24(8): 817-833.

García, M., Hernández-Molina, F.J., Llave, E., Stow, D.A.V., León, R., Fernández-Puga, M.C., Diaz del Río, V. and Somoza, L., 2009. Contourite erosive features caused by the Mediterranean Outflow

Water in the Gulf of Cadiz: Quaternary tectonic and oceanographic implications. Marine Geology, 257(1-4): 24-40.

Gascard, J.C. and Richez, C., 1985. Water masses and circulation in the Western Alboran Sea and in the Straits of Gibraltar. Progress In Oceanography, 15: 157-216.

Gonthier, E., Faugères, J.-C. and Stow, D.A.V., 1984. Contourite facies of the Faro Drift, Gulf of Cadiz. In: D.A.V. Stow and D.J.W. Piper (Editors), Fine Grained Sediments, Deep-Water Processes and Facies. Special Publication. Geological Society, London, pp. 275-291.

Gonzalez, R., Dias, J.M.A., Lobo, F. and Mendes, I., 2004. Sedimentological and paleoenvironmental characterisation of transgressive sediments on the Guadiana Shelf (Northern Gulf of Cadiz, SW Iberia). Quaternary International, 120(1): 133-144.

Gràcia, E., Dañobeitia, J., Vergés, J., Bartolomé, R. and Córdoba, D., 2003. Crustal architecture and tectonic evolution of the Gulf of Cadiz (SW Iberian margin) at the convergence of the Eurasian and African plates. Tectonics, 22(4): 1033.

Grant, K.M., Rohling, E.J., Ramsey, C.B., Cheng, H., Edwards, R.L., Florindo, F., Heslop, D., Marra, F., Roberts, A.P., Tamisiea, M.E. and Williams, F., 2014. Sea-level variability over five glacial cycles. Nat Commun, 5: 5076.

Gutscher, M.A., Malod, J., Rehault, J.P., Contrucci, I., Klingelhoefer, F., Mendes-Victor, L. and Spakman, W., 2002. Evidence for Active Subduction Beneath Gibraltar. Geology, 30(12): 1071-1074.

Habgood, E., Kenyon, N.H., Masson, D.G., Akhmetzhanov, A.M., Weaver, P.P.E., Gardner, J. and Mulder, T., 2003. Deep-water sediment wave fields, bottom current sand channels and gravity flow channel-lobe systems: Gulf of Cadiz, NE Atlantic. Sedimentology, 50: 483-510.

Hanquiez, V., Mulder, T., Lecroart, P., Gonthier, E., Marchès, E. and Voisset, M., 2007. High resolution seafloor images in the Gulf of Cadiz, Iberian margin. Marine Geology, 246(1): 42-59.

Hays, J.D., Imbrie, J. and Shackleton, N.J., 1976. Variations in the Earth's orbit: pacemaker of the ice ages. Science, 194(4270): 1121-1132.

Helland-Hansen, W. and Gjelberg, J.G., 1994. Conceptual basis and variability in sequence stratigraphy: a different perspective. Sedimentary Geology, 92(1): 31-52.

Helland-Hansen, W. and Hampson, G.J., 2009. Trajectory analysis: concepts and applications. Basin Research, 21(5): 454-483.

Henriksen, S., Hampson, G.J., Helland-Hansen, W., Johannessen, E.P. and Steel, R.J., 2009. Shelf edge and shoreline trajectories, a dynamic approach to stratigraphic analysis. Basin Research, 21(5): 445-453.

Hernández-Molina, F.J., Llave, E., Preu, B., Ercilla, G., Fontan, A., Bruno, M., Serra, N., Gomiz, J.J., Brackenridge, R.E., Sierro, F.J., Stow, D.A.V., García, M., Juan, C., Sandoval, N. and Arnaiz, A., 2014b. Contourite processes associated with the Mediterranean Outflow Water after its exit from the Strait of Gibraltar: Global and conceptual implications. Geology, 42(3): 227-230.

Hernández-Molina, F.J., Llave, E., Somoza, L., Fernandez-Puga, M.C., Maestro, A., Leon, R., Medialdea, T., Barnolas, A., Garcia, M., del Rio, V.D., Fernandez-Salas, L.M., Vazquez, J.T., Lobo, F., Dias, J.M.A., Rodero, J. and Gardner, J., 2003. Looking for clues to paleoceanographic imprints: A diagnosis of the Gulf of Cadiz contourite depositional systems. Geology, 31(1): 19-22.

Hernández-Molina, F.J., Llave, E., Stow, D.A.V., Garcia, M., Somoza, L., Vazquez, J.T., Lobo, F.J., Maestro, A., del Rio, V.D., Leon, R., Medialdea, T. and Gardner, J., 2006. The contourite depositional system of the Gulf of Cadiz: A sedimentary model related to the bottom current activity of the Mediterranean outflow water and its interaction with the continental margin. Deep-Sea Research Part II-Topical Studies in Oceanography, 53(11-13): 1420-1463.

Hernández-Molina, F.J., Sierro, F.J., Llave, E., Roque, C., Stow, D.A.V., Williams, T., Lofi, J., Van der Schee, M., Arnáiz, A., Ledesma, S., Rosales, C., Rodríguez-Tovar, F.J., Pardo-Igúzquiza, E. and Brackenridge, R.E., 2016a. Evolution of the gulf of Cadiz margin and southwest Portugal contourite depositional system: Tectonic, sedimentary and paleoceanographic implications from IODP expedition 339. Marine Geology, 377: 7-39.

Hernández-Molina, F.J., Somoza, L. and Lobo, F., 2000. Seismic stratigraphy of the Gulf of Cádiz continental shelf: a model for Late Quaternary very high-resolution sequence stratigraphy and response to sea-level fall. In: D.W. Hunt and R.L. Gawthorpe (Editors), Sedimentary responses to Forced Regressions. Geological Society, London, Special Publications, 172, pp. 329-362.

Hernández-Molina, F.J., Somoza, L., Rey, J. and Pomar, L., 1994. Late Pleistocene-Holocene sediments on the Spanish continental shelves: Model for very high resolution sequence stratigraphy. Marine Geology, 120(3): 129-174.

Hernández-Molina, F.J., Somoza, L., Vazquez, J.T., Lobo, F., Fernandez-Puga, M.C., Llave, E. and Diaz-del Rio, V., 2002. Quaternary stratigraphic stacking patterns on the continental shelves of the southern Iberian Peninsula: their relationship with global climate and palaeoceanographic changes. Quaternary International, 92: 5-23.

Hernández-Molina, F.J., Stow, D.A.V., Alvarez-Zarikian, C., Acton, G., Bahr, A., Balestra, B., Ducassou, E., Flood, R.D., Flores, J.A., Furota, S., Grunert, P., Hodell, D.A., Jimenez-Espejo, F., Kim, J.K., Krissek, L., Kuroda, J., Li, B., Llave, E., Lofi, J., Lourens, L.J., Miller, M., Nanayama, F., Nishida, N., Richter, C., Roque, C., Pereira, H., Sanchez Goñi, M.F., Sierro, F.J., Singh, A.D., Sloss, C., Takashimizu, Y., Tzanova, A., Voelker, A., Williams, T. and Xuan, C., 2014a. Onset of Mediterranean outflow into the north Atlantic. Science, 344(6189): 1244-1250.

Hernández-Molina, F.J., Wåhlin, A., Bruno, M., Ercilla, G., Llave, E., Serra, N., Rosón, G., Puig, P., Rebesco, M., Van Rooij, D., Roque, D., González-Pola, C., Sánchez, F., Gómez, M., Preu, B., Schwenk, T., Hanebuth, T.J.J., Sánchez Leal, R.F., García-Lafuente, J., Brackenridge, R.E., Juan, C., Stow, D.A.V. and Sánchez-González, J.M., 2016b. Oceanographic processes and morphosedimentary products along the Iberian margins: A new multidisciplinary approach. Marine Geology, 378: 127-156.

Hodell, D., Crowhurst, S., Skinner, L., Tzedakis, P.C., Margari, V., Channell, J.E.T., Kamenov, G., Maclachlan, S. and Rothwell, G., 2013. Response of Iberian Margin sediments to orbital and suborbital forcing over the past 420 ka. Paleoceanography, 28(1): 185-199.

Hübscher, C. and Spieß, V., 2005. Forced regression systems tracts on the Bengal Shelf. Marine Geology, 219(4): 207-218.

Hunt, D. and Tucker, M.E., 1992. Stranded parasequences and the forced regressive wedge systems tract: deposition during base-level fall. Sedimentary Geology, 81: 1-9.

Hunt, D. and Tucker, M.E., 1995. Stranded parasequences and the forced regressive wedge systems tract: deposition during base-level fall—reply. Sedimentary Geology, 95(1): 147-160.

Johnson, J. and Stevens, I., 2000. A fine resolution model of the eastern North Atlantic between the Azores, the Canary Islands and the Gibraltar Strait. Deep Sea Research I, 47: 875-899.

Johnson, J.G., 1971. Timing and Coordination of Orogenic, Epeirogenic, and Eustatic Events. GSA Bulletin, 82(12): 3263-3298.

Johnson, J.G., Klapper, G. and Sandberg, C.A., 1985. Devonian eustatic fluctuations in Euramerica. GSA Bulletin, 96(5): 567-587.

Johnson, J.G. and Murphy, M.A., 1984. Time-rock model for Siluro-Devonian continental shelf, western United States. GSA Bulletin, 95(11): 1349-1359.

Jouet, G., Berné, S., Rabineau, M., Bassetti, M.A., Bernier, P., Dennielou, B., Sierro, F.J., Flores, J.A. and Taviani, M., 2006. Shoreface migrations at the shelf edge and sea-level changes around the Last Glacial Maximum (Gulf of Lions, NW Mediterranean). Marine Geology, 234(1-4): 21-42.

Kaboth, S., Bahr, A., Reichart, G.-J., Jacobs, B. and Lourens, L.J., 2016. New insights into upper MOW variability over the last 150kyr from IODP 339 Site U1386 in the Gulf of Cadiz. Marine Geology, 377: 136-145.

Kaboth, S., de Boer, B., Bahr, A., Zeeden, C. and Lourens, L.J., 2017. Mediterranean Outflow Water dynamics during the past ~570 kyr: Regional and global implications. Paleoceanography, 32(6): 634-647.

Kolla, V., Biondi, P., Long, B. and Fillon, R., 2000. Sequence stratigraphy and architecture of the Late Pleistocene Lagniappe delta complex, northeast Gulf of Mexico. In: D.W. Hunt and R.L. Gawthorpe (Editors), Sedimentary responses to Forced Regressions. Geological Society, London, Special Publications, 172, pp. 291-327.

Kolla, V., Posamentier, H.W. and Eichenseer, H., 1995. Stranded parasequences and the forced regressive wedge systems tract: deposition during base-level fall - discussion. Sedimentary Geology, 95(1): 139-145.

Koulali, A., Ouazar, D., Tahayt, A., King, R.W., Vernant, P., Reilinger, R.E., McClusky, S., Mourabit, T., Davila, J.M. and Amraoui, N., 2011. New GPS constraints on active deformation along the Africa–Iberia plate boundary. Earth and Planetary Science Letters, 308(1-2): 211-217.

Labaune, C., Jouet, G., Berné, S., Gensous, B., Tesson, M. and Delpeint, A., 2005. Seismic stratigraphy of the Deglacial deposits of the Rhône prodelta and of the adjacent shelf. Marine Geology, 222-223: 299-311.

Lambeck, K. and Chappell, J., 2001. Sea Level Change Through the Last Glacial Cycle. Science, 292: 679-686.

Lambeck, K., Esat, T.M. and Potter, E.-K., 2002. Links between climate and sea levels for the past three million years. Nature, 419: 199-206.

Lea, D.W., Martin, P.A., Pak, D.K. and Spero, H.J., 2002. Reconstructing a 350 ky history of sea level using planktonic Mg/Ca and oxygen isotope records from a Cocos Ridge core. Quaternary Science Reviews, 21: 283-293.

Liquete, C., Canals, M., De Mol, B., De Batist, M. and Trincardi, F., 2008. Quaternary stratal architecture of the Barcelona prodeltaic continental shelf (NW Mediterranean). Marine Geology, 250(3-4): 234-250.

Lisiecki, L.E. and Raymo, M.E., 2005. A Pliocene-Pleistocene stack of 57 globally distributed benthic $\delta^{18}O$ records. Paleoceanography, 20(2): PA1003.

Llave, E., Hernández-Molina, F.J., Somoza, L., Diaz-del Rio, V., Stow, D.A.V., Maestro, A. and Alveirinho Dias, J.M., 2001. Seismic stacking pattern of the Faro-Albufeira contourite system (Gulf of Cadiz): a Quaternary record of paleoceanographic and tectonic influences. Marine Geophysical Researches, 22: 487-508.

Llave, E., Hernández-Molina, F.J., Somoza, L., Stow, D.A.V. and Diaz del Rio, G., 2007. Quaternary evolution of the contourite depositional system in the Gulf of Cadiz. In: A.R. Viana and M. Rebesco (Editors), Economic and Palaeoceanographic Significance of Contourite Deposits. Special Publication. Geological Society, London, pp. 49-79.

Llave, E., Matias, H., Hernández-Molina, F.J., Ercilla, G., Stow, D.A.V. and Medialdea, T., 2011. Pliocene-Quaternary contourites along the northern Gulf of Cadiz margin: sedimentary stacking pattern and regional distribution. Geo-Marine Letters, 31(5-6): 377-390.

Llave, E., Schönfeld, J., Hernández-Molina, F.J., Mulder, T., Somoza, L., Diaz-del Rio, V. and Sanchez-Almazo, I., 2006. High-resolution stratigraphy of the Mediterranean outflow contourite system in the Gulf of Cadiz during the late Pleistocene: The impact of Heinrich events. Marine Geology, 277: 241-262.

Lobo, F.J., 1995. Estructuración y evolución morfosedimentaria de un sector del margen continental septentrional del Golfo de Cádiz durante el Cuaternario Terminal. Dissertation, University of Cádiz, Puerto Real (Cádiz, Spain), 200 pp.

Lobo, F.J., Dias, J.M.A., Hernández-Molina, F.J., Gonzalez, R., Fernandez-Salas, L.M. and Diaz-Del-Rio, V., 2005a. Late Quaternary shelf-margin wedges and upper slope progradation in the Gulf of Cadiz margin (SW Iberian Peninsula). In: D.M. Hodgson and S.S. Flint (Editors), Submarine Slope Systems: Processes and Products. Geological Society, London, Special Publications, 244, pp. 7-25.

Lobo, F.J., Fernández-Salas, L.M., Hernández-Molina, F.J., González, R., Dias, J.M.A., del Río, V.D. and Somoza, L., 2005b. Holocene highstand deposits in the Gulf of Cadiz, SW Iberian Peninsula: A high-resolution record of hierarchical environmental changes. Marine Geology, 219(2): 109-131.

Lobo, F.J., García, M., Luján, M., Mendes, I., Reguera, M.I. and Van Rooij, D., 2018. Morphology of the last subaerial unconformity on a shelf: insights into transgressive ravinement and incised valley occurrence in the Gulf of Cádiz. Geo-Marine Letters, 38(1): 33-45.

Lobo, F.J., Hernández-Molina, F.J., Somoza, L. and Díaz del Río, V., 2001. The sedimentary record of the post-glacial transgression on the Gulf of Cadiz continental shelf (Southwest Spain). Marine Geology, 178(1): 171-195.

Lobo, F.J., Hernández-Molina, F.J., Somoza, L., Díaz del Río, V. and Dias, J.M.A., 2002. Stratigraphic evidence of an upper Pleistocene TST to HST complex on the Gulf of Cádiz continental shelf (south-west Iberian Peninsula). Geo-Marine Letters, 22(2): 95-107.

Lobo, F.J. and Ridente, D., 2014. Stratigraphic architecture and spatio-temporal variability of high-frequency (Milankovitch) depositional cycles on modern continental margins: An overview. Marine Geology, 352(0): 215-247.

Lobo, F.J., Sánchez, R., González, R., Dias, J.M.A., Hernández-Molina, F.J., Fernández-Salas, L.M., Díaz del Río, V. and Mendes, I., 2004. Contrasting styles of the Holocene highstand sedimentation and sediment dispersal systems in the northern shelf of the Gulf of Cadiz. Continental Shelf Research, 24(4-5): 461-482.

Lofi, J., Voelker, A.H.L., Ducassou, E., Hernández-Molina, F.J., Sierro, F.J., Bahr, A., Galvani, A., Lourens, L.J., Pardo-Igúzquiza, E., Pezard, P., Rodríguez-Tovar, F.J. and Williams, T., 2016. Quaternary chronostratigraphic framework and sedimentary processes for the Gulf of Cadiz and Portuguese Contourite Depositional Systems derived from Natural Gamma Ray records. Marine Geology, 377: 40-57.

Louarn, E. and Morin, P., 2011. Antarctic Intermediate Water influence on Mediterranean Sea Water outflow. Deep Sea Research Part I: Oceanographic Research Papers, 58(9): 932-942.

Lu, H. and Fulthorpe, C.S., 2004. Controls on sequence stratigraphy of a middle Miocene–Holocene, current-swept, passive margin: Offshore Canterbury Basin, New Zealand. GSA Bulletin, 116(11-12): 1345-1366.

Maldonado, A., Somoza, L. and Pallarés, L., 1999. The Betic orogen and the Iberian-African boundary in the Gulf of Cadiz: geological evolution (central North Atlantic). Marine Geology, 155: 9-43.

Marchès, E., Mulder, T., Cremer, M., Bonnel, C., Hanquiez, V., Gonthier, E. and Lecroart, P., 2007. Contourite drift construction influenced by capture of Mediterranean Outflow Water deep-sea current by the Portimao submarine canyon (Gulf of Cadiz, South Portugal). Marine Geology, 242(4): 247-260.

Marchès, E., Mulder, T., Gonthier, E., Cremer, M., Hanquiez, V., Garlan, T. and Lecroart, P., 2010. Perched lobe formation in the Gulf of Cadiz: Interactions between gravity processes and contour currents (Algarve Margin, Southern Portugal). Sedimentary Geology, 229(3): 81-94.

Maselli, V., Trincardi, F., Cattaneo, A., Ridente, D. and Asioli, A., 2010. Subsidence pattern in the central Adriatic and its influence on sediment architecture during the last 400 kyr. Journal of Geophysical Research: Solid Earth, 115(B12).

Maslin, M.A. and Brierley, C.M., 2015. The role of orbital forcing in the Early Middle Pleistocene Transition. Quaternary International, 389: 47-55.

McHugh, C.M., Fulthorpe, C.S., Hoyanagi, K., Blum, P., Mountain, G.S. and Miller, K.G., 2017. The sedimentary imprint of glacio-eustasy: implications for global correlations of seismic sequences. Geosphere, 14(1): 1-21.

Medialdea, T., Vegas, R., Somoza, L., Vázquez, J.T., Maldonado, A., Díaz-del-Río, V., Maestro, A., Córdoba, D. and Fernández-Puga, M.C., 2004. Structure and evolution of the "Olistostrome" complex of the Gibraltar Arc in the Gulf of Cádiz (eastern Central Atlantic): evidence from two long seismic cross-sections. Marine Geology, 209(1-4): 173-198.

Miall, A.D., 1991. Stratigraphic sequences and their chronostratigraphic correlation. Journal of Sedimentary Research, 61(4): 497-505.

Miall, A.D., 1992. Exxon global cycle chart: An event for every occasion? Geology, 20(9): 787-790.

Milankovitch, M., 1930. Matematische klimalehre und astronomische theorie der klimaschwankungen. In: W. Köppen and R. Geiger (Editors), Hanbuch der klimatologie, IA. Gebrüder Bontraeger, Berlin, pp. 1-176.

Miller, K.G., Mountain, G.S., Browning, J.V., Katz, M.E., Monteverde, D., Sugarman, P.J., Ando, H., Bassetti, M.A., Bjerrum, C.J., Hodgson, D., Hesselbo, S., Karakaya, S., Proust, J.-N. and Rabineau, M., 2013. Testing sequence stratigraphic models by drilling Miocene foresets on the New Jersey shallow shelf. Geosphere, 9(5): 1236-1256.

Millot, C., 2009. Another description of the Mediterranean Sea outflow. Progress in Oceanography, 82(2): 101-124.

Mitchum, R.M., Jr., Vail, P.R. and Sangree, J.B., 1977. Seismic Stratigraphy and Global Changes of Sea Level, Part 6: Stratigraphic Interpretation of Seismic Reflection Patterns in Depositional Sequences In: C.E. Payton (Editor), Seismic Stratigraphy — Applications to Hydrocarbon Exploration. American Association of Petroleum Geologists.

Mulder, T., Lecroart, P., Hanquiez, V., Marches, E., Gonthier, E., Guedes, J.-C., Thiébot, E., Jaaidi, B., Kenyon, N., Voisset, M., Perez, C., Sayago, M., Fuchey, Y. and Bujan, S., 2006. The western part of the Gulf of Cadiz: contour currents and turbidity currents interactions. Geo-Marine Letters, 26(1): 31-41.

Mulder, T., Voisset, M., Lecroart, P., Le Drezen, E., Gonthier, E., Hanquiez, V., Faugeres, J.C., Habgood, E., Hernández-Molina, F.J., Estrada, F., Llave-Barranco, E., Poirier, D., Gorini, C., Fuchey, Y., Voelker, A., Freitas, P., Sanchez, F.L., Fernandez, L.M., Kenyon, N.H. and Morel, J., 2003. The Gulf of Cadiz: an unstable giant contouritic levee. Geo-Marine Letters, 23(1): 7-18.

Neal, J. and Abreu, V., 2009. Sequence stratigraphy hierarchy and the accommodation succession method. Geology, 37(9): 779-782.

Neal, J.E., Abreu, V., Bohacs, K.M., Feldman, H.R. and Pederson, K.H., 2016. Accommodation succession (δA/δS) sequence stratigraphy: observational method, utility and insights into sequence boundary formation. Journal of the Geological Society, 173(5): 803-816.

Nelson, C.H., Baraza, J., Maldonado, A., Rodero, J., Escutia, C. and Barber, J.H., 1999. Influence of the Atlantic inflow and Mediterranean outflow currents on Late Quaternary sedimentary facies of the Gulf of Cadiz continental margin. Marine Geology, 155(1-2): 99-129.

Nelson, C.H., Baraza, J. and Maldonaldo, A., 1993. Mediterranean undercurrent sandy contourites, Gulf of Cadiz, Spain. Sedimentary Geology, 82: 103-131.

Ochoa, J. and Bray, N.A., 1991. Water mass exchange in the Gulf of Cadiz. Deep Sea Research Part A. Oceanographic Research Papers, 38: S465-S503.

Payton, C.E., 1977. Seismic Stratigraphy - Applications to Hydrocarbon Exploration. AAPG Memoir 26, 516 pp.

Pellegrini, C., Asioli, A., Bohacs, K.M., Drexler, T.M., Feldman, H.R., Sweet, M.L., Maselli, V., Rovere, M., Gamberi, F., Valle, G.D. and Trincardi, F., 2018. The Late Pleistocene Po River lowstand wedge in the Adriatic Sea: Controls on architecture variability and sediment partitioning. Marine and Petroleum Geology, 96: 16-50.

Pellegrini, C., Maselli, V., Cattaneo, A., Piva, A., Ceregato, A. and Trincardi, F., 2015. Anatomy of a compound delta from the post-glacial transgressive record in the Adriatic Sea. Marine Geology, 362: 43-59.

Posamentier, H.W. and Allen, G.P., 1993. Variability of the sequence stratigraphic model: effects of local basin factors. Sedimentary Geology, 86(1): 91-109.

Posamentier, H.W., Allen, G.P., James, D.P. and Tesson, M., 1992. Forced Regressions in a Sequence Stratigraphic Framework: Concepts, Examples, and Exploration Significance. The American Association of Petroleum Geologists Bulletin, 76(11): 1687-1709.

Posamentier, H.W., Jervey, M.T. and Vail, P.R., 1988. Eustatic Controls on Clastic Deposition I - Conceptual Framework. In: C.K. Wilgus, B.S. Hastings, H. Posamentier, J.V. Wagoner, C.A. Ross and C.G.S.C. Kendall (Editors), Sea-Level Changes: An Integrated Approach. SEPM Society for Sedimentary Geology, pp. 109-124.

Posamentier, H.W. and Vail, P.R., 1988. Eustatic Controls on Clastic Deposition II—Sequence and Systems Tract Models. In: C.K. Wilgus, B.S. Hastings, H. Posamentier, J.V. Wagoner, C.A. Ross and C.G.S.C. Kendall (Editors), Sea-Level Changes: An Integrated Approach. SEPM Society for Sedimentary Geology, pp. 125-154.

Price, J., Baringer, M.O., Lueck, R.G., Johnson, G.C., Ambar, I., Parrilla, G., Cantos, A., Kennelly, M.A. and Sanford, T.B., 1993. Mediterranean Outflow Mixing and Dynamics. Science, 259: 1277-1282.

Proust, J.-N., Pouderoux, H., Ando, H., Hesselbo, S.P., Hodgson, D.M., Lofi, J., Rabineau, M. and Sugarman, P.J., 2018. Facies architecture of Miocene subaqueous clinothems of the New Jersey passive margin: Results from IODP-ICDP Expedition 313. Geosphere, 14(4): 1564-1591.

Rabineau, M., Berné, S., Aslanian, D., Olivet, J.-L., Joseph, P., Guillocheau, F., Bourillet, J.-F., Ledrezen, E. and Granjeon, D., 2005. Sedimentary sequences in the Gulf of Lion: A record of 100,000 years climatic cycles. Marine and Petroleum Geology, 22(6-7): 775-804.

Rabineau, M., Berné, S., Olivet, J.-L., Aslanian, D., Guillocheau, F. and Joseph, P., 2006. Paleo sea levels reconsidered from direct observation of paleoshoreline position during Glacial Maxima (for the last 500,000 yr). Earth and Planetary Science Letters, 252(1-2): 119-137.

Rabineau, M., Leroux, E., Aslanian, D., Bache, F., Gorini, C., Moulin, M., Molliex, S., Droz, L., dos Reis, A.T., Rubino, J.L., Guillocheau, F. and Olivet, J.L., 2014. Quantifying subsidence and isostatic readjustment using sedimentary paleomarkers, example from the Gulf of Lion. Earth and Planetary Science Letters, 388: 353-366.

Riboulot, V., Cattaneo, A., Berné, S., Schneider, R.R., Voisset, M., Imbert, P. and Grimaud, S., 2012. Geometry and chronology of late Quaternary depositional sequences in the Eastern Niger Submarine Delta. Marine Geology, 319-322: 1-20.

Ridente, D., 2016. Releasing the sequence stratigraphy paradigm. Overview and perspectives. Journal of the Geological Society, 173(5): 845-853.

Ridente, D., Petrungaro, R., Falese, F. and Chiocci, F.L., 2012. Middle–Upper Pleistocene record of 100-ka depositional cycles on the Southern Tuscany continental margin (Tyrrhenian Sea, Italy). Marine Geology, 326-328: 1-13.

Ridente, D., Trincardi, F., Piva, A. and Asioli, A., 2009. The combined effect of sea level and supply during Milankovitch cyclicity: Evidence from shallow-marine $\delta^{18}O$ records and sequence architecture (Adriatic margin). Geology, 37(11): 1003-1006.

Ridente, D., Trincardi, F., Piva, A., Asioli, A. and Cattaneo, A., 2008. Sedimentary response to climate and sea level changes during the past ∼400 ka from borehole PRAD1-2 (Adriatic margin). Geochemistry, Geophysics, Geosystems, 9(9).

Rodero, J., Pallarés, L. and Maldonaldo, A., 1999. Late Quaternary seismic facies of the Gulf of Cadiz Spanish margin: depositional processes influenced by sea-level change and tectonic controls. Marine Geology, 155: 131-156.

Rogerson, M., Colmenero-Hidalgo, E., Levine, R.C., Rohling, E.J., Voelker, A.H.L., Bigg, G.R., Schönfeld, J., Cacho, I., Sierro, F.J., Löwemark, L., Reguera, M.I., de Abreu, L. and Garrick, K., 2010. Enhanced Mediterranean-Atlantic exchange during Atlantic freshening phases. Geochemistry Geophysics Geosystems, 11(8): Q08013.

Rohling, E.J., Foster, G.L., Grant, K.M., Marino, G., Roberts, A.P., Tamisiea, M.E. and Williams, F., 2014. Sea-level and deep-sea-temperature variability over the past 5.3 million years. Nature, 508(7497): 477-82.

Roque, C., 1998. Análise morfosedimentar da sequência deposicional do Quaternário Superior da plataforma continental Algarvia entre Faro e a foz do Rio Guadiana. Dissertation, University of Lisbon, 221 pp.

Roque, C., Duarte, H., Terrinha, P., Valadares, V., Noiva, J., Cachão, M., Ferreira, J., Legoinha, P. and Zitellini, N., 2012. Pliocene and Quaternary depositional model of the Algarve margin contourite drifts (Gulf of Cadiz, SW Iberia): Seismic architecture, tectonic control and paleoceanographic insights. Marine Geology, 303–306: 42-62.

Rosas, F.M., Duarte, J.C., Terrinha, P., Valadares, V. and Matias, L., 2009. Morphotectonic characterization of major bathymetric lineaments in Gulf of Cadiz (Africa–Iberia plate boundary): Insights from analogue modelling experiments. Marine Geology, 261(1-4): 33-47.

Rosenbaum, G., Lister, G.S. and Duboz, C., 2002. Relative motions of Africa, Iberia and Europe during Alpine orogeny. Tectonophysics, 359: 117-129.

Roveri, M., Flecker, R., Krijgsman, W., Lofi, J., Lugli, S., Manzi, V., Sierro, F.J., Bertini, A., Camerlenghi, A., De Lange, G., Govers, R., Hilgen, F.J., Hübscher, C., Meijer, P.T. and Stoica, M., 2014. The Messinian Salinity Crisis: Past and future of a great challenge for marine sciences. Marine Geology, 352: 25-58.

Ruddiman, W.F., 2003. Orbital insolation, ice volume, and greenhouse gases. Quaternary Science Reviews, 22(15-17): 1597-1629.

Ruddiman, W.F., Raymo, M.E. and McIntyre, A., 1986. Matuyama 41,000-year cycles: North Atlantic Ocean and northern hemisphere ice sheets. Earth and Planetary Science Letters, 80: 117-129.

Sánchez-Leal, R.F., Bellanco, M.J., Fernández-Salas, L.M., García-Lafuente, J., Gasser-Rubinat, M., González-Pola, C., Hernández-Molina, F.J., Pelegrí, J.L., Peliz, A., Relvas, P., Roque, D., Ruiz-Villarreal, M., Sammartino, S. and Sánchez-Garrido, J.C., 2017. The Mediterranean Overflow in the Gulf of Cadiz: A rugged journey. Science Advances, 3(11).

Schlitzer, R., 2017. Ocean Data View, odv.awi.de.

Schwarzacher, W., 2000. Repetitions and cycles in stratigraphy. Earth-Science Reviews, 50(1-2): 51-75.

Shackleton, N.J. and Opdyke, N.D., 1973. Oxygen isotope and palaeomagnetic stratigraphy of equatorial Pacific core V28-238: oxygen isotope temperature and ice volumes on a 10^5 and 10^6 year scale. Quaternary Research, 3(1): 39-59.

Sheridan, R.E., Ashley, G.M., Miller, K.G., Waldner, J.S., Hall, D.W. and Uptegrove, J., 2000. Offshore-onshore correlation of upper Pleistocene strata, New Jersey Coastal Plain to continental shelf and slope. Sedimentary Geology, 134(1): 197-207.

Siddall, M., Rohling, E.J., Almogi-Labin, A., Hemleben, C., Meischner, D., Schmelzer, I. and Smeed, D.A., 2003. Sea-level fluctuations during the last glacial cycle. Nature, 423(6942): 853-858.

Sierro, F.J., Andersen, N., Bassetti, M.A., Berné, S., Canals, M., Curtis, J.H., Dennielou, B., Flores, J.A., Frigola, J., Gonzalez-Mora, B., Grimalt, J.O., Hodell, D.A., Jouet, G., Pérez-Folgado, M. and Schneider, R., 2009. Phase relationship between sea level and abrupt climate change. Quaternary Science Reviews, 28(25): 2867-2881.

Somoza, L., Hernández-Molina, F.J., De Andres, J.R. and Rey, J., 1997. Continental shelf architecture and sea-level cycles: Late Quaternary high-resolution stratigraphy of the Gulf of Cadiz, Spain. Geo-Marine Letters, 17: 133-139.

Srivastava, S.P., Schouten, H., Roest, W.R., Klitgord, K.D., Kovacs, L.C., Verhoef, J. and Macnab, R., 1990. Iberian plate kinematics: a jumping plate boundary between Eurasia and Africa. Nature, 344: 756-759.

Stow, D.A.V., Faugères, J.-C. and Gonthier, E., 1986. Facies distribution and textural variation in Faro Drift contourites: Velocity fluctuation and drift growth. Marine Geology, 72: 71-100.

Stow, D.A.V., Faugères, J.-C., Gonthier, E., Cremer, M., Llave, E., Hernández-Molina, F.J., Somoza, L. and Díaz-Del-Río, V., 2002. Faro-Albufeira drift complex, northern Gulf of Cadiz. Geological Society, London, Memoirs, 22(1): 137-154.

Stow, D.A.V., Hernández-Molina, F.J., Alvarez Zarikian, C.A. and Expedition 339 Scientists, 2013. Proc. IODP, 339. Integrated Ocean Drilling Program Management International, Tokyo.

Terrinha, P., Matias, L., Vicente, J., Duarte, J., Luís, J., Pinheiro, L., Lourenço, N., Diez, S., Rosas, F., Magalhães, V., Valadares, V., Zitellini, N., Roque, C. and Víctor, L.M., 2009. Morphotectonics and strain partitioning at the Iberia–Africa plate boundary from multibeam and seismic reflection data. Marine Geology, 267(3-4): 156-174.

Toucanne, S., Mulder, T., Schönfeld, J., Hanquiez, V., Gonthier, E., Duprat, J., Cremer, M. and Zaragosi, S., 2007. Contourites of the Gulf of Cadiz: A high-resolution record of the paleocirculation of the Mediterranean outflow water during the last 50,000 years. Palaeogeography, Palaeoclimatology, Palaeoecology, 246(2-4): 354-366.

Voelker, A.H.L., Lebreiro, S.M., Schonfeld, J., Cacho, I., Erlenkeuser, H. and Abrantes, F., 2006. Mediterranean outflow strengthening during northern hemisphere coolings: A salt source for the glacial Atlantic? Earth and Planetary Science Letters, 245(1-2): 39-55.

Waelbroeck, C., Labeyrie, L., Michel, E., Duplessy, J.C., McManus, J.F., Lambeck, K., Balbon, E. and Labracherie, M., 2002. Sea-level and deep water temperature changes derived from benthic foraminifera isotopic records. Quaternary Science Reviews, 21(1-3): 295-305.

Yoo, D.-G., Kim, K.-J., Lee, G.-S., Kim, G.-Y. and Bae, S.-H., 2017. Seismic stratigraphic reconstruction of late Pleistocene lowstand wedges on the shelf margin and trough region of the Korea Strait: a review. Geosciences Journal, 21(6): 933-949.

Zazo, C., 1999. Interglacial sea levels. Quaternary International, 55: 101-113.

Zazo, C., Silva, P.G., Goy, J.L., Hillaire-Marcel, C., Ghaleb, B., Lario, J., Bardají, T. and González, A., 1999. Coastal uplift in continental collision plate boundaries: data from the Last Interglacial marine terraces of the Gibraltar Strait area (south Spain). Tectonophysics, 301(1): 95-109.

Zecchin, M. and Catuneanu, O., 2013. High-resolution sequence stratigraphy of clastic shelves I: Units and bounding surfaces. Marine and Petroleum Geology, 39(1): 1-25.

Zenk, W., 1975. On the Mediterranean outflow west of Gibraltar. "Meteor" Forsch.-Ergebnisse, 16: 23-34.

Zitellini, N., Gracia, E., Matias, L., Terrinha, P., Abreu, M.A., DeAlteriis, G., Henriet, J.P., Danobeitia, J.J., Masson, D.G., Mulder, T., Ramella, R., Somoza, L. and Diez, S., 2009. The quest for the Africa-Eurasia plate boundary west of the Strait of Gibraltar. Earth and Planetary Science Letters, 280(1-4): 13-50.

earlier work		*this work*			*SHELF*			*UPPER SLOPE*			*MIDDLE SLOPE*		
					ext. shape	*config. & facies*	*terminations*	*ext. shape*	*config. & facies*	*terminations*	*ext. shape*	*config. & facies*	*terminations*
Q6	H2	**U1**		**mws1**	sheet to bank*	subpar. (chaotic, par.-oblique*), mod. A	T: conf. – toplap B: conf. – onlap	sheet	subparallel – wavy, high A	T: conf. – e.t. B: conf. (onlap)	sheet	parallel low A (with upward incr.)	T: conf. B: conf.
	H1	**U2**	U2.1	is2	wedge	subpar. – wavy progr. (chaotic), mod. A	T: e.t. B: onlap – downlap*	wedge	chaotic – wavy, transparent – mod. A	T: conf. (e.t.) B: conf. (downlap)	sheet	(sub)parallel upward incr. A	T: conf. (e.t.) B: conf.
			U2.2	**mws2**	X	X	X	X	X	X		parallel low A	T: conf. B: conf. (onlap)
	G3	**U3**	U3.1	is3.1	wedge	par. – tangential oblique progr., mod. – high* A	T: toplap – e.t.* B: downlap	wedge to sheet	wavy – contorted (chaotic), low A (high A at foot)	T: conf. (e.t.) B: conf.	sheet	parallel upward incr. A	T: conf. (e.t.) B: conf.
	G2		U3.2	is3.2	lens	low-angle par.-oblique progr., mod. A	T: toplap B: downlap		subpar. – wavy (chaotic), low – mod. A	T: toplap B: onlap		smooth, parallel low A (with upward incr.)	T: conf. B: conf.
			U3.3	is3.3	X	X	X		X	X		smooth, parallel mod. – high A	T: conf. (e.t.) B: conf.
	G1		U3.4	**mws3**	lens	low-angle par.-oblique progr.	T: toplap B: onlap – downlap*		subpar. – wavy, low A	T: toplap B: conf. (onlap)		parallel low – mod. A	T: conf. B: conf.
		U4	U4.1	is4	wedge – lobate to bank	par.-oblique progr. (chaotic), mod. – high* A	T: toplap – e.t.* B: downlap	sheet	subparallel, low A	T: conf. (e.t.) B: conf.	sheet	parallel mod. A	T: conf. (e.t.) B: conf.
Q5	F3		U4.2	**mws4**	X	X	X	X	X	X		par., low – mod. (high) A	T: conf. (e.t.) B: conf.
	F2	**U5**	U5.1	is5	wedge	contorted – par.-oblique progr., low A	T: toplap – e.t.* B: downlap	wedge	wavy – hummocky, mod. A	T: conf. (e.t.) B: conf.	sheet	smooth, parallel high A	T: conf. (e.t.) B: conf.
	F1		U5.2	**mws5**	lens	subpar. (chaotic), low – mod. A	T: conf. B: downlap		subpar. – wavy, very low A	T: conf. (e.t.) B: conf. (onlap)		smooth, parallel low A	T: conf. B: conf.

Table 1.

(sub-)unit		*MIS*	*age (ka)*
U1		MIS2 → present	27 → 0
U2	U2.1	MIS5 → MIS2	115 → 27
	U2.2	MIS6 → MIS5	135 → 115
U3	U3.1	MIS7.3 → MIS6	200 → 135
	U3.2	MIS7.4 → MIS7.3	225 → 200
	U3.3	MIS7.5 → MIS7.4	240 → 225
	U3.4	MIS8 → MIS7.5	262 → 240
U4	U4.1	MIS9 → MIS8	310 → 262
	U4.2	MIS10 → MIS9	335 → 310
U5	U5.1	MIS11 → MIS10	400 → 335
	U5.2	MIS12 → MIS11	435 → 400

Table 2.

Events (of the relative SL curve) & stages	Standard sequence stratigraphic models				Sequence stratigraphic approach in **this study**
	Depositional Sequence *	**Depositional Sequence ****	**Genetic Sequence**	**T – R Sequence**	
HNR *end of T*	HST *mfs*	HST *mfs*	HST *mfs = SB*	RST *mfs*	TST + HST
T *end of R*	TST *mrs*	TST *mrs*	TST *mrs*	TST *mrs = SB*	*mrs = SB*
LNR *end of rel. SL fall*	late LST (w)	LST *cc** = SB*	late LST (w)	RST	RST (FSST + LST)
FR *onset of rel. SL fall*	early LST (f) *cc* = SB*	FSST *bsfr*	early LST (f) *bsfr*		*bsfr*
HNR	HST	HST	HST		TST + HST

↑ time ↑

Table 3.

U1386			
depth (mcd)	**depth (mbsf)**	**age (ka)**	**ref.**
0,00	0,00	0,0	Kaboth et al. (2016)
2,00	1,80	10,6	
2,70	2,43	11,3	
3,70	3,33	16,8	
12,50	11,26	31,1	
13,40	12,07	32,4	
13,70	12,34	33,3	
14,00	12,61	34,6	
14,70	13,24	35,9	
15,50	13,96	37,7	
16,20	14,59	38,6	
16,40	14,77	39,2	
16,75	15,09	40,4	
17,10	15,40	41,2	
17,50	15,76	42,0	
18,20	16,39	43,3	
18,70	16,84	44,2	
19,40	17,47	46,3	
19,50	17,56	47,0	
20,20	18,19	48,1	
24,00	21,62	56,0	
25,00	22,52	58,0	
27,21	24,51	65,0	
28,05	25,26	70,0	
28,10	25,31	71,2	
29,00	26,12	75,0	
29,55	26,61	75,5	
30,05	27,06	84,2	
30,15	27,15	86,2	
34,50	31,07	104,6	
37,70	33,95	110,1	
40,45	36,43	116,5	
43,70	39,36	127,6	
44,40	39,99	133,1	
45,04	40,57	134,8	
48,05	43,28	150,0	
	47,50	159,0	Lofi et al. (2016)
	60,90	198,0	
	63,80	208,0	
	75,10	245,0	
	81,80	267,0	
	86,60	283,0	
	95,20	312,0	
	100,50	327,0	
	104,60	341,0	
	123,70	398,0	
	147,50	482,0	

U1387			
depth (mcd)	**depth (mbsf)**	**age (ka)**	**ref.**
1,80	1,63	10,7	Bahr et al. (2014)
2,64	2,39	13,7	
3,54	3,20	16,0	
9,64	8,72	29,0	
9,88	8,94	30,1	
9,91	8,97	30,7	
10,48	9,48	32,8	
10,70	9,68	33,6	
11,18	10,12	35,3	
11,49	10,40	36,3	
12,43	11,25	38,5	
12,59	11,39	39,9	
12,71	11,50	41,0	
13,94	12,62	42,5	
14,51	13,13	44,4	
15,32	13,86	47,4	
15,50	14,03	48,4	
17,24	15,60	53,8	
17,89	16,19	56,0	
18,28	16,54	59,5	
21,46	19,42	70,4	
21,88	19,80	70,7	
22,27	20,15	71,8	
22,87	20,70	75,0	
25,20	22,81	83,6	
25,93	23,47	86,7	
27,57	24,95	103,3	
28,07	25,40	106,1	
29,56	26,75	109,9	
29,77	26,94	110,8	
32,92	29,79	131,1	
33,58	30,39	134,9	
	35,20	159,0	Lofi et al. (2016)
	46,40	198,0	
	48,60	208,0	
	57,90	245,0	
	63,40	267,0	
	67,40	283,0	
	74,50	312,0	
	78,00	327,0	
	81,60	341,0	
	95,60	398,0	
	116,50	482,0	

Supplementary table 1.

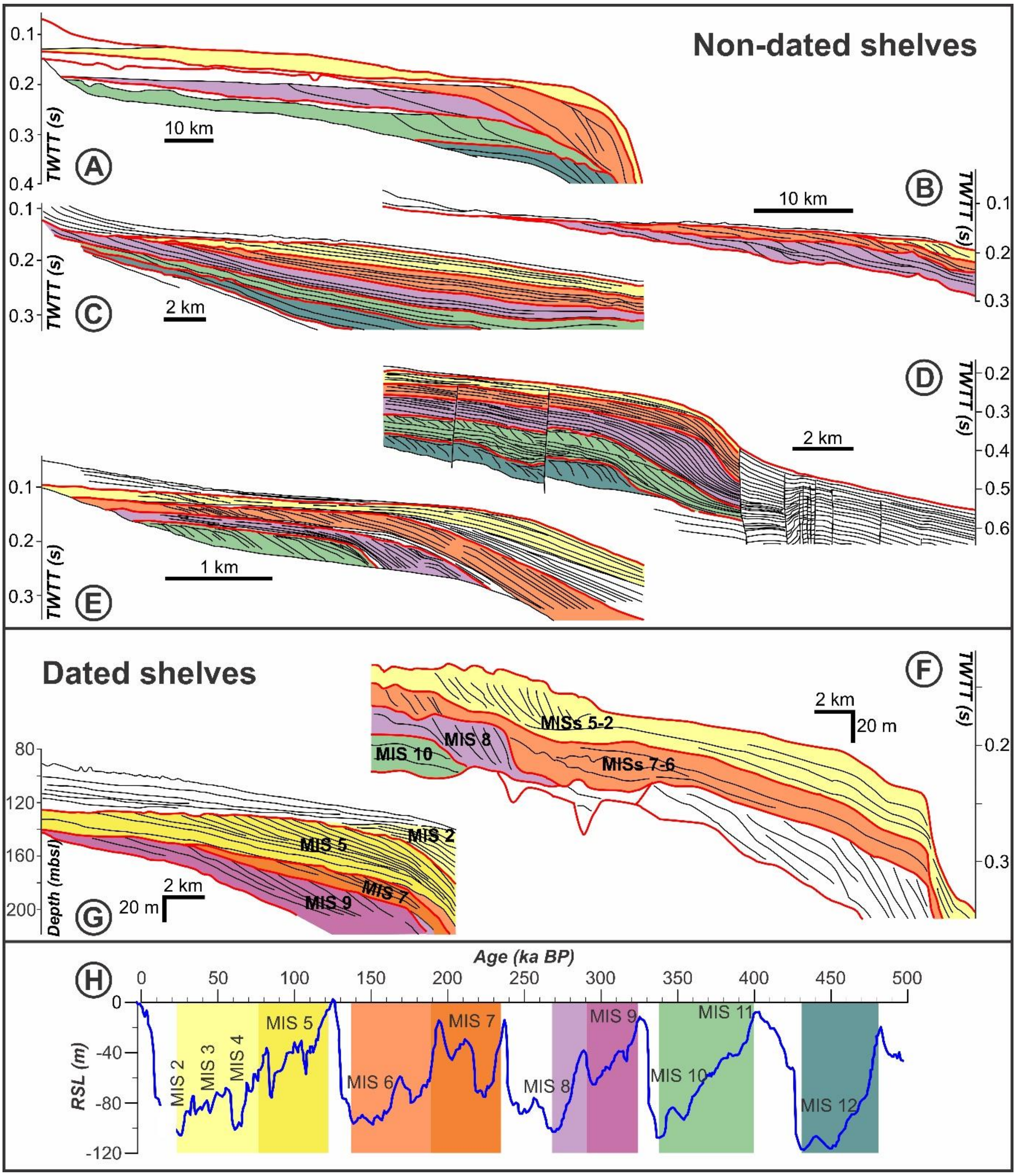

Non-dated shelves
Dated shelves
TWTT (s)
10 km
2 km
1 km
20 m
Depth (mbsl)
MISs 5-2
MIS 8
MIS 10
MISs 7-6
MIS 5
MIS 2
MIS 7
MIS 9
Age (ka BP)
RSL (m)
MIS 2
MIS 3
MIS 4
MIS 5
MIS 6
MIS 7
MIS 8
MIS 9
MIS 10
MIS 11
MIS 12

Figure 1.

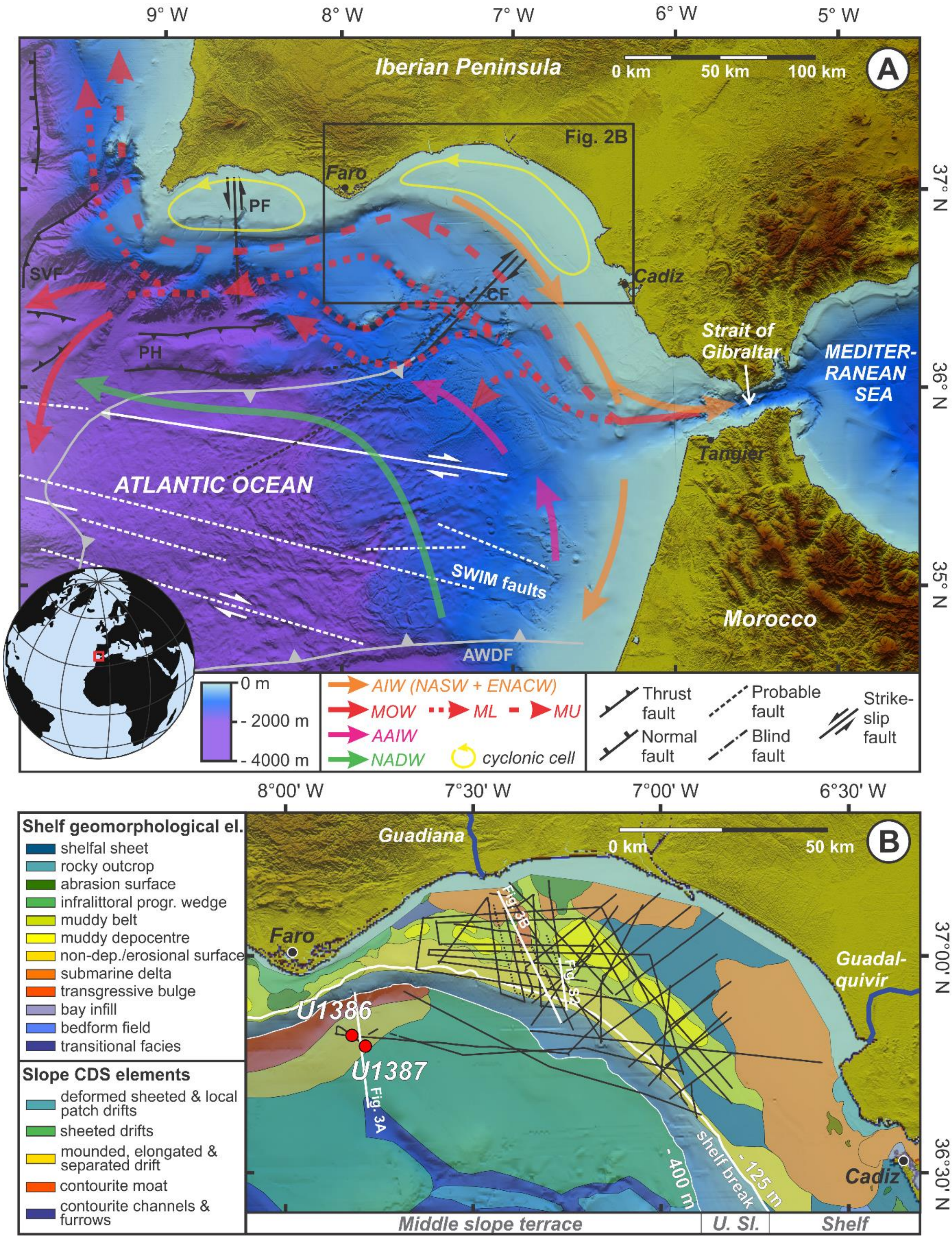
9° W
8° W
7° W
6° W
5° W
Iberian Peninsula
0 km
50 km
100 km
A
Fig. 2B
Faro
PF
Cadiz
CF
SVF
PH
Strait of Gibraltar
MEDITER-RANEAN SEA
Tangier
ATLANTIC OCEAN
SWIM faults
Morocco
AWDF
37° N
36° N
35° N
0 m
- 2000 m
- 4000 m
AIW (NASW + ENACW)
MOW
ML
MU
AAIW
NADW
cyclonic cell
Thrust fault
Normal fault
Probable fault
Blind fault
Strike-slip fault
8°00' W
7°30' W
7°00' W
6°30' W
Shelf geomorphological el.
shelfal sheet
rocky outcrop
abrasion surface
infralittoral progr. wedge
muddy belt
muddy depocentre
non-dep./erosional surface
submarine delta
transgressive bulge
bay infill
bedform field
transitional facies
Slope CDS elements
deformed sheeted & local patch drifts
sheeted drifts
mounded, elongated & separated drift
contourite moat
contourite channels & furrows
Guadiana
0 km
50 km
B
Faro
Fig. 3B
Fig. 8
U1386
U1387
Fig. 3A
Guadal-quivir
- 400 m
shelf break
- 125 m
Cadiz
37°00' N
36°30' N
Middle slope terrace
U. Sl.
Shelf

Figure 2.

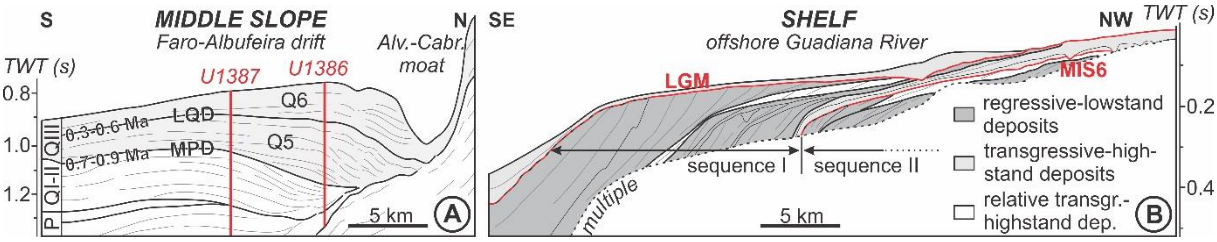
S
MIDDLE SLOPE
Faro-Albufeira drift
N
Alv.-Cabr. moat
TWT (s)
U1387
U1386
0.8
1.0
1.2
Q6
LQD
0.3-0.6 Ma
Q5
MPD
0.7-0.9 Ma
QIII
QI-II
P
5 km
A
SE
SHELF
offshore Guadiana River
NW
TWT (s)
LGM
MIS6
0.2
0.4
sequence I
sequence II
multiple
5 km
regressive-lowstand deposits
transgressive-high-stand deposits
relative transgr.-highstand dep.
B

Figure 3.

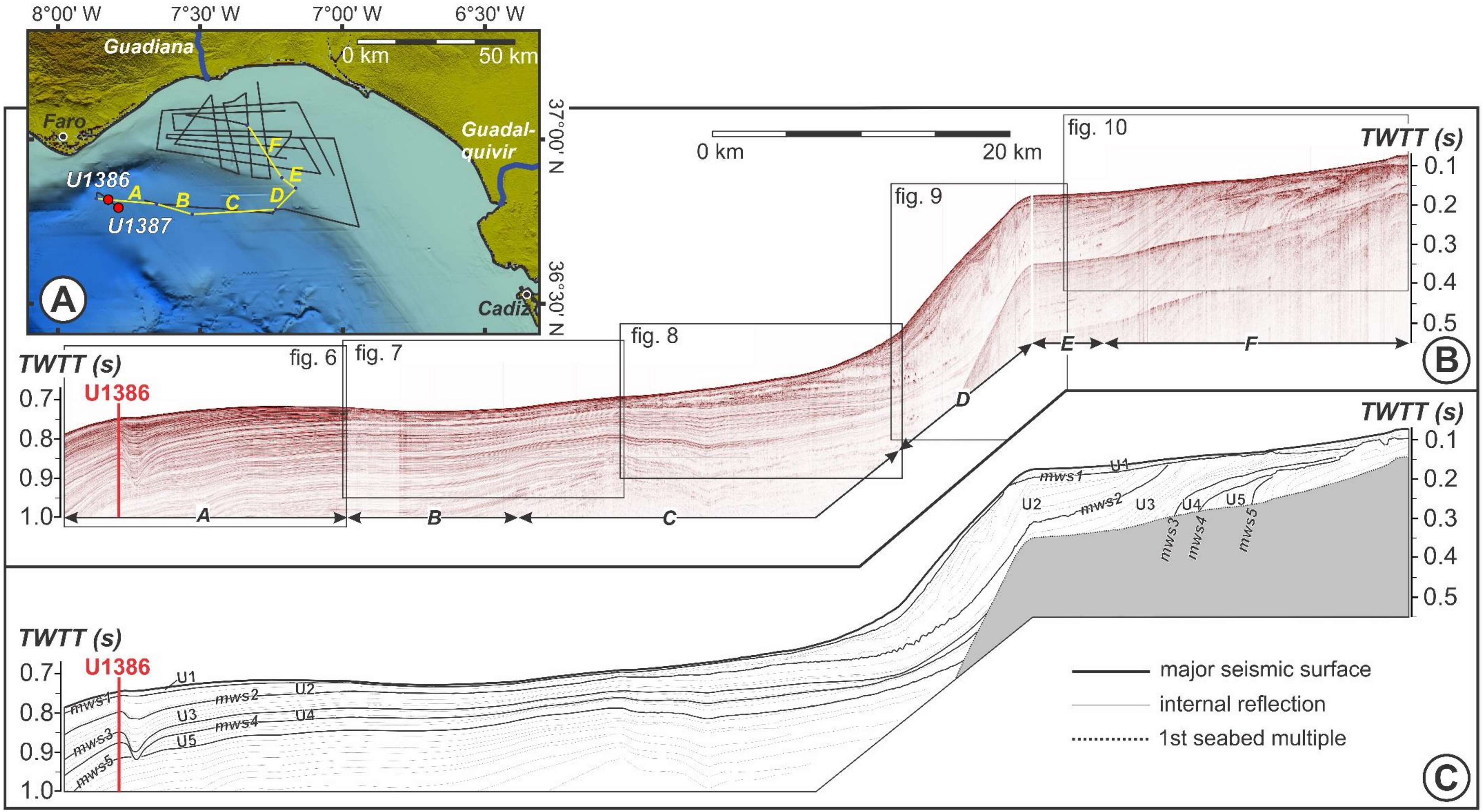

8°00' W
7°30' W
7°00' W
6°30' W
Guadiana
0 km
50 km
Faro
Guadal-
quivir
37°00' N
36°30' N
U1386
U1387
A
B
C
D
E
F
Cadiz
0 km
20 km
TWTT (s)
fig. 6
fig. 7
fig. 8
fig. 9
fig. 10
U1386
U1
U2
U3
U4
U5
mws1
mws2
mws3
mws4
mws5
major seismic surface
internal reflection
1st seabed multiple

Figure 4.

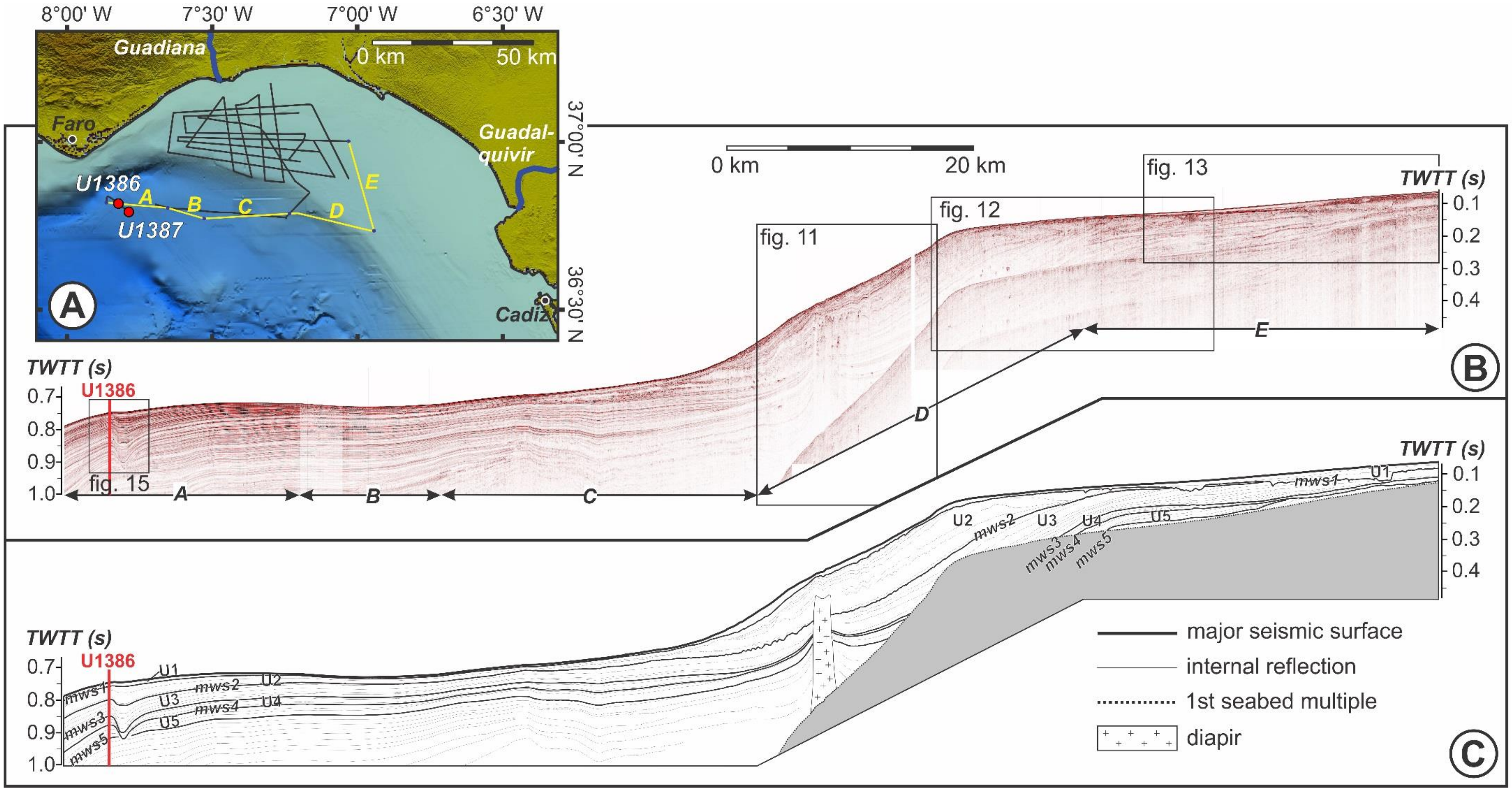

8°00' W
7°30' W
7°00' W
6°30' W
Guadiana
0 km
50 km
Faro
37°00' N
Guadal-
quivir
U1386
U1387
A
B
C
D
E
36°30' N
Cadiz
0 km
20 km
fig. 13
fig. 12
fig. 11
fig. 15
TWTT (s)
U1386
0.1
0.2
0.3
0.4
0.7
0.8
0.9
1.0
mws1
mws2
mws3
mws4
mws5
U1
U2
U3
U4
U5
major seismic surface
internal reflection
1st seabed multiple
diapir

Figure 5.

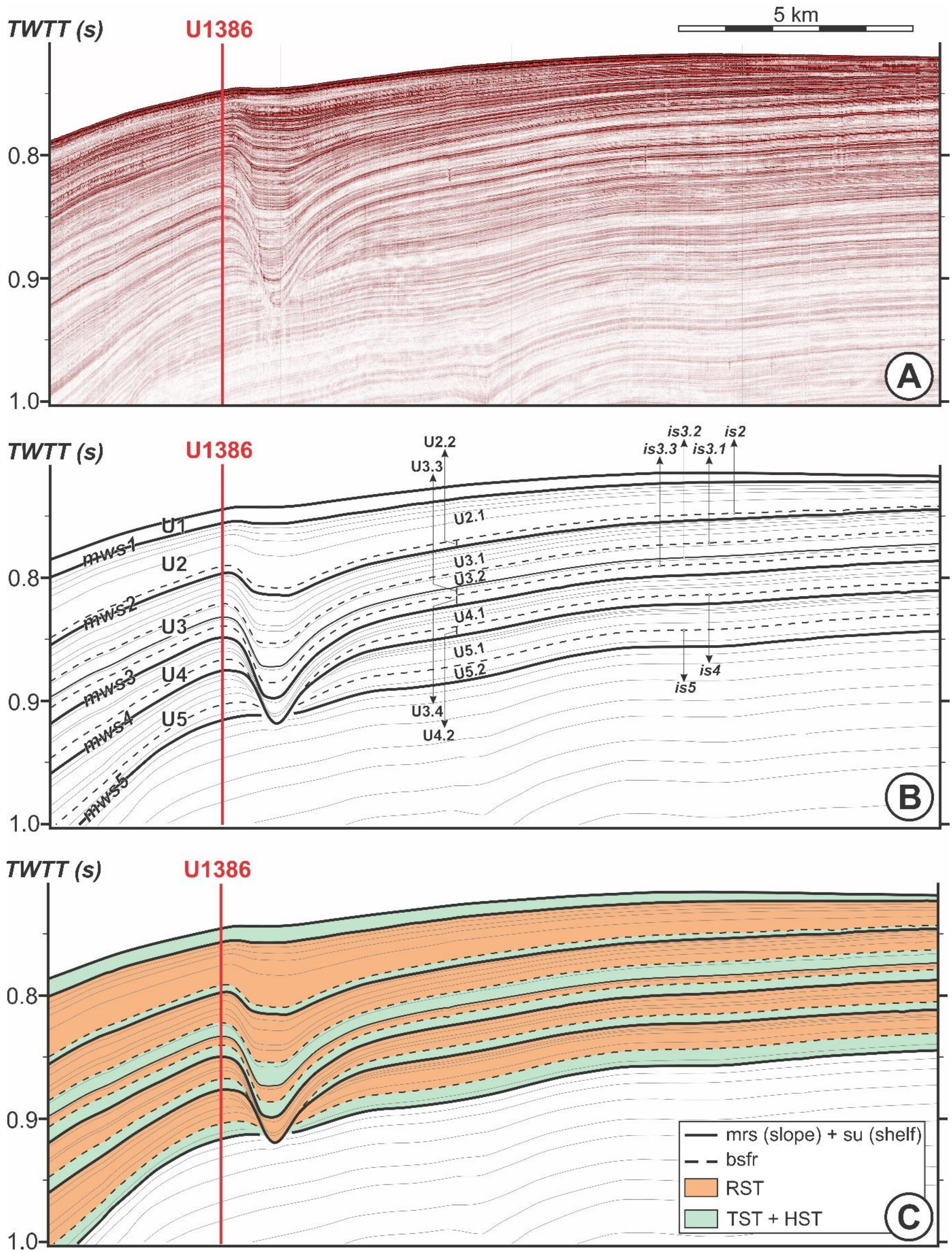

TWTT (s)
U1386
5 km
0.8
0.9
1.0
A
TWTT (s)
U1386
U2.2
U3.3
is3.2
is3.3
is3.1
is2
U1
U2.1
mws1
U2
U3.1
U3.2
0.8
mws2
U4.1
U3
U5.1
U5.2
mws3
U4
is4
is5
0.9
U3.4
mws4
U5
U4.2
mws5
1.0
B
TWTT (s)
U1386
0.8
0.9
1.0
mrs (slope) + su (shelf)
bsfr
RST
TST + HST
C

Figure 6.

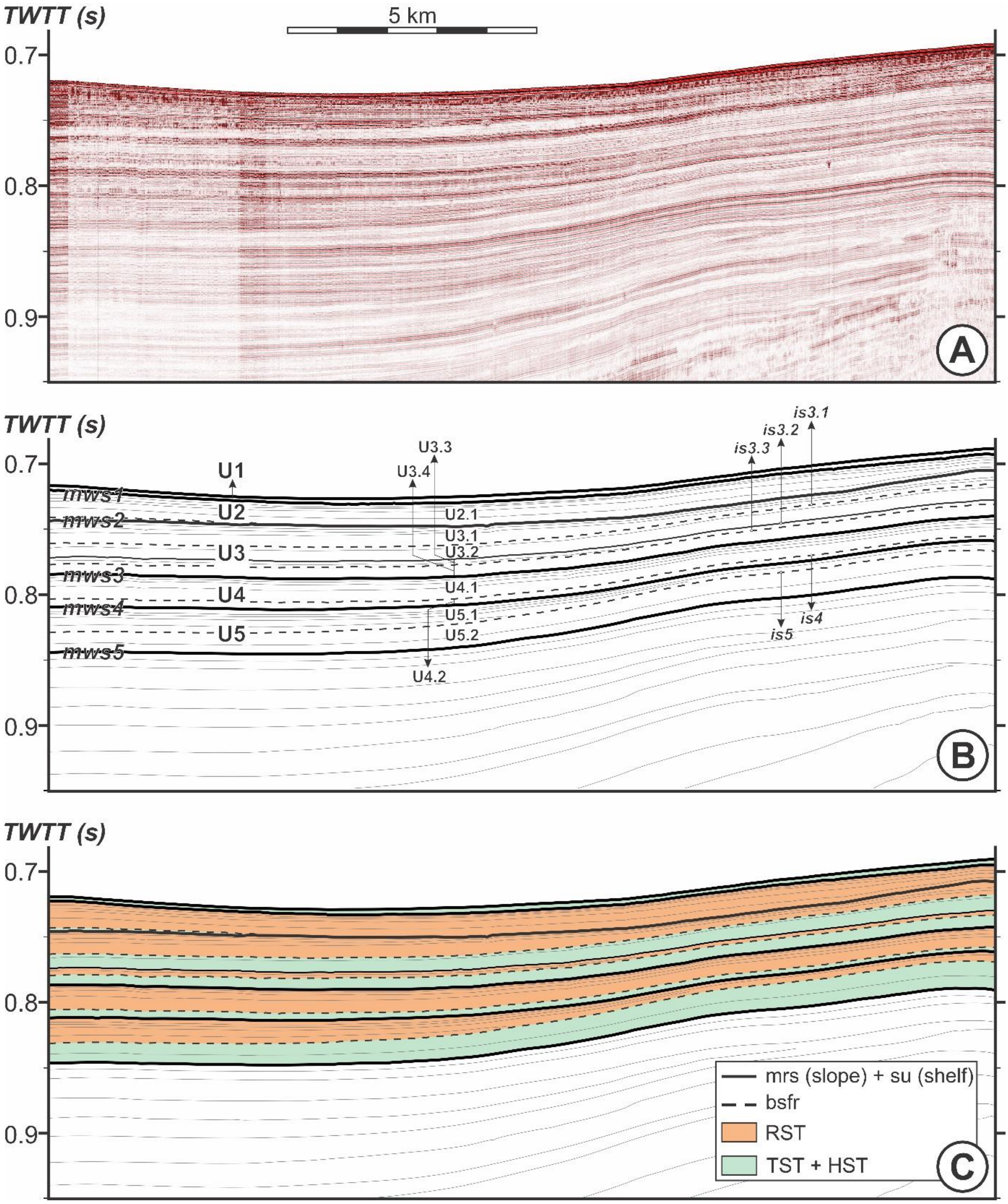
TWTT (s)
5 km
0.7
0.8
0.9
A
U1
U2
U3
U4
U5
mws1
mws2
mws3
mws4
mws5
U3.3
U3.4
U2.1
U3.1
U3.2
U4.1
U5.1
U5.2
U4.2
is3.1
is3.2
is3.3
is4
is5
B
mrs (slope) + su (shelf)
bsfr
RST
TST + HST
C

Figure 7.

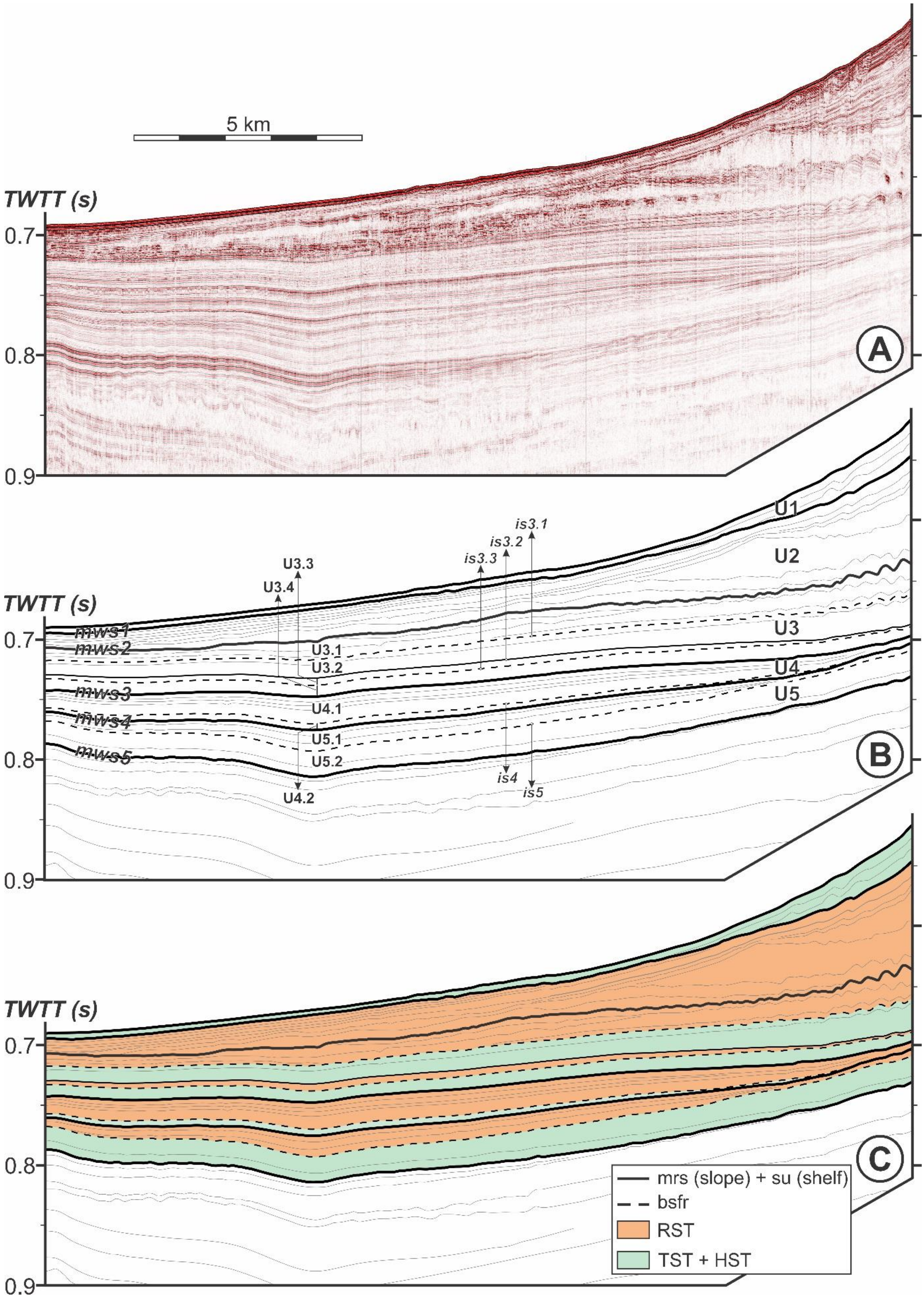

5 km
TWTT (s)
0.7
0.8
0.9
A
U1
U2
U3
U4
U5
U3.3
U3.4
is3.1
is3.2
is3.3
mws1
mws2
mws3
mws4
mws5
U3.1
U3.2
U4.1
U5.1
U5.2
U4.2
is4
is5
B
C
mrs (slope) + su (shelf)
bsfr
RST
TST + HST

Figure 8.

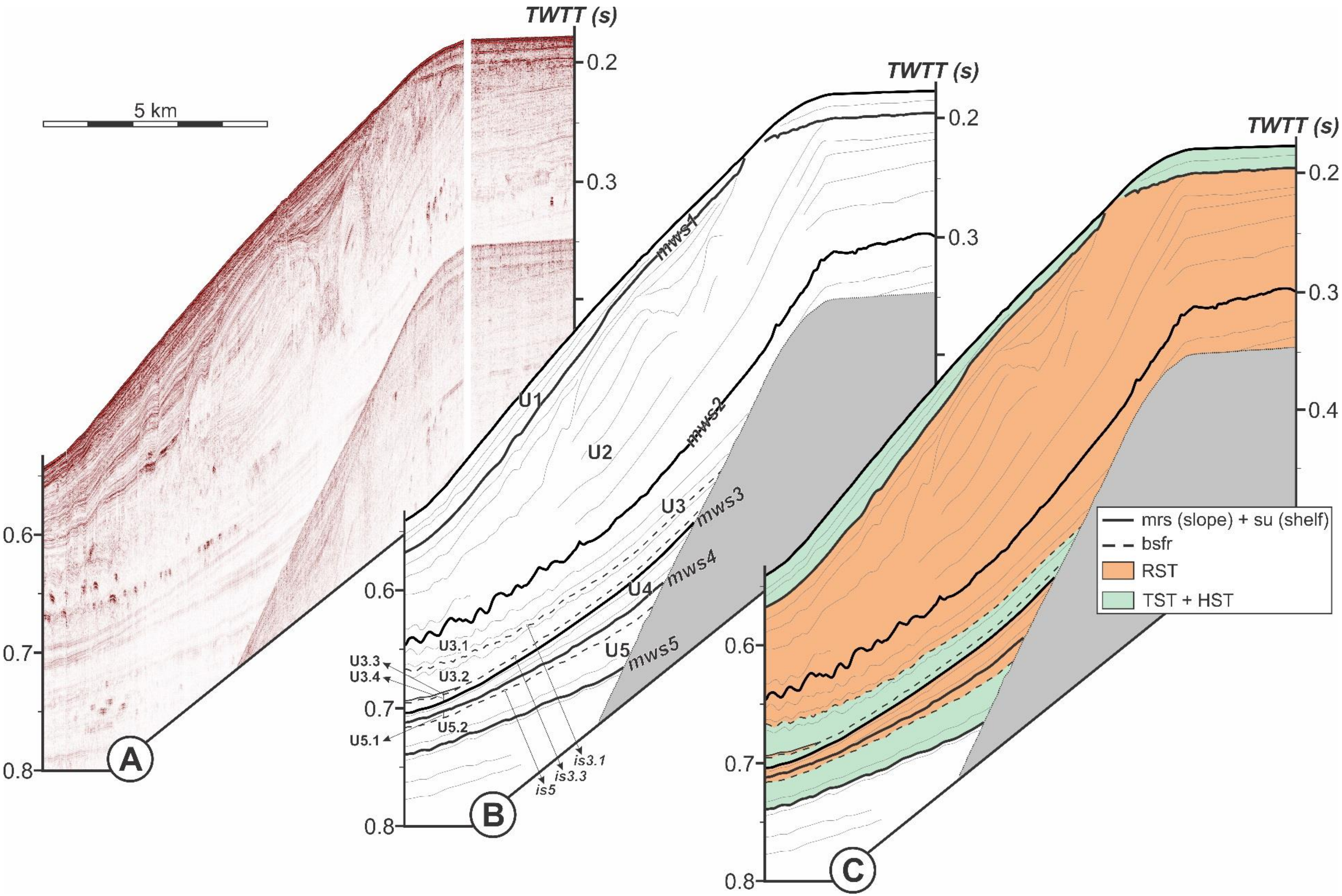

TWTT (s)
5 km
0.2
0.3
0.6
0.7
0.8
A
TWTT (s)
0.2
0.3
mws1
U1
U2
mws2
U3
mws3
U4
mws4
U5
mws5
U3.1
U3.2
U3.3
U3.4
U5.1
U5.2
is3.1
is3.3
is5
0.6
0.7
0.8
B
TWTT (s)
0.2
0.3
0.4
mrs (slope) + su (shelf)
bsfr
RST
TST + HST
0.6
0.7
0.8
C

Figure 9.

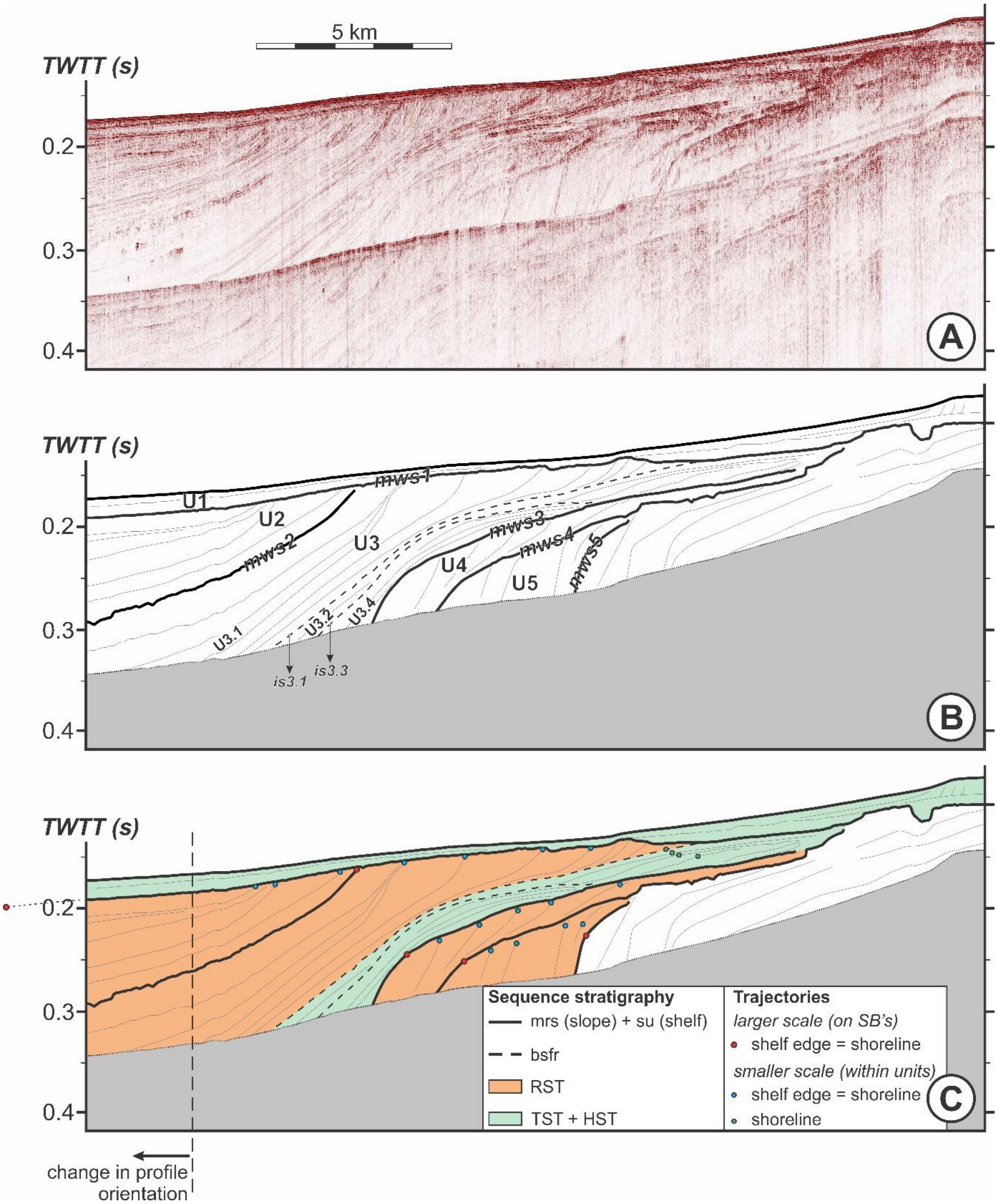
5 km
TWTT (s)
0.2
0.3
0.4
A
TWTT (s)
U1
U2
U3
U4
U5
mws1
mws2
mws3
mws4
mws5
U3.1
U3.2
U3.4
is3.1
is3.3
B
TWTT (s)
Sequence stratigraphy
mrs (slope) + su (shelf)
bsfr
RST
TST + HST
Trajectories
larger scale (on SB's)
shelf edge = shoreline
smaller scale (within units)
shelf edge = shoreline
shoreline
C
change in profile orientation

Figure 10.

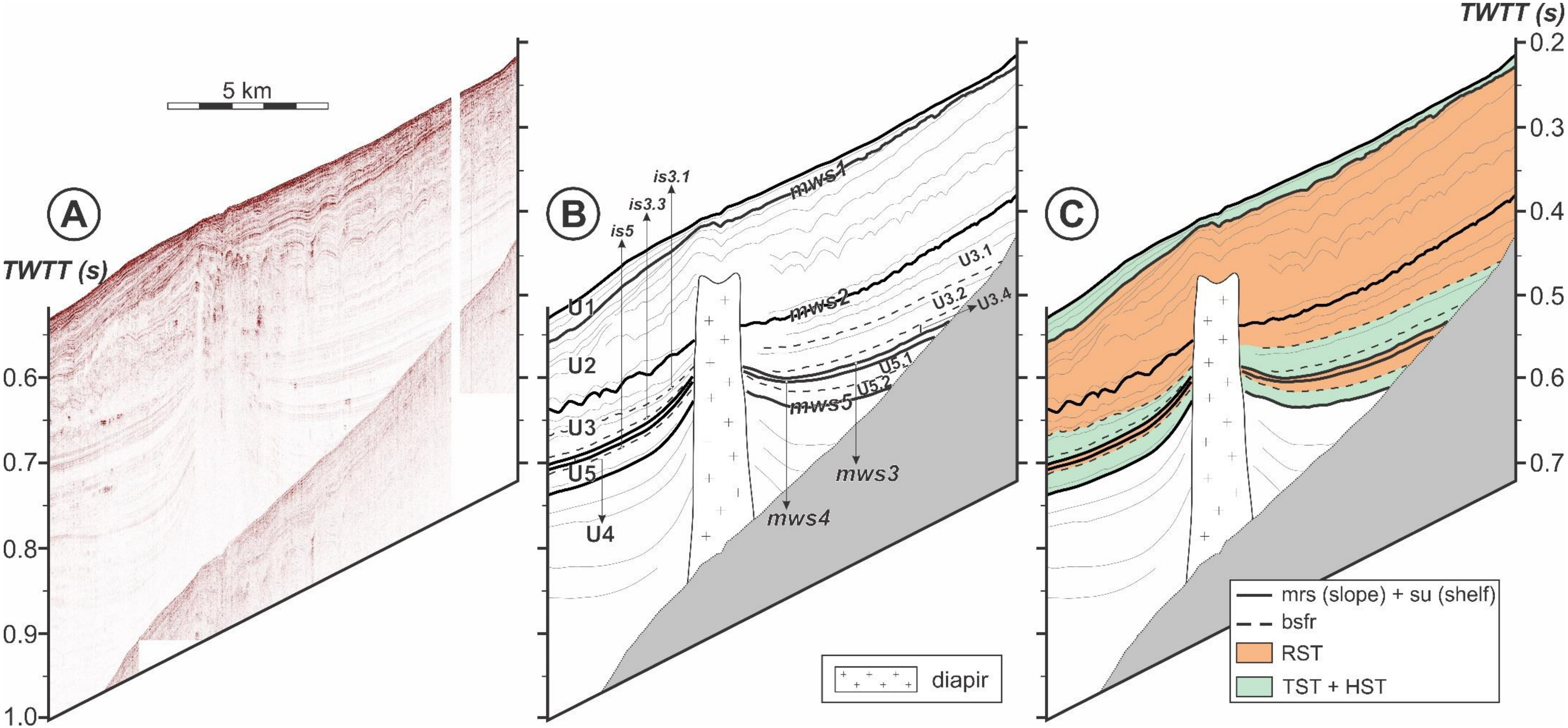

5 km
A
TWTT (s)
0.6
0.7
0.8
0.9
1.0
B
is3.1
is3.3
is5
mws1
mws2
U1
U2
U3
U5
U4
U3.1
U3.2
U3.4
U5.1
U5.2
mws5
mws3
mws4
diapir
C
TWTT (s)
0.2
0.3
0.4
0.5
0.6
0.7
mrs (slope) + su (shelf)
bsfr
RST
TST + HST

Figure 11.

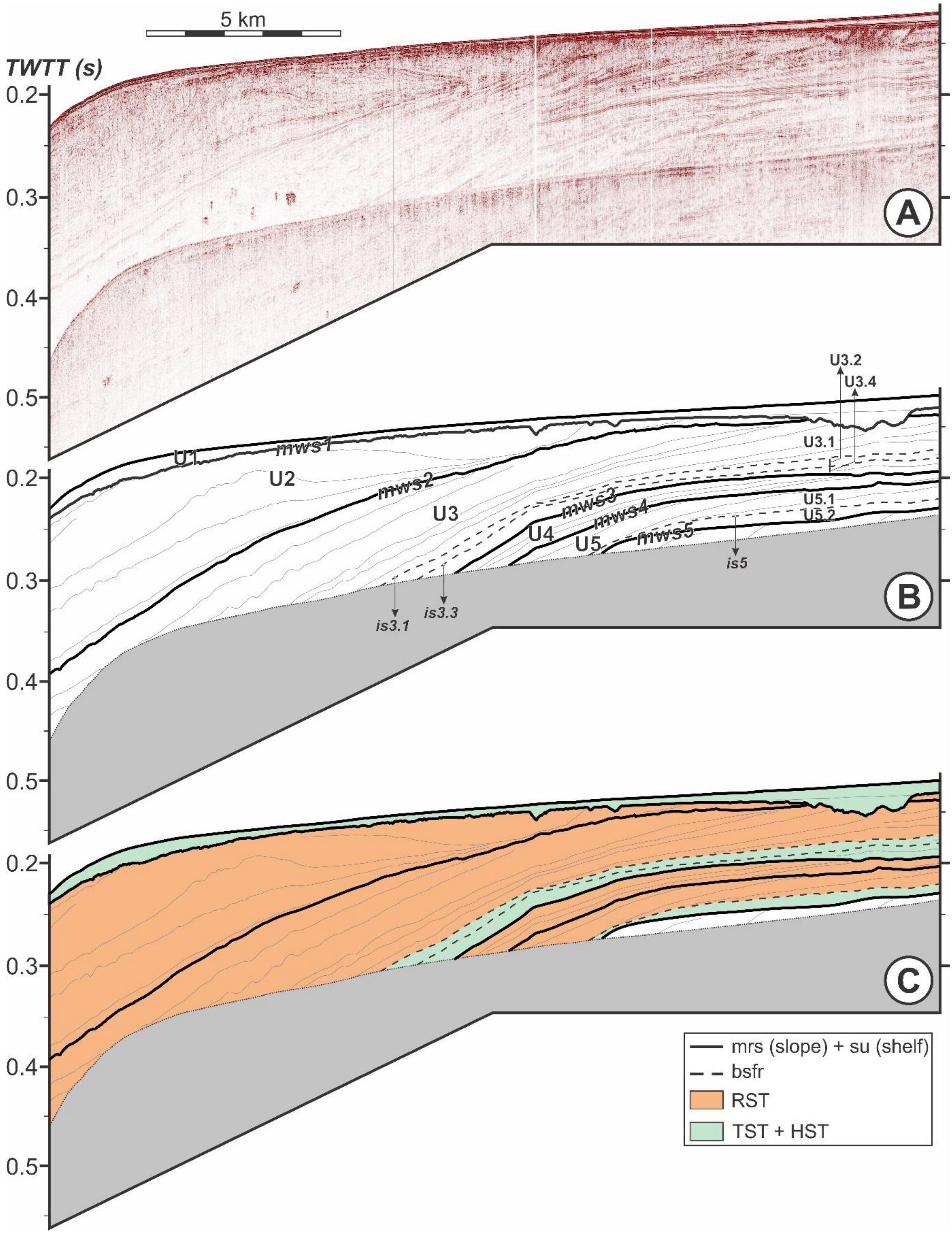
5 km
TWTT (s)
0.2
0.3
0.4
0.5
A
U3.2
U3.4
U3.1
U1
mws1
U2
mws2
U3
mws3
mws4
U4
U5
mws5
U5.1
U5.2
is5
is3.1
is3.3
B
C
mrs (slope) + su (shelf)
bsfr
RST
TST + HST

Figure 12.

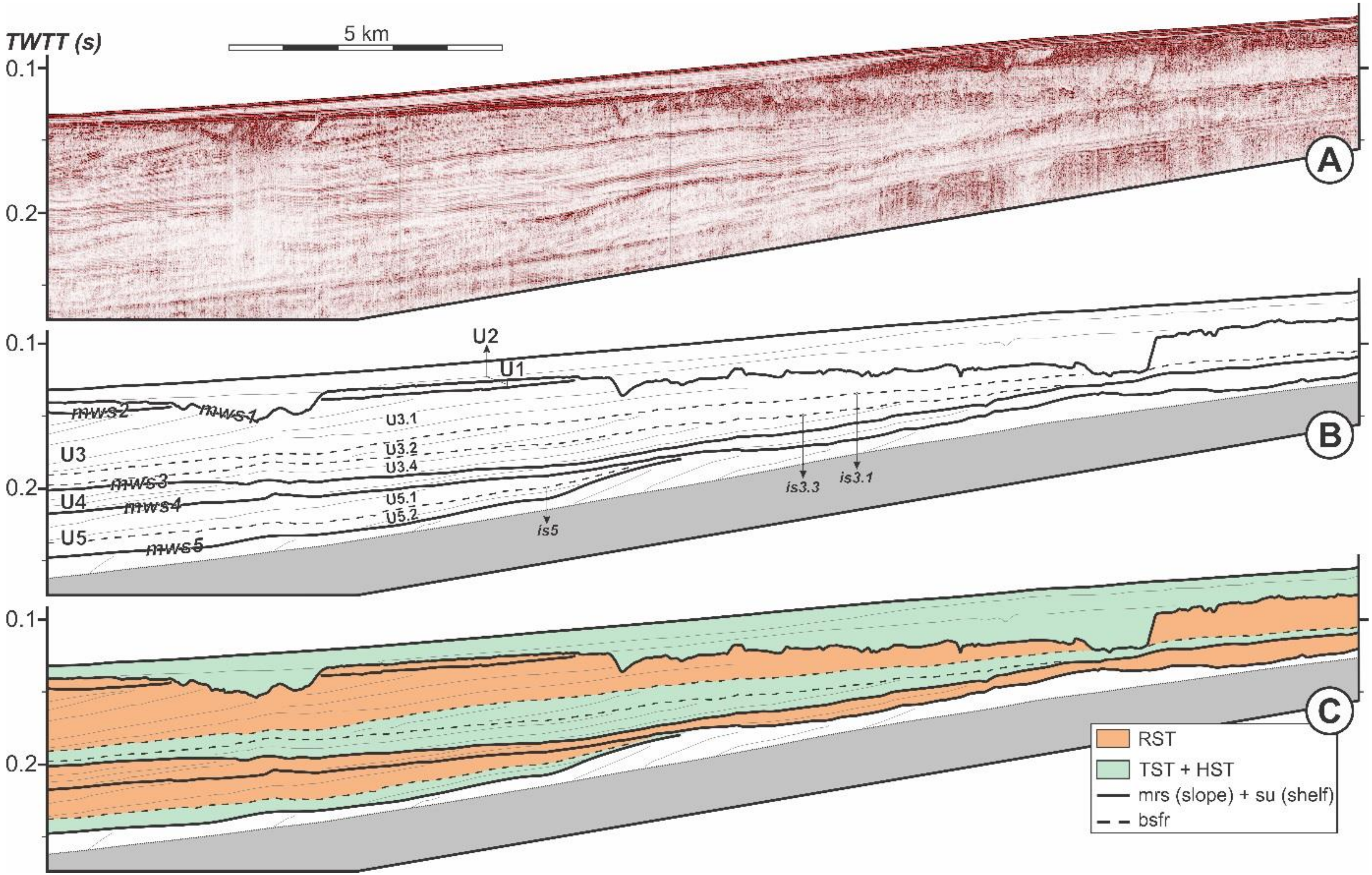

TWTT (s)
5 km
0.1
0.2
A
B
U2
U1
mws2
mws1
U3.1
U3
U3.2
U3.4
mws3
U4
mws4
U5.1
U5.2
U5
mws5
is5
is3.3
is3.1
C
RST
TST + HST
mrs (slope) + su (shelf)
bsfr

Figure 13.

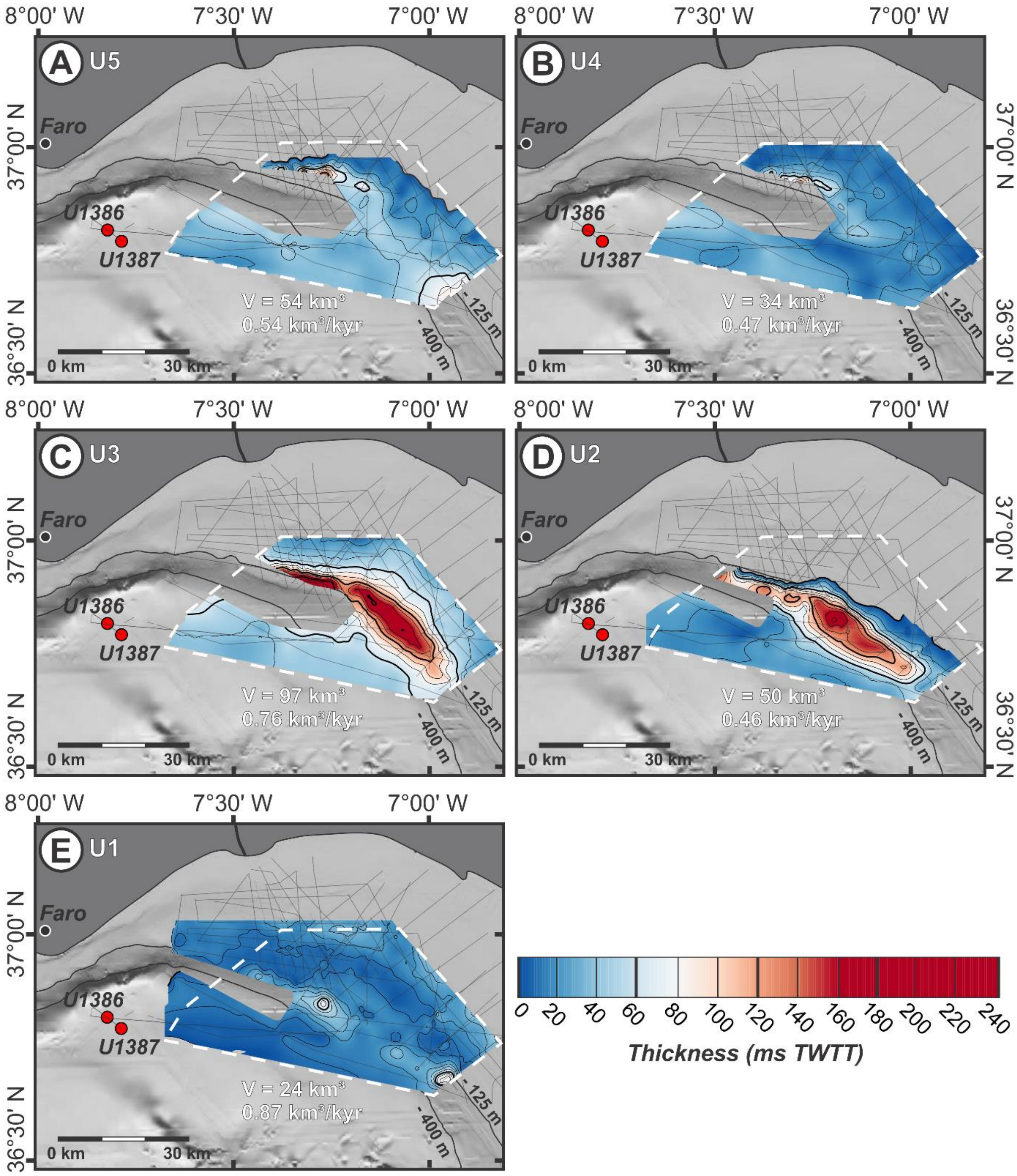
A U5
B U4
C U3
D U2
E U1
8°00' W
7°30' W
7°00' W
37°00' N
36°30' N
Faro
U1386
U1387
V = 54 km³
0.54 km³/kyr
V = 34 km³
0.47 km³/kyr
V = 97 km³
0.76 km³/kyr
V = 50 km³
0.46 km³/kyr
V = 24 km³
0.87 km³/kyr
125 m
400 m
0 km
30 km
0 20 40 60 80 100 120 140 160 180 200 220 240
Thickness (ms TWTT)

Figure 14.

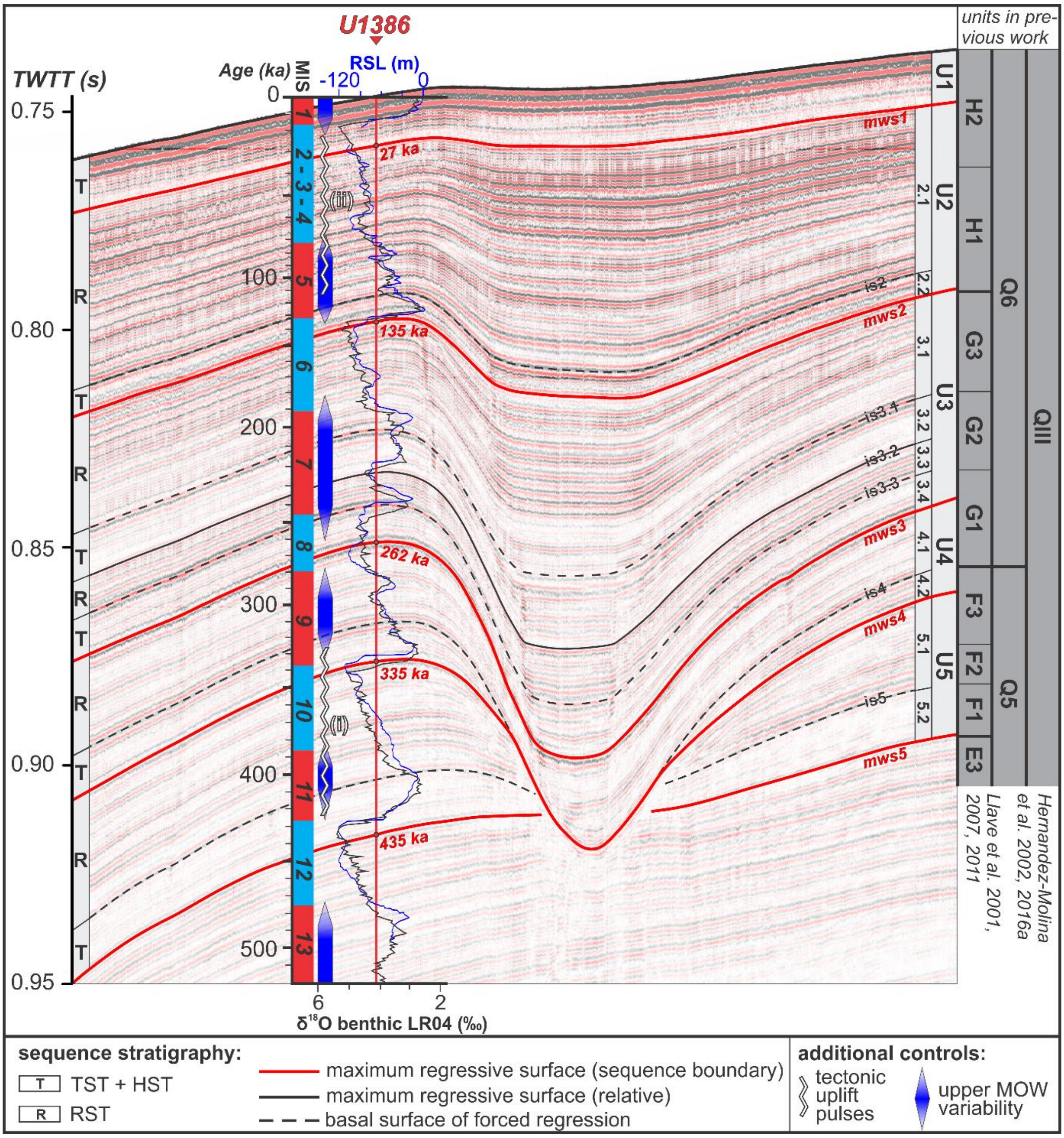

U1386
units in previous work
TWTT (s)
Age (ka)
MIS
RSL (m)
-120
0
0.75
0.80
0.85
0.90
0.95
100
200
300
400
500
27 ka
135 ka
262 ka
335 ka
435 ka
mws1
mws2
mws3
mws4
mws5
is2
is3.1
is3.2
is3.3
is4
is5
U1
U2
U3
U4
U5
H2
H1
G3
G2
G1
F3
F2
F1
E3
Q6
Q5
QII
Llave et al. 2001, 2007, 2011
Hernandez-Molina et al. 2002, 2016a
δ18O benthic LR04 (‰)
sequence stratigraphy:
TST + HST
RST
maximum regressive surface (sequence boundary)
maximum regressive surface (relative)
basal surface of forced regression
additional controls:
tectonic uplift pulses
upper MOW variability

Figure 15.

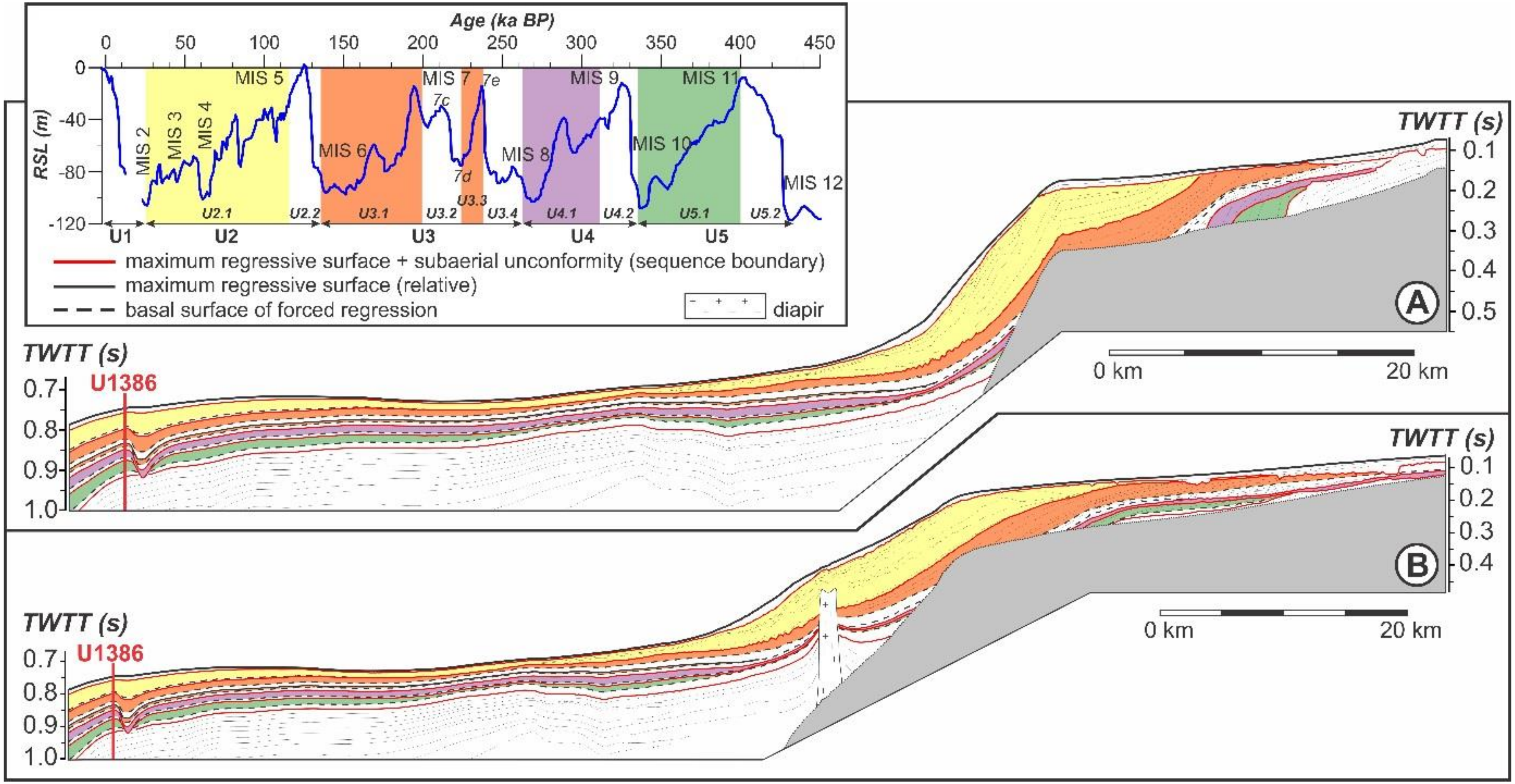

Age (ka BP)
0
50
100
150
200
250
300
350
400
450
RSL (m)
-40
-80
-120
MIS 2
MIS 3
MIS 4
MIS 5
MIS 6
MIS 7
7c
7d
7e
MIS 8
MIS 9
MIS 10
MIS 11
MIS 12
U2.1
U2.2
U3.1
U3.2
U3.3
U3.4
U4.1
U4.2
U5.1
U5.2
U1
U2
U3
U4
U5
maximum regressive surface + subaerial unconformity (sequence boundary)
maximum regressive surface (relative)
basal surface of forced regression
diapir
TWTT (s)
0.1
0.2
0.3
0.4
0.5
A
0 km
20 km
TWTT (s)
0.7
0.8
0.9
1.0
U1386
TWTT (s)
0.1
0.2
0.3
0.4
B
0 km
20 km
TWTT (s)
0.7
0.8
0.9
1.0
U1386

Figure 16.

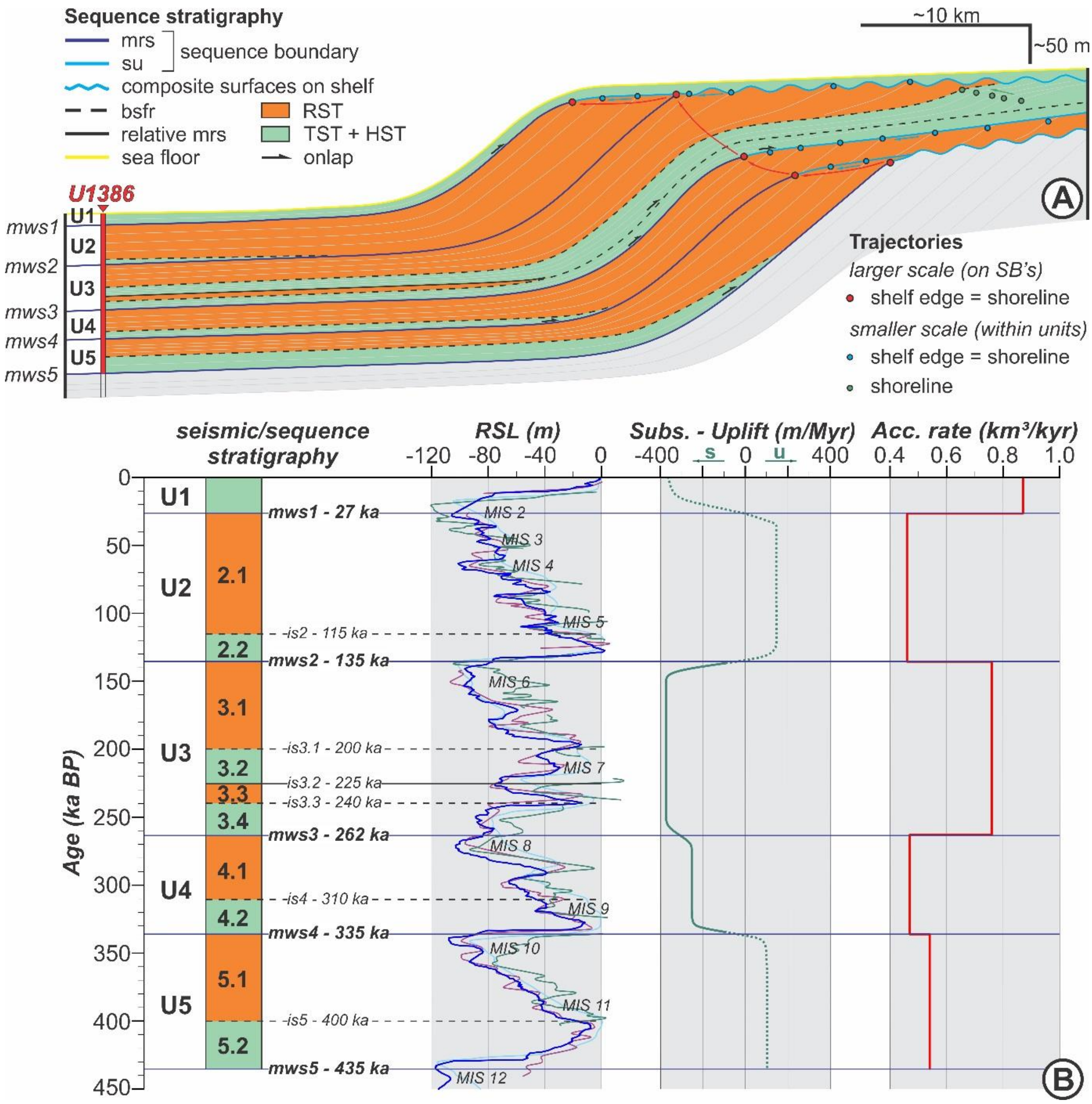

Sequence stratigraphy
mrs
su
sequence boundary
composite surfaces on shelf
bsfr
relative mrs
sea floor
RST
TST + HST
onlap
~10 km
~50 m
U1386
U1
U2
U3
U4
U5
mws1
mws2
mws3
mws4
mws5
A
Trajectories
larger scale (on SB's)
shelf edge = shoreline
smaller scale (within units)
shelf edge = shoreline
shoreline
seismic/sequence stratigraphy
RSL (m)
Subs. - Uplift (m/Myr)
Acc. rate (km³/kyr)
Age (ka BP)
2.1
2.2
3.1
3.2
3.3
3.4
4.1
4.2
5.1
5.2
mws1 - 27 ka
is2 - 115 ka
mws2 - 135 ka
is3.1 - 200 ka
is3.2 - 225 ka
is3.3 - 240 ka
mws3 - 262 ka
is4 - 310 ka
mws4 - 335 ka
is5 - 400 ka
mws5 - 435 ka
MIS 2
MIS 3
MIS 4
MIS 5
MIS 6
MIS 7
MIS 8
MIS 9
MIS 10
MIS 11
MIS 12
B

Figure 17.

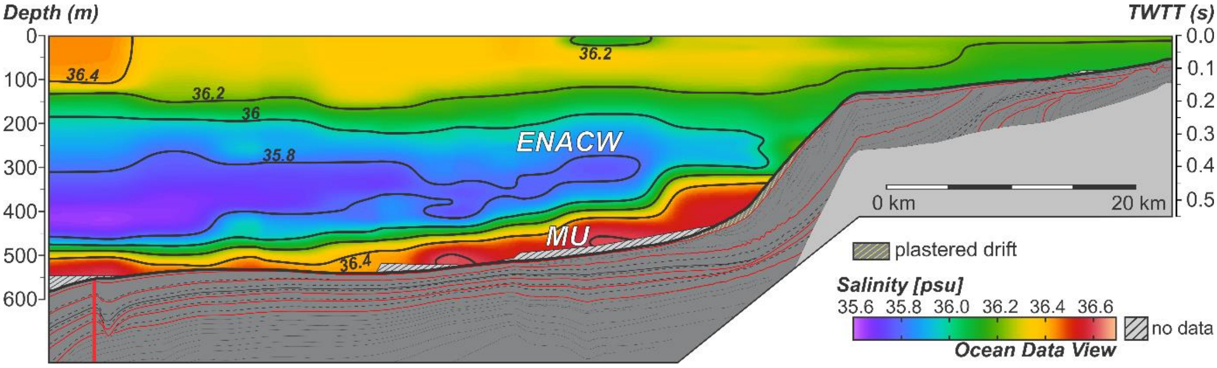
Depth (m)
TWTT (s)
0
100
200
300
400
500
600
0.0
0.1
0.2
0.3
0.4
0.5
36.4
36.2
36.2
36
35.8
ENACW
MU
36.4
0 km
20 km
plastered drift
Salinity [psu]
35.6 35.8 36.0 36.2 36.4 36.6
no data
Ocean Data View

Figure 18.

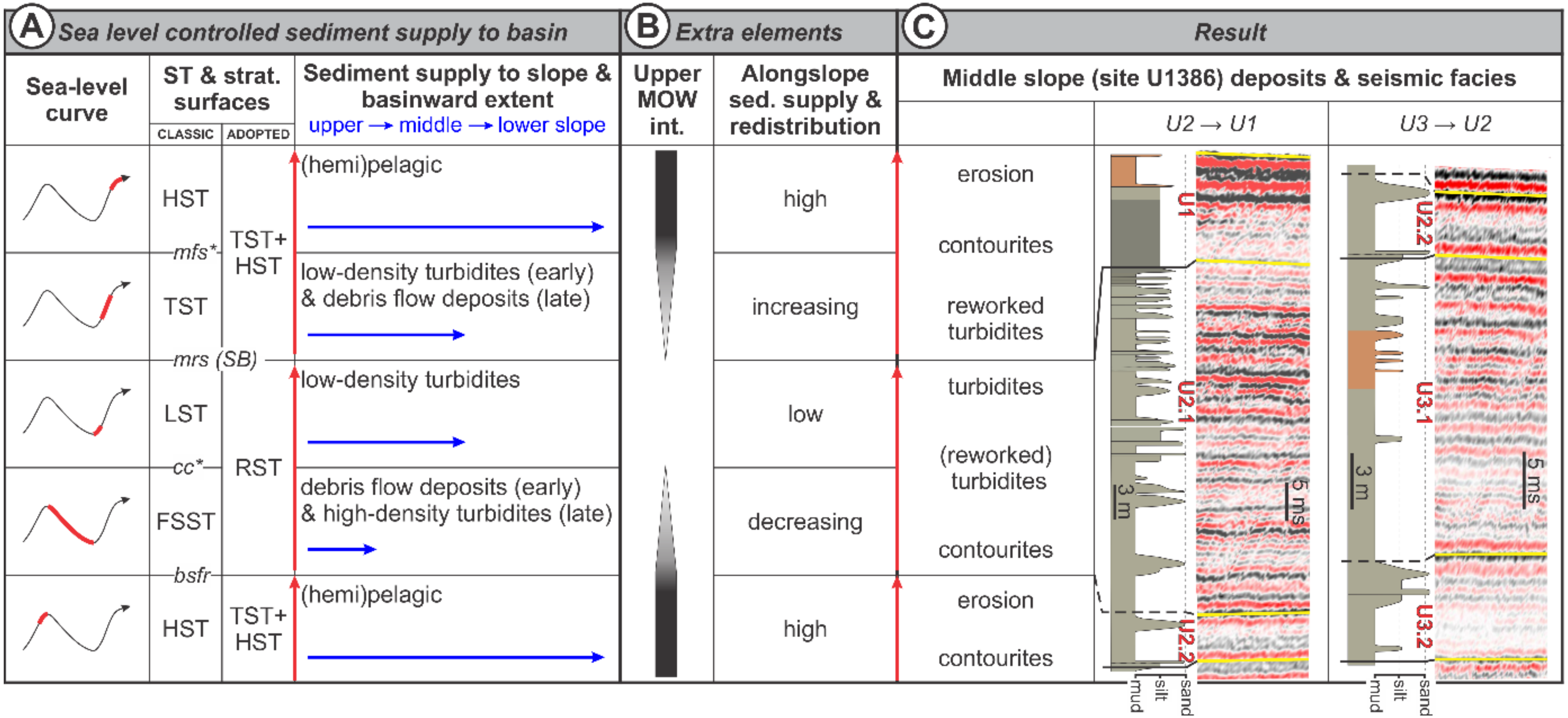

A Sea level controlled sediment supply to basin
B Extra elements
C Result
Sea-level curve
ST & strat. surfaces
CLASSIC
ADOPTED
Sediment supply to slope & basinward extent
upper → middle → lower slope
Upper MOW int.
Alongslope sed. supply & redistribution
Middle slope (site U1386) deposits & seismic facies
U2 → U1
U3 → U2
HST
mfs*
TST
mrs (SB)
LST
cc*
FSST
bsfr
HST
TST+ HST
RST
TST+ HST
(hemi)pelagic
low-density turbidites (early) & debris flow deposits (late)
low-density turbidites
debris flow deposits (early) & high-density turbidites (late)
(hemi)pelagic
high
increasing
low
decreasing
high
erosion
contourites
reworked turbidites
turbidites
(reworked) turbidites
contourites
erosion
contourites
U1
U2.1
U2.2
U2.2
U3.1
U3.2
3 m
5 ms
3 m
5 ms
mud
silt
sand
mud
silt
sand

Figure 19.

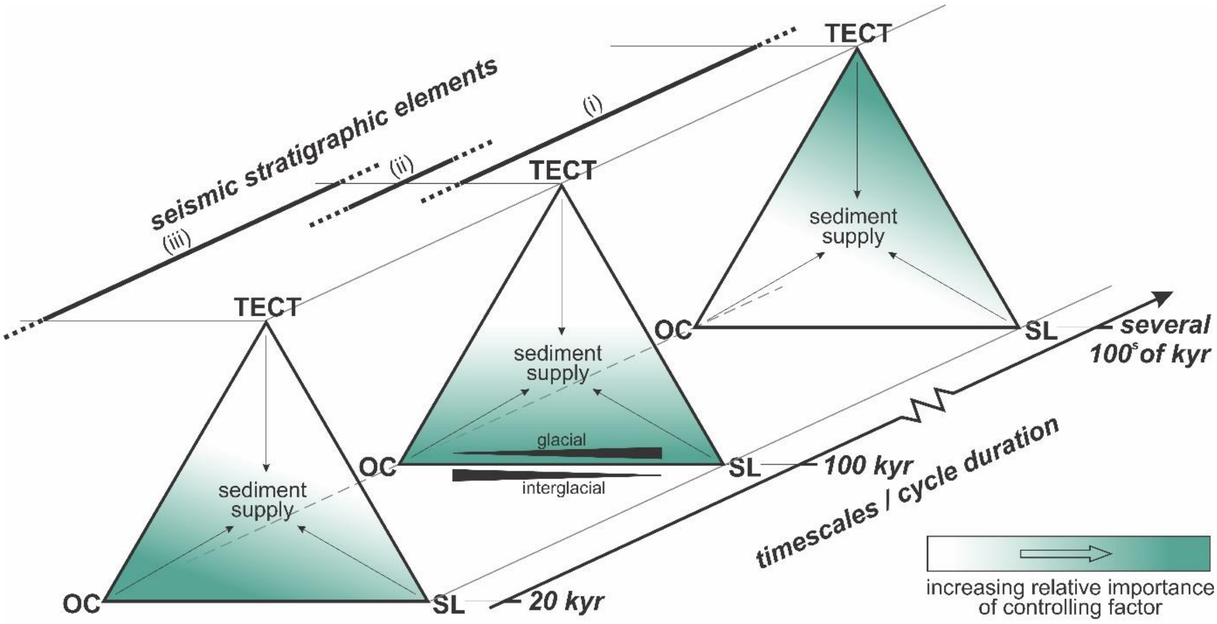
seismic stratigraphic elements
(i)
(ii)
(iii)
TECT
sediment supply
OC
SL
glacial
interglacial
20 kyr
100 kyr
several 100s of kyr
timescales / cycle duration
increasing relative importance of controlling factor

Figure 20.

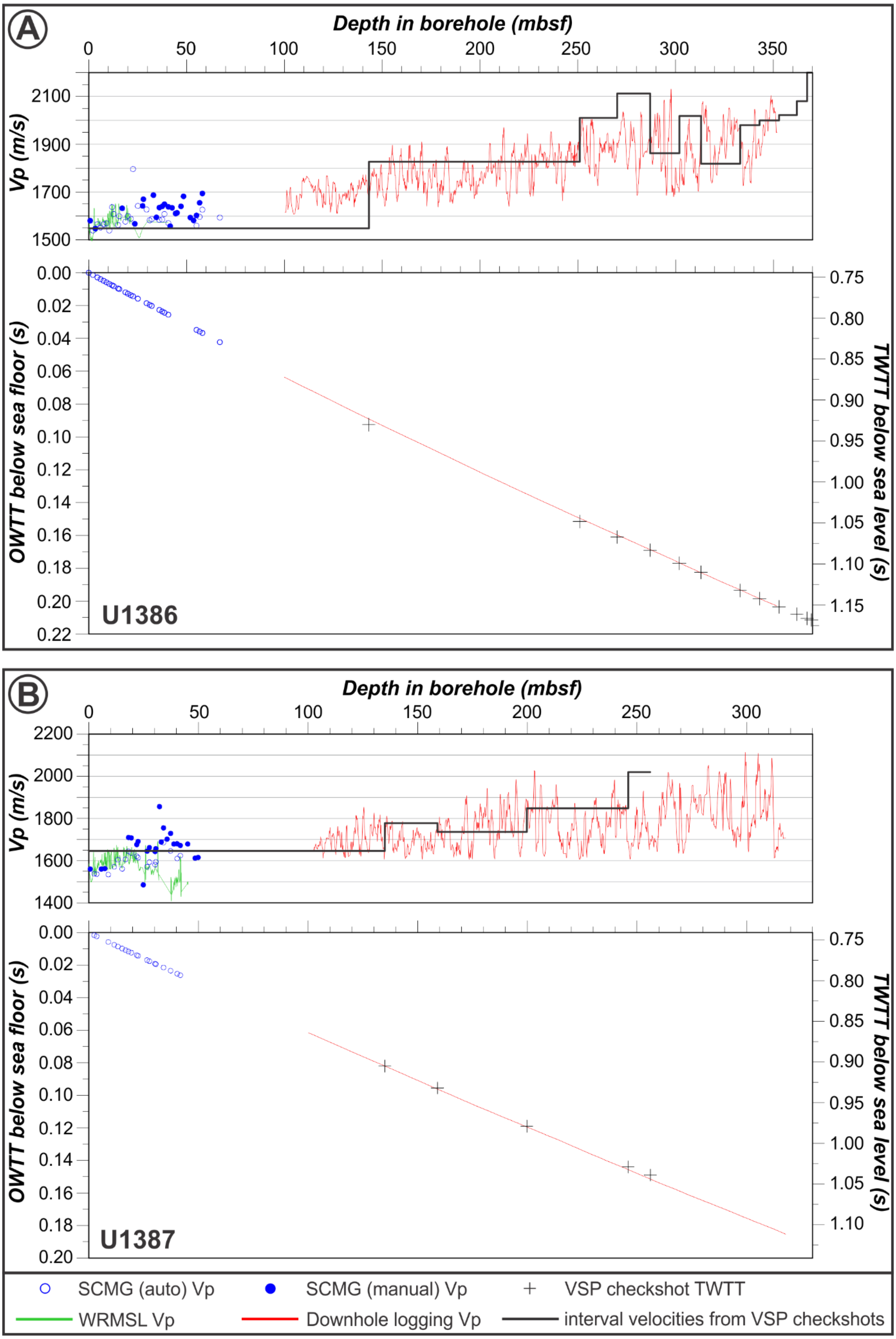

Supplementary figure 1.

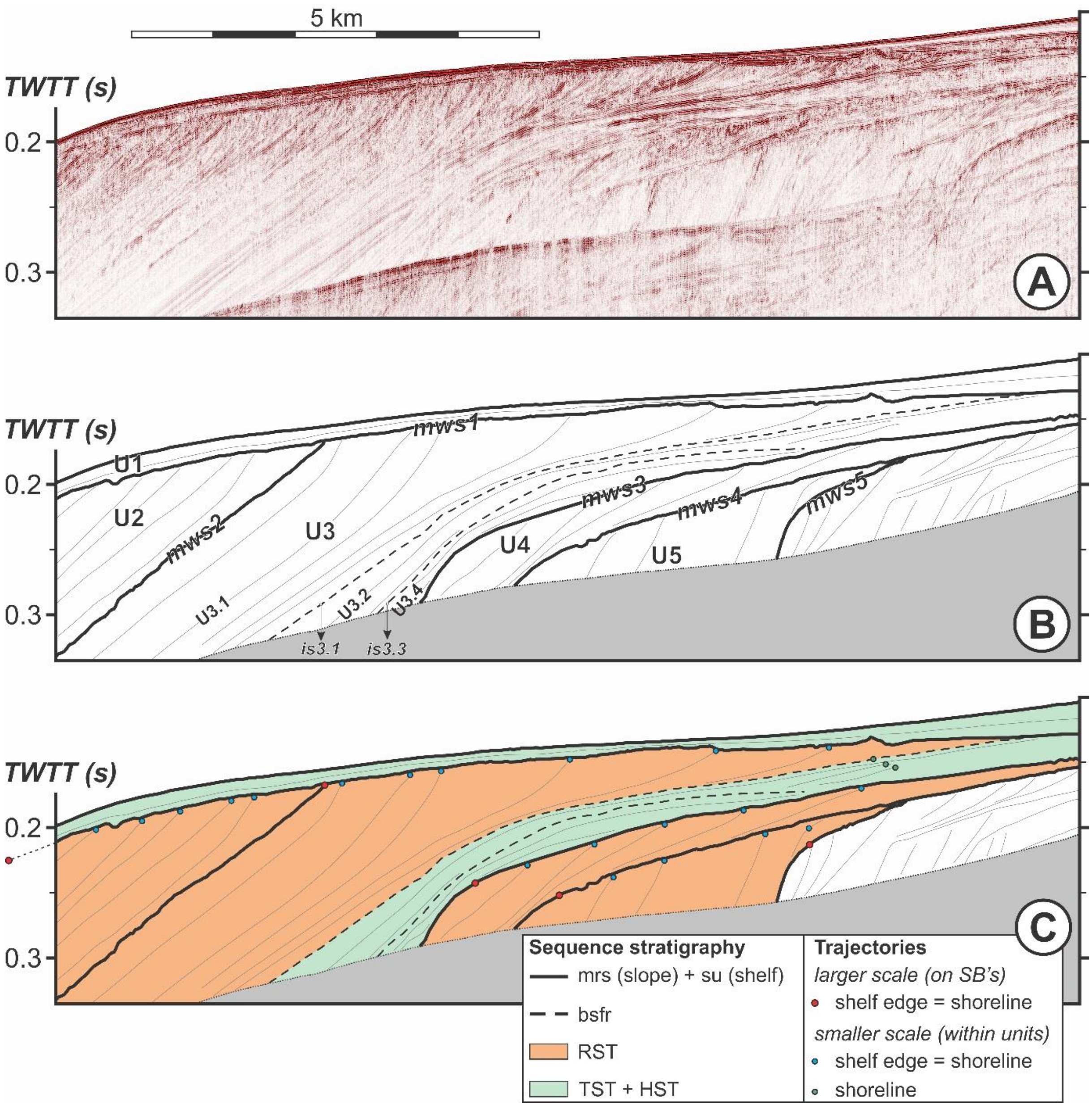

Supplementary figure 2.

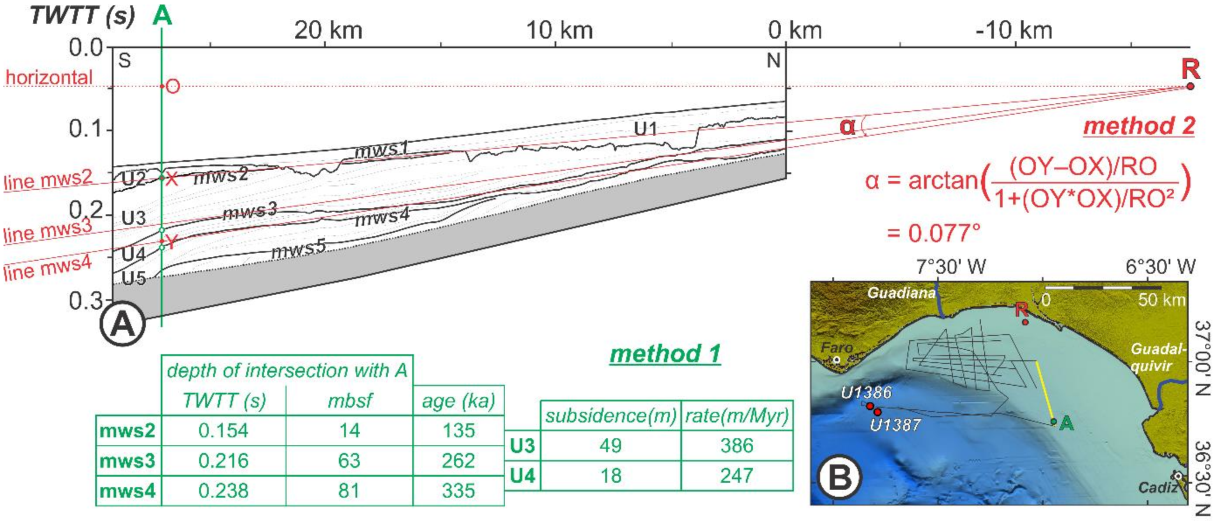

	depth of intersection with A		
	TWTT (s)	mbsf	age (ka)
mws2	0.154	14	135
mws3	0.216	63	262
mws4	0.238	81	335

	subsidence(m)	rate(m/Myr)
U3	49	386
U4	18	247

Supplementary figure 3.

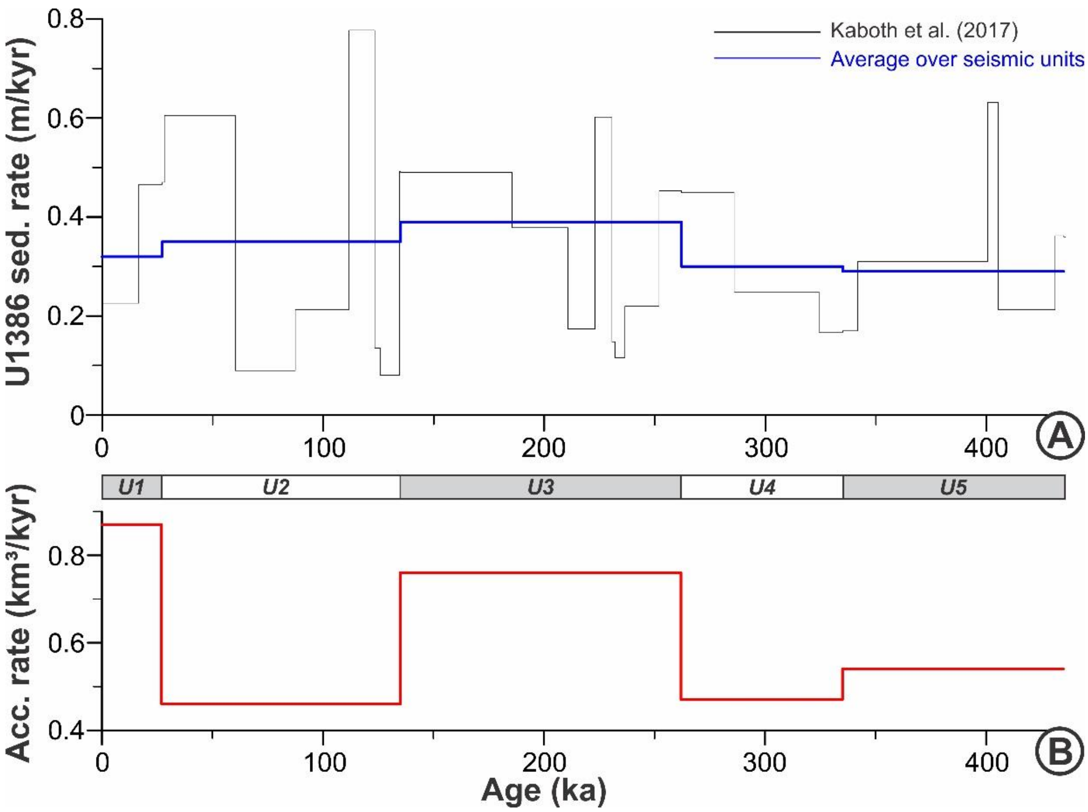

Supplementary figure 4.